Fall 2012

Use of high volume fly ash-wood fiber and polyurea layers for blast mitigation

Anthony Francis Wulfers

Department:

USE OF HIGH VOLUME FLY ASH-WOOD FIBER AND POLYUREA LAYERS FOR BLAST MITIGATION

by

ANTHONY FRANCIS WULFERS

A THESIS

Presented to the Faculty of the Graduate School of the

MISSOURI UNIVERSITY OF SCIENCE AND TECHNOLOGY

In Partial Fulfillment of the Requirements for the Degree

MASTERS OF SCIENCE IN CIVIL ENGINEERING

2012

Approved by

JOHN J. MYERS – ADVISOR
JASON BAIRD
JEFFERY VOLZ

ABSTRACT

This project is a continuation of research done by Natalia Carey and John Myers. The first part of Natalia's research was to develop and characterize an e-glass discrete fiber-reinforced polyurea (DFRP) system for infrastructure applications. She then recommended two polyurea systems (A and B) be further examined. These polyurea systems were then applied to plain reinforced concrete and steel fiber reinforced concrete panels (SFRC). Carey found that the SFRC panels sustained less overall damage.

For this project SFRC was used as the base layer in combination with the DFRP systems. In addition to the DFRP and SFRC a high-volume fly ash-wood fiber (FA-WF) material was added to act as a sacrificial layer on the panels. The FA-WF is a material that has been under development at Missouri University of Science and Technology (Missouri S&T). These panels were then tested with explosives at the Missouri S&T Mine. The panels were compared visually and analytically. The visual observations were used to compare dramatic differences in the panels, while more analytical means, like residual deflections and estimated mass loss allows panels with very similar damage to be compared. After comparing the results significantly less damage was observed in the hybrid panels that contained a foam-gap and a DFRP layer. Results from this study will be used to evaluate alternative construction methods and coating systems to protect at-risk structures and their inhabitants.

ACKNOWLEDGEMENTS

I would like to thank my advisor Dr. John J. Myers for his guidance throughout this project. Dr. Myers provided support, encouragement, and most of all an opportunity to continue my education. I would like to thank Natalia Carey for her assistance and guidance throughout this project. I would also like to thank my committee members Dr. Jason Baird and Dr. Jeffery Volz for their guidance and involvement in this research project.

I would like to thank the parties that assisted in putting this project together Awareness and Localization of Explosives Related Threats (ALERT) center of excellence at Northeastern University, my advisor Dr. John J. Myers, and the funding provided by the Department of Homeland Security.

I greatly appreciate the generous donations of materials and time provided by LINE-X, Propex, Owings-Corning, Encore Building Solutions, and Labadie Power Plant. I would specifically like to acknowledge the contributions by Jeff Jira of LINE-X and Dave Edmundson of Propex.

I gratefully acknowledge the support and assistance by students and staff members of the Department of Civil, Architectural and Environmental Engineering (CArEE), the Center for Infrastructure Engineering Studies and the Rock Mechanics and Explosives Center (RMERC) at Missouri University of Science and Technology (Missouri S&T)..

I would like to especially thank my parents for their endless support throughout my research.

TABLE OF CONTENTS

LIST OF ILLUSTRATIONS

LIST OF TABLES

NOMENCLATURE

Symbol	Description
b	Decay coefficient
E	Modulus of elasticity
M	Dry mass
M_s	Wet mass
p(t)	Pressure as a function of time
p_o	Atmospheric pressure
P_s^+	Peak overpressure
R	Standoff distance
s	Stress
t	Time elapsed
T^+	Positive phase duration
V	Volume
W	Charge weight
Z	Scaled distance
ε	Strain
ρ_w	Density of water

1. INTRODUCTION

1.1 OVERVIEW

The importance of research into blast mitigation has been increasing with the increasing terrorist threats (Wright and Ichniowski 2002). It does not take a special degree or large capital to create an explosive (Michel and Herbeck 2001). Important cultural and governmental buildings present themselves as targets for adversaries and due to the lack of consideration for blast in the design of buildings, many of these buildings are at risk of collapsing after an explosive attack, resulting in fatalities. However, in recent years blast has become more and more commonly considered in design (Security Management Consulting 2010).

Blast was rarely considered in building design (Carey and Myers 2009) prior to the Oklahoma City bombing. Shortly after the bombing on April 19, 2005 the General Services Administration published a Security Design Criteria which was a major step in preventing another event like the Oklahoma City Bombing. The Security Design Criteria have been updated a few times since its inception and typically recommends some type of barrier be constructed outside the building to create a standoff distance (Security Management Consulting 2010). After the terrorist attacks of 9/11/2001, Jersey barriers were placed around many of the American Federal Buildings, which created an eyesore and a restrictive environment in many urban areas (Hill 2004). Barriers reduce possible damage from explosive events by increasing the standoff distance, but when the desired standoff distance is 30 m (100 feet) it is sometimes impossible to achieve in urban environments (Nadel 2002).

Barriers are designed against certain breaches, but if one should occur, like what happened during 9/11/2001 terrorist attacks, many of the current federal buildings are at risk of collapse. This does not mean that there is a need to design all federal buildings for the use of airplanes as weapons, but it means that consideration should be given to the ability of our enemies to breach a barrier and then detonate an explosive. New federal buildings are designed to resist progressive collapse; however, it is difficult to retrofit an existing building to resist progressive collapse (Gonchar 2002). One method is to contain the blast within the exterior shell, which is investigated in this study. This study examines using two materials that may have applications as retrofit or new construction material.

1.2 PURPOSE AND RESEARCH OBJECTIVES

This research study is the fourth phase of a multi-organizational effort to mitigate blast damage and harden structural systems. The project was undertaken under the Awareness and Localization of Explosive Related Threats (ALERT) center of excellence at Northeastern University. The study was funded by the Department of Homeland Security (DHS). Personnel from the Department of Civil, Architectural, and Environmental Engineering (CArEE) and the Rock Mechanics and Explosives Research Center (RMERC) at Missouri University of Science and Technology (Missouri S&T) were engaged in the effort.

This study examined the use of a high-volume fly ash-wood fiber (FA-WF) material as a sacrificial material with and without other hybrid technologies for blast mitigation and dissipation. A study by Tinsley and Myers (2007) has already been completed on the benefits of FA-WF for blast mitigation. The study done by Tinsley and

Myers (2007) at Missouri S&T concluded that the FA-WF material provided a dramatic benefit in blast mitigation. The FA-WF material is a low strength and low density material that is highly ductile thus allowing for greater energy absorption (Tinsley and Myers 2007). The research presented in this study was aimed at investigating the benefits of a FA-WF layer, but also examined the benefits of a polyurea compound on a concrete panel with a FA-WF layer and the use of internal steel fibers in some hybrid systems.

The benefits of plain polyurea during a blast event have already been well established through many previous studies and it is even being used currently by the United States (U.S.) Military (Applied Research Associates, Inc. 2004). So this study investigates using an e-glass, discrete fiber reinforced polyurea (DFRP). E-glass is electrically conductive glass. In a previous study done by Greene and Myers (2010) this same polyurea material with discrete e-glass fiber was investigated for its effects in strengthening existing structural members. In Greene's study, she indicated that the e-glass DFRP exhibited strengthening qualities for flexure and shear. The discrete e-glass fiber material was studied to investigate its feasibility as a multi-functional retrofitting material. The e-glass DFRP could be a material that could be used to not only harden against blast, but also strengthen deteriorating or obsolete structures. This research attempts to discover if the added e-glass fiber contributes to the stiffness of a panel while also containing any fragments from a blast for various hybrid systems.

The high volume fly ash-wood fiber (FA-WF) material was chosen for examination as a sacrificial material since it is a low strength yet ductile material. It was also chosen since both the wood fiber and the fly ash are byproducts of two industries: the lumber and coal power industries, respectively. This makes the material not only

beneficial in terms of properties but also in terms of a renewable and sustainability perspective. The FA-WF material was intended to be used as a sacrificial material on the compression face of steel fiber reinforced concrete (SFRC) base. A recently completed study by Carey compared SFRC and reinforced concrete (RC) and found that the SFRC is significantly better at containing. This study decided to use SFRC in almost all the panels to better understand the benefits of SFRC in combination with e-glass DFRP coatings and sacrificial FA-WF layers.

The focus of this overall research study was on the combination of FA-WF, SFRC, and DFRP coatings. This study examined the benefits from the FA-WF and polyurea. The SFRC was not investigated for its benefits in this study since that study was undertaken by Carey and Myers (2012).

2. RELATED WORK

Summaries of several studies and available literature in the fields of FA-WF, polyurea coatings, and blast mitigation testing are presented in this section. These research projects provided the foundation for this study.

2.1 EXPLOSIVES

The wave from a high explosive decays with distance and time as it propagates through the air. **Equations 2.1 – 2.2** were used to account for the impact of distance on the decay in the wave, and calculate the initial overpressure (P_s^+) in bar given a scaled distance (Z) in m away from a trinitrotoluene (TNT) charge. **Equation 2.1** only applies to P_s^+ values that are greater than or equal to 10 bar and **Eq. 2.2** accounts for P_s^+ values between 0.1 and 10 bar. The scaled distance, which was calculated using **Eq. 2.3**, accounted for the distance to the explosive (R) (i.e. standoff distance) in m and weight (W) in kg of the TNT charge (Chock and Kapania 2001). Explosive materials release a certain amount of energy based on the chemical composition of the material and weight allowing any explosive to be converted to a weight of TNT called a TNT equivalent, and for C-4 the TNT equivalent is 1.3 (National Counterterroism Center 2011). **Equations 2.1 – 2.3** assume that the explosive is TNT, so the TNT equivalence of an explosive allowed these equations to be used. Once the peak overpressure was found at a specific location the decay in time was represented by **Eq. 2.4** or the modified Friedlander's equation (Chock and Kapania 2001), which is illustrated in **Figure 2.1**. The modified

Friedlander's equation calculates pressure (p(t)) given a duration of time (t), atmospheric pressure (p_o), peak overpressure, and the decay coefficient (b) (Tinsley and Myers 2007).

$$P_s^+ = \frac{6.7}{z^3} + 1, (P_s^+ \geq 10) \quad (2.1)$$

$$P_s^+ = \frac{0.975}{z} + \frac{1.455}{z^2} + \frac{5.85}{z^3} - 0.19, (0.1 \leq P_s^+ < 10) \quad (2.2)$$

$$Z = R/W^{1/3} \quad (2.3)$$

$$p(t) = p_o + (P_s^+) * (1 - \frac{t}{T^+}) e^{-b\frac{t}{T^+}} \quad (2.4)$$

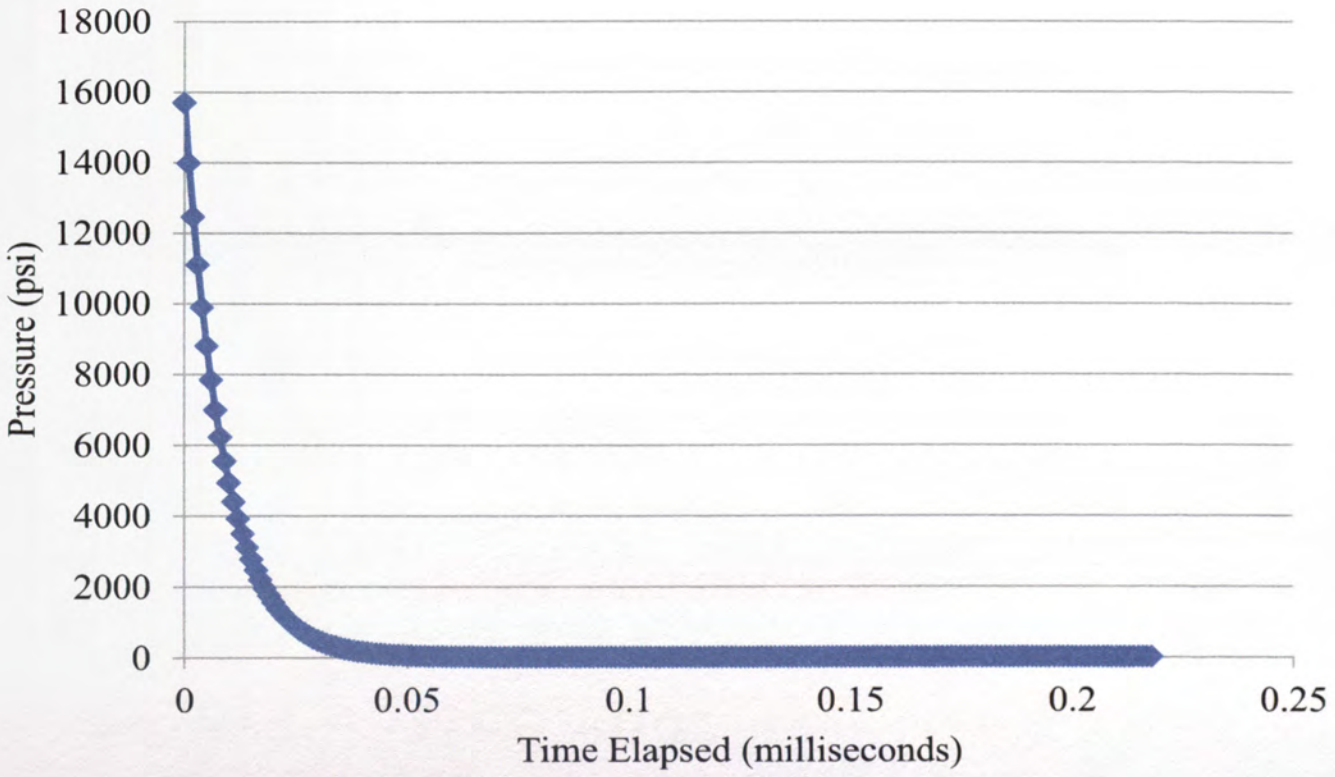

Figure 2.1 – Modified Friedlander's Equation

As a blast wave travels from one medium into the next medium the way it is transmitted into that medium is based on the shock wave impedance of the two materials. The shock wave impedance is based on the density of a material and the material's shock velocity. As a blast wave transitions from a lower shock impedance medium into a higher shock impedance medium, the wave is transmitted as a compression wave. If the wave is going from a higher to lower shock impedance the wave is transmitted as rarefaction or as a tensile wave if the medium is a solid. The greater the shock impedance mismatch is, the greater the amount of wave that is reflected, thus decreasing the amount of wave transmitted (Cooper 1996).

2.2 DEVELOPMENT OF A FA-WF MATERIAL

Society has encouraged many industries to adapt and attempt to recycle and reuse products to become more environmentally friendly. Concrete and construction industries have been in search of more environmentally friendly products and practices. This has led to looking at the waste products of other industries as possible sources of construction materials.

Fly ash, which is now commonly used in concrete, is a byproduct of the coal power industry. Fly ash was first studied for use in concrete as a pozzolan in 1937 (Halstead 1986), so its use in concrete is nothing new, but usage has been steadily increasing from 2000 to 2010 (American Coal Ash Association 2012). Fly ash presents itself as a substitute for a certain portion of the cement in concrete due to its pozzolanic properties, which allow it to increase long-term strength, chemical resistivity, and durability. Fly ash's spherical shape also allows it to improve the workability of concrete

(American Coal Ash Association 2003). Although usage has increased there is still a significant amount going to waste—62% (American Coal Ash Association 2012). So the need for increasing the usage of fly ash is still present and this project investigates using fly ash as a major component of the sacrificial FA-WF blast material.

The use of wood fiber in concrete is at least 70 years old (Durisol Building Systems, Inc. 2011) thus it is not a new technology either. The study of wood fiber concrete however, is somewhat limited. A few studies have been conducted regarding the durability of wood fiber concrete, including one by Coatanlem et al. (2006) which tested the effect of soaking the wood chips with a solution of sodium silicate on bond strength between the wood fibers and cementitous material. Coatanlem research found that the sodium silicate did in fact improve the bond strength and the material was able to maintain strength even after 16 months of exposure to harsh environments (Coatanlem, Jauberthie and Rendell 2006). In studies performed by Durisol Building Systems, Inc. it was discovered that the wood fiber concrete-insulated concrete forms they produce have fire rating of 4 hours and were resistant to termites despite being made of wood fibers (Durisol Building Systems, Inc. 2006).

Combining fly ash in high volumes with wood fibers for use as a construction material has barely been researched. This is partly because the FA-WF material has been under development at Missouri S&T since a project by Joshi and Myers in 2005. The study performed by Joshi and Myers examined FA-WF for use as a construction material in walls. The study investigated the mechanical properties including strength, ductility, freeze-thaw, and shrinkage. Joshi found that the material provided some benefits such as sound resistance, ductile behavior, thermal resistance, and damping capability. Due to the

materials ductile behavior Joshi recommended that future studies investigate using this material in blast mitigation (Joshi and Myers 2005).

2.3 FA-WF LAYER FOR BLAST MITIGATION

Based on the recommendation by Joshi and Myers three later studies examined the blast resistance of FA-WF, including this one. The second phase of a project by Tinsley and Myers was the first to investigate FA-WF's performance during blast events. The test matrices for the two phases of the blast research are recorded in **Tables 2.1 – 2.2**. The tables also outline the materials present in the 1180 x 1180 mm (46.5 x 46.5 in) panels, which all had a 90. mm (3.5 in) base. The bi-layered panels had an additional 50 mm (2 in) high volume FA-WF blast mitigation material (BMM) layer (Tinsley and Myers 2007).

The panels were tested at the University of Missouri-Rolla experimental mine with varying weights of an RDX-based C-4 explosive at varying standoff distances. Two to four blast events were used for each panel and are detailed in **Tables 2.1 – 2.2**. The test set up is illustrated in **Figure 2.2** (Tinsley and Myers 2007).

Table 2.1 – Tinsley's Phase 1 Test Matrix

Panel No.	Event No.	Charge weight (g)	Standoff distance (mm)	Description
Panel 1A	1	454	915	Bi-layered construction with concrete base and top layer of BMM 0.2% reinforcement ratio in concrete and 0.16% in BMM layer [140 mm (5.5 in) thick]
	2	680	610	
	3	907	305	
	4	1360	305	
Panel 2A	1	225	915	High volume fly ash-wood fiber blast mitigation material with reinforcement ratio of 0.2% in each direction [89 mm (3.5 in) thick]
	2	454	915	
	3	680	610	
	4	907	305	
Panel 3A	1	454	915	Normal-weight concrete with addition of 6% wood fibers by weight with 0.2% reinforcement ratio in each direction [89 mm (3.5 in) thick]
	2	680	610	
	3	907	305	
Panel 4A	1	454	910	Normal-weight concrete with 0.5% reinforcement ratio in each direction [89 mm (3.5 in) thick]
	2	1134	305	
	3	1360	152	
Panel 5A	1	454	915	Bi-layered construction with 0.5% reinforced concrete base and top layer BMM [140 mm (5.5 in) thick]
	2	1134	305	
	3	1360	305	
	4	1360	Contact	

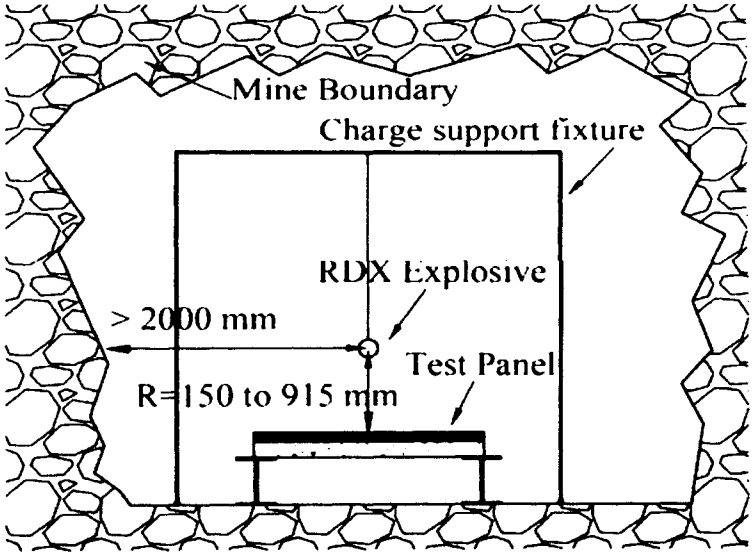

Figure 2.2 – Blast Test Setup (Tinsley and Myers 2007)

Table 2.2 – Tinsley's Phase 2 Test Matrix

Panel No.	Event No.	Charge weight (g)	Standoff distance (mm)	Description
Panel 1B	1	680	610	Bi-layered construction with concrete base and top layer of BMM 0.2% reinforcement ratio in concrete and 0.16% in BMM layer coated with polyurea
	2	907	305	
	3	1360	305	
	4	1360	152	
Panel 2B	1	680	610	High volume fly ash-wood fiber blast mitigation material with reinforcement ratio of 0.2% each direction. Coated with polyurea
	2	907	305	
Panel 3B	1	680	610	Normal-weight concrete with addition of 6% wood fibers by weight with 0.2% reinforcement ratio in each direction. Coated with polyurea
	2	907	305	
	3	1360	152	
Panel 4B	1	680	610	Normal-weight concrete with 0.5% reinforcement ratio in each direction. Coated with polyurea
	2	1134	305	
	3	1360	152	
Panel 5B	1	680	610	FA-C-WF panel and RC panel seperated by 19 mm (0.75 in) air gap. Reinforcement ratio of each Panel was 0.2%
	2	907	305	
	3	1360	305	
	4	1360	152	

Tinsley tested each panel until a failure was noticed. He then compared the panels based on the blast loading each panel absorbed prior to failure and by comparing the damage caused by the common 0.68 kg (1.5 lb) charge at a standoff distance of 610 mm (24 in) shared by all but two panels. From his comparisons he concluded that the FA-WF material was beneficial when used in a bi-layered setup as a sacrificial layer, but that the FA-WF material was not as effective as reinforced concrete when used individually at mitigating blast damage.

Following Tinsley's work, a project conducted by Carey and Myers (2009) examined the use of FA-WF and polyurea in blast barriers. The project investigated six barriers which are described in the test matrix, **Table 2.3**. This project was on larger scale blast testing than Tinsley and Myers (2007) project. In the work done by Carey and Myers (2009) the barrier size was 3.3 x 0.61 x 1.07 m (130 x 24 x 42 in). The testing for this project was done at the Air Force Research Laboratory (AFRL) at Tyndall Air Force Base in Florida.

Table 2.3 – Carey's Barrier Test Matrix

Barrier No.	Description
Barrier #1	Standard reinforced concrete barrier (external coating system: polyurea and chopped glass fibers
Barrier #2	Standard Reinforced concrete barrier (external coating system: polyurea)
Barrier #3	Hybrid construction, concrete barrier with a layer of WF-FA (external coating system: polyurea)
Barrier #4	Hybrid construction, concrete barrier with a layer of WF-FA (external coating system: polyurea and chopped glass fibers)
Barrier #5	Hybrid construction, concrete barrier with a layer of WF-FA
Barrier #6	Standard reinforced concrete barrier

The tested panel was placed in a chain of support barriers and an undisclosed charge was placed on the front face of the panel. A standard video was taken from the same side of the barrier as the where the charge was placed while a high speed video was taken from the other side of the barrier. A pressure gauge was placed 15 m from the center; the entire setup illustrated in **Figure 2.3**. The visual surface area damage, mass loss and debris scatter were all recorded to compare the barrier systems.

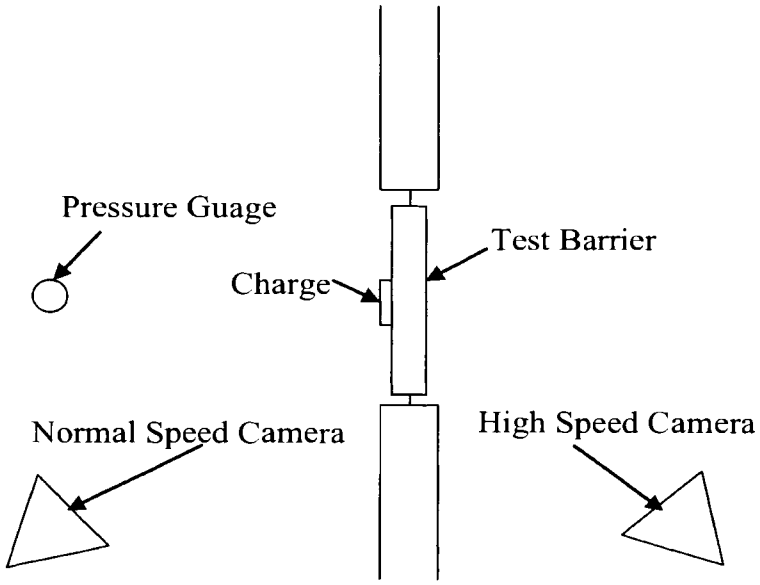

Figure 2.3 – Blast Test Setup

Carey concluded from her results that the polyurea significantly reduced the damage in all the categories investigated. Another finding was that the FA-WF's only positive benefit was a reduced scatter only in the uncoated panels. Overall barrier #2, the standard reinforced concrete barrier with plain polyurea, performed the best considering the three parameters recorded (Carey and Myers 2009).

2.4 DEVELOPMENT OF A DISCRETE FIBER REINFORCED POLYUREA

Polyurea is formed by the chemical reaction between an isocyanate and an amine-terminated resin blend (Polyurea Development Association 2010). An isocyanate is a chain of nitrogen, carbon and oxygen with an overall negative one imbalance of electrons (-NCO) (Occupational Safety & Health Administration 2008). An amine is a basic

organic compound containing Nitrogen (HyperPhysics 2010). Polyurea has been investigated since the 1990s for its use in design and retrofit of blast resistant elements. Much of the research done on polyurea was funded by the military and thus not readily available in the public domain. Some military vehicles use polyurea coatings because it provides a higher level of protection per weight than rolled homogeneous armor, which was traditionally used for blast protection. As of 2004, 96 high mobility multipurpose vehicle doors have been retrofitted with polyurea. The ease of application, ability to absorb some of the blast, and ability to contain fragmentation has made the polyurea an ideal product for use in military vehicles (Applied Research Associates, Inc. 2004).

Research done by Davidson et al in 2004 investigated using polyurea on masonry walls. Davidson built dual wall sections at the AFRL at TAFB and then applied the polyurea to one wall. He then detonated a charge outside the structure and then analyzed the results. **Figure 2.4** illustrates post-event behavior after one of the events. The section of the wall on the right side in **Figure 2.4** was coated with polyurea, while the wall section on the left that was reduced to rubble was not coated with polyurea. Davidson found that the polyurea was very effective at strengthening a masonry wall against blast (Davidson, et al. 2004).

Figure 2.4 – External Test 1 Results. (Davidson, et al. 2004)

LINE-X the same company that provided material for this investigation currently uses a product called PAXCON 3350 in U.S. military buildings (LINE-X Protective Coatings Corp. 2004). Some of the structures that have been coated with PAXCON 3350 for blast protection are the U.S. Pentagon, the Federal Courthouse in New York and the Washington Naval Base. The material was also used in over 50,000 armor plates worn by soldiers in Iraq and Afghanistan, and has even saved at least one life (PAXCON 2011).

Polyurea has been proven as an effective blast resistant material. Researchers at Missouri S&T have been investigating combining polyurea in a discrete fashion with e-glass fiber to create an easily applied, multi-hazard, retrofit material. The research undertaken by Carey and Myers (2009) was the first to investigate this e-glass DFRP material. The results from this research showed no significant impact in reducing fragmentation, with low fiber ratios from adding the e-glass fibers (Carey and Myers 2009). These results lead to the effort to develop and characterize various e-glass DFRP

systems that may perform better in blast resistance and act as a possible strengthening agent. In a subsequent project by Carey and Myers (2010) five types of polyurea were examined under direct tension testing. This study also investigated the addition of discrete E-glass fibers, which included determining an optimal fiber length and fiber ratio. The test matrix for this study is reported in **Table 2.4**. The length of glass fiber was controlled by setting the spacing of the blades in the chop gun. The percentage of fiber was regulated by the fiber feed rate (i.e. number of turns applied to a dial on the spray gun).

Table 2.4 – Test Matrix

Material	Fiber Length, mm (in)	Fiber Chopping Speed (# of dial turns)
Polyurea A	6 (0.25)	3, 3.5, 3.75, 4, 5
Polyurea A	13 (0.5)	3, 3.5, 3.75, 4
Polyurea A	38 (1.5)	3, 3.5, 3.75
Polyurea B	6 (0.25)	3, 4, 5, 6, 7, 9
Polyurea C	6 (0.25)	3, 4, 5, 6, 7, 8
Polyurea D	6 (0.25)	3, 4, 5, 6, 7, 8
Polyurea E	6 (0.25)	3, 4, 5, 6, 7, 8

The first set of specimens created and tested were the three sets of different fiber length polyurea a specimens. These were tested and analyzed prior to making any other specimens to determine optimal fiber length. From this testing series it was determined that a fiber length of 6.4 mm (0.25 in) was optimal for the E-glass fiber used. The longer fiber length increased the ability for fiber rupture, but dramatically decreased the ultimate strain at failure. Subsequent studies focused on the integration of 6.4 mm (0.25 in) fibers. The tensile strength and fiber ratio were then found for each specimen. From this data

Carey concluded that Polyurea B and E should be further investigated. **Figures 2.5 – 2.6** are graphs of the stress versus strain for Polyurea B and E respectively. Polyurea B was chosen because of its higher yield strength while Polyurea E was chosen because of its moderate yield strength and durability (Carey and Myers 2010).

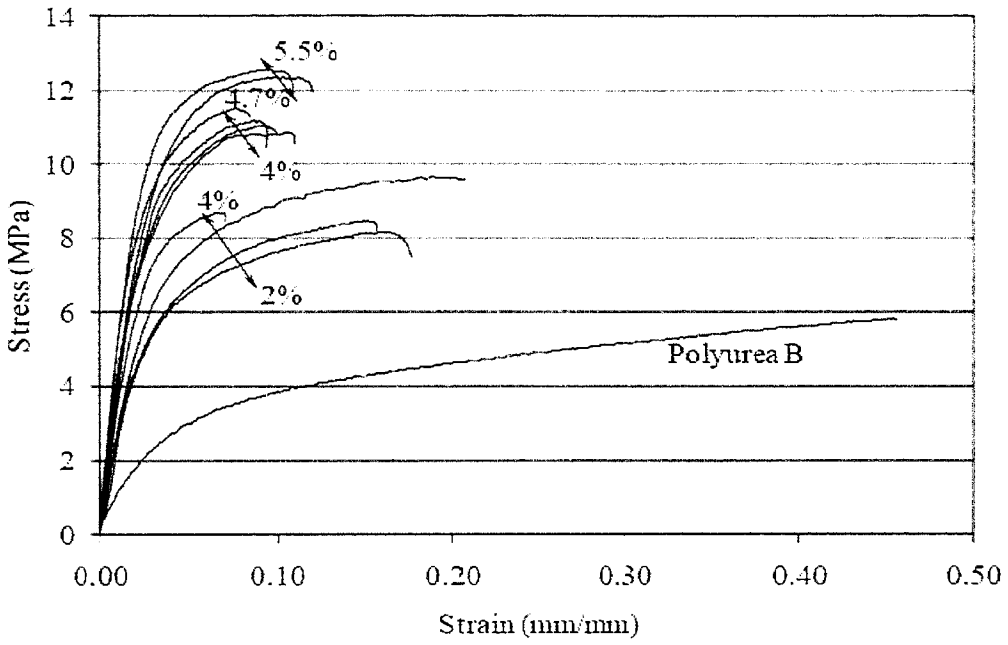

Unit conversion: 1 MPa=0.14504 ksi

Figure 2.5 – Stress-strain behavior of fiber-reinforced polyurea B systems

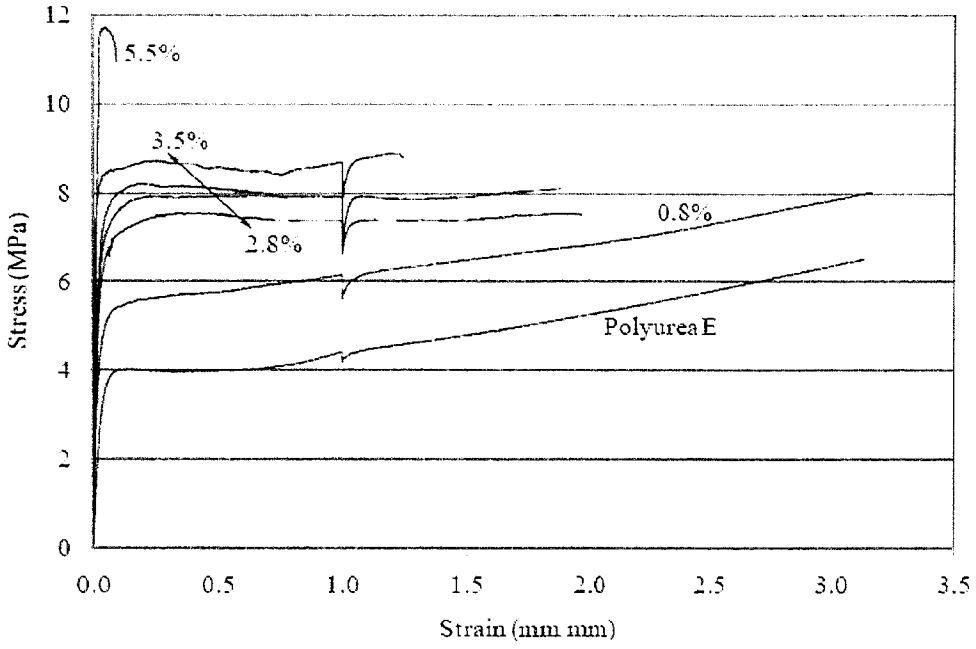

Unit conversion: 1 MPa=0.14504 ksi

Figure 2.6 – Stress-strain behavior of fiber-reinforced polyurea E systems

The next phase of research on e-glass DFRP was undertaken by Greene and Myers (2010). Polyurea B and E from Carey's work were used in Greene's study and were termed as Polyurea A and B, respectively (Polyurea B now is Polyurea A, and Polyurea E now is Polyurea B). Greene investigated the use of e-glass DFRP as a strengthening agent for columns and beams. She used three different strength concrete mixes to create cylinders that were then sprayed with the polyurea to investigate if the polyurea provides any strength gains from confinement. The results indicated that the both polyurea A & = had minimal impact on strength and modulus of elasticity.

Another part of her research was on DFRP strengthened beams, for this phase full scale beams were fabricated and tested until failure. Polyurea A did not provide any strength gains for the beams, but the polyurea B systems provided additional flexural

strength, increased residual deflections, and improved shear strength. This disparity between the two polyurea materials was attributed to the set times. Polyurea A has a 3-6 second gel time while polyurea B has an 11-13 second gel time. This additional gel time allowed the fibers to more easily mix or assimilate into the polyurea (Greene and Myers 2010). The results from Greene's study indicate that the e-glass DFRP provided additional flexural strength which could be beneficial in multi-hazard mitigation.

3. EXPERIMENTAL PROGRAM

3.1 SPECIMEN FABRICATION AND TEST SETUP

A total of thirteen panels were fabricated in the Missouri S&T Structural Engineering High Bay Research Laboratory (SERL). **Table 3.1** shows the test matrix used for this experiment. All the panels consisted of a combination of some of the following: steel fiber reinforced concrete (SFRC), plain reinforced concrete (RC), high-volume fly ash-wood fiber (FA-WF), and a polyurea compound. These composites were investigated based on previous work by Tinsley and Myers (2007) and Carey and Myers (2009). The SFRC acted as the base material in most of the panels and the FA-WF material was designed to perform as a sacrificial layer during the blast. The polyurea layer was designed to primarily contain any spalling or fragmentation.

Table 3.1 – Experimental Test Matrix

	Panel Name					
			Polyurea			
FA-WF Layer	Control		XS100	Fiber XS100	XS430	Fiber XS430
None	SFRC-3.5	SFRC-5.5				
	1-RC	2-RC				
50 mm	1-H	2-H	H-A	H-A/F	H-B	H-B/F
50 mm + Foam Gap	H-FG			H-FG-A/F		H-FG-B/F

All the panels were 1180 x 1180 mm (46.5 x 46.5 in) with varying depths, between 90. mm (3.5 in) and 220 mm (8.5 in). Drawing of the profiles of the panels can be found in **Appendix A**. The nomenclature for the panel names in **Table 3.1** were based

on the materials that comprised the panels. For the SFRC and RC panels the ID notations indicate the only material that comprised the panel. For panels with a number prior to the name it indicates that there were more than one panel of the same configuration and the numbering is just differentiating the panels. Panels with a number after indicate that the depth in inches of that panel. The hybrid panels consisting of a base SFRC layer and FA-WF layer use the designation of H. The panels incorporating a foam-gap use H-FG to describe a hybrid panel (H) with a foam-gap (FG). The polyurea's appellation of A for XS100 and B for XS430 is consistent with the study by Greene and Myers (2010). The presence of discrete glass fibers in the polyurea layer is indicated by adding a /F to the polyurea type. For example, the H-FG-A/F panel consists of a steel fiber reinforced concrete base with a layer of high-volume fly ash-wood fiber separated by a foam-gap and coated with the XS100 polyurea combined with discrete glass fibers.

3.1.1 Materials. The following materials were used in the construction of the test panels: Class C fly ash, type I Portland cement, wood fibers, polyurea, E-glass fibers, steel fibers, mild steel reinforcement, coarse aggregate and fine aggregate.

The ASTM Class C fly ash (ASTM C618-08a 2008) was donated by Labadie Power Plant of St. Louis, Missouri. The fly ash was a key ingredient in the FA-WF material. The chemical composition of the fly ash is reported in **Table 3.2** (Ameren Corporation 2011). **Figure 3.1a** displays the fly ash used in this project.

Table 3.2 – Chemical Compositions of Class C Fly Ash and Type I Portland Cement

Component	Labadie Class C Fly Ash (%)	Monarch Type I Portland Cement (%)
Silicon Dioxide (SiO_2)	33.46	21.80
Aluminum Oxide (Al_2O_3)	19.53	4.56
Ferric Oxide (Fe_2O_3)	6.28	3.46
Calcium Oxide (CaO)	26.28	63.28
Magnesium Oxide (MgO)	5.54	2.04
Sulfur Trioxide (SO_3)	2.40	2.65
Loss of Ignition	0.34	0.53
Mositure	0.15	-
Potassium Oxide (K_2O)	0.45	0.55
Phosphorus Pentoxide (P_2O_5)	1.30	-
Titanium Dioxide (TiO_2)	1.48	-
Sodium Oxide (Na_2O)	1.73	0.18
Manganic Oxide (Mn_2O_3)	0.04	-
Zinc Oxide (ZnO)	0.02	-
Chromium Oxide (CrO)	0.01	-
Barium Oxide (BaO)	0.84	-
Strontium Oxide (SrO)	0.40	-
Insoluble Residue	-	0.26

Monarch type I Portland cement (ASTM C150/C150M-11 2011) was purchased from a local contractor supplier. Portland cement was a key ingredient in the sacrificial FA-WF layer. The chemical composition for the cement (The Monarch Cement Company 2011) is reported in **Table 3.2** along with the fly ash. **Figure 3.1b** displays the cement used in this project.

(a) Class C Fly Ash (b) Type I Portland Cement

Figure 3.1 – Cementitious Materials

The milled oak wood fibers were donated by Encore Building Solutions of St. Louis (EBS) and are milled from recycled wood pallets. The typical size of the wood fibers was 6.4 to 13 mm (0.25 to 0.50 in) with some very fine particles but few particles longer than 13 mm (0.50 in). **Table 3.3** presents the mechanical properties of the milled oak wood fibers and **Figure 3.2** displays a sample of the wood fibers.

Table 3.3 – Mechanical Properties of Oak

Mechanical Properties	Green	Air Dried
Weight (kg/m^3)	1009	753
Modulus of Rupture (MPa)	55.85	95.84
Modulus of Elasticity (MPa)	8274	11170
Maximum crushing strength parallel to grain (MPa)	24.3	48.5
Compression perpendicular to grains (MPa)	5.86	9.72
Maximum shearing strength parallel to grain (MPa)	8.76	13.03

Unit conversion 1.00 kg/m^3=0.0624 lb/ft^3, 1.00 MPa=145 psi

Figure 3.2 – Wood Fibers

The polyurea was purchased and applied by LINE-X of Columbia, MO. The polyurea is typically used as a commercial grade spray-on bed liner for vehicles and contain zero volatile organic compounds (VOC). Two different polyureas were used: XS-100 (Polyurea A) and XS-430 (Polyurea B). The XS-100 is LINE-X's base material is typically used as a bed liner and is rapid setting. The XS-430 is a higher grade, slower set material. Material properties for the LINE-X products used are reported in **Table 3.4** (Greene and Myers 2010). **Figure 3.3a** displays a plain polyurea B coupon specimen.

Table 3.4 – Polyurea Material Properties

	Polyurea Designation	
Mechanical Properties	A	B
Density (kg/m^3)	928	878
Elongation (%)-ASTM D412-06a	91	445
Tensile Strength (Mpa)-ASTM D412-06a	14.8	19.3
Gel Time (sec)	3-6	11-13
Tack Free Time (sec)	6-9	78-85

Unit Conversions: 1.00 kg/m^3=0.0624 lb/ft^3, 1.00 MPa=145 psi

The E-glass fiber was procured from Owens Corning. This material was combined with the polyurea to create the DFRP by using a chopper attachment on the polyurea spray gun. The chopper attachment runs on compressed air and is similar to what is found in fiberglass installation. The speed of the chopper was adjustable as was the length of the fibers. Based on the recommendations of earlier work performed at Missouri S&T 6.4 mm (0.25 in) fibers were used (Carey and Myers 2010). The mechanical properties of the e-glass presented in **Table 3.5** were provided by the manufacturer. An image from the Owens Corning's website shows what the chopped fibers looked like after processing (**Figure 3.3b**). An e-glass DFRP B burn off specimen is illustrated in **Figure 3.3c**.

Table 3.5 – Glass Fiber Material Properties

Mechanical Properties	Dry Range
Tensile Strength (Mpa)-ASTM D638-10	59-98
Tensile Modulus (Mpa)-ASTM D638-10	7542-14893
Flexural Strength (Mpa)-ASTM D790-10	166-307
Flexural Modulus (Mpa)-ASTM D790-10	6939-12065

Unit Conversion: 1.00 MPa=145 psi

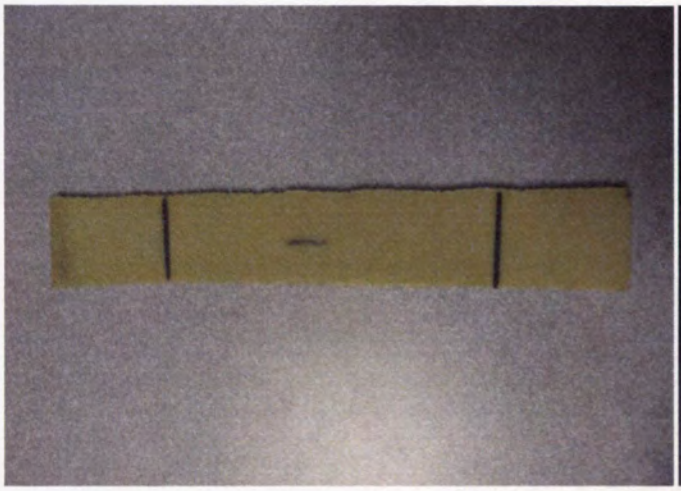

(a) Plain Polyurea B

(b) Chopped Glass Fibers (Owens Corning 2012)

(c) Polyurea B with Discrete E-glass Fibers

Figure 3.3 – Polyurea and E-glass

The steel fiber was procured from Propex. Their product Novocon 1050HE was recommended by the manufacturer for blast resistance. This material was used in the construction of the base for most of the panels. The steel fiber has also been used in a concurrent project by Carey and Myers. Steel fibers have been proven to improve the flexural performance and toughness of concrete, so based on this and the good results from Carey's work it was selected for this phase of study. **Figure 3.4** shows a sample of

the steel fibers while **Table 3.6** displays the fiber properties provided by the manufacturer (Propex Concrete Systems 2007).

Table 3.6 – Steel Fiber Properties

Property	1050HE
Fiber Length (mm)	50
Diameter (mm)	1
Tensile Strength (Mpa)	1050

Unit Conversions: 1.00 mm=0.0394 in 1.00 MPa=145 psi

Figure 3.4 – Propex Novocon 1050H Steel Fiber

Steel reinforcement was purchased from Nu-Way Construction in Jefferson City, MO. ASTM number 3 bars (ASTM A615/A615M-09b 2009) were used as longitudinal reinforcement and 6.0 mm (0.25 in) cold rolled round bars were used for stirrups in the bi-layered systems. The 10. mm (0.38 in) rebar was tested according to ASTM

A370/A370M-11a for quality assurance using the Tinius Olsen to have an actual yield strength of 441.2 MPa (64.0 ksi) at a 0.5 percent offset and an ultimate strength of 712.5 MPa (103.3 ksi).

The concrete was supplied by Rolla Ready Mix, in Rolla, MO. A 25 mm (1.0 in) nominal maximum size aggregate, 27.5 MPa (4000 psi) mix was used in combination with the steel fibers to construct all the bases of the panels. This basic mix design was consistent with concurrent project by Carey and Myers and also with the project performed by Tinsley and Myers in 2007 to provide comparable bench marking.

3.1.2 Test Specimen Fabrication. The panels were fabricated using oiled wooden forms. Two forms from a previous project, Tinsley and Myers 2007, along with two additional forms, constructed for this project were used to fabricate the panels. The new forms had removable side walls to allow for changeable depths, which was important for fabrication of the hybrid panels. The adjustable walls allowed the forms to be flush with the concrete layer and then could be raised for the placing of the FA-WF layer on top. The two forms from the existing project had permanently attached side walls with one having a depth of 90. mm (3.5 in) and the other having a depth of 140 mm (5.5 in). All the forms were constructed to fabricate an 1180 x 1180 mm (46.5 x 46.5 in) panels and either had adjustable depth or was fixed at 90. mm (3.5 in) or 140 mm (5.5 in). Annotated drawings of panel dimensions are displayed in **Appendix A**. A few days prior to the placement of the concrete the forms were cleaned and adjusted if necessary. For the placement of the concrete layer all the forms were adjusted or marked for a 90. mm (3.5 in) depth. On the day before concrete placement the forms were coated in bar chain oil

and set out in the Missouri S&T SERL on top of a large amount of plastic sheeting. On the day of the placement bar chain oil was again amply applied to the forms prior to concrete placement to allow the panels to be lifted out of the forms. The first coat of oil allows the wood to absorb the oil so that the second coat will not be absorbed and thus allow for ease in stripping the forms.

All the panels also had the same longitudinal reinforcing steel layout, which is illustrated in **Figure 3.5** and an annotated drawing of the rebar layout is displayed in **Appendix A**. Seven number 3 ASTM grade 60 mild steel bars extended in both directions providing a reinforcement ratio of 0.5% for the typical depth panels. The reinforcement ratio and layout was based on the results and recommendations of Tinsley and Myers (2007) study. The SFRC-5.5 had the same reinforcement layout which provided a reinforcement ratio of 0.32%. The clear cover from the sides and the extreme tension fiber was 25 mm (1.0 in) based on the nominal maximum aggregate size. To create the clear cover steel running chairs were used. Panels that included the FA-WF layer also had two 6.4 mm (0.25 in) cold rolled round bars used as stirrups and to connect the two layers. The stirrups were cut into 3 m (10 ft) lengths and then bent. All the reinforcement was delivered in 6 m (20 ft) lengths and the longitudinal reinforcement was cut to lengths of around 1130 mm (44.5 in). They were then placed into a tying table that was constructed for this project and is illustrated in **Figure 3.6**. The steel was then tied with tie wire and a manual twister tool. This was all done days before a scheduled concrete placement. Then on the day of the placement, chairs and stirrups were tied to the cages and then the assembly was set into the oiled forms.

Figure 3.5 – Reinforcing Steel Layout in Forms

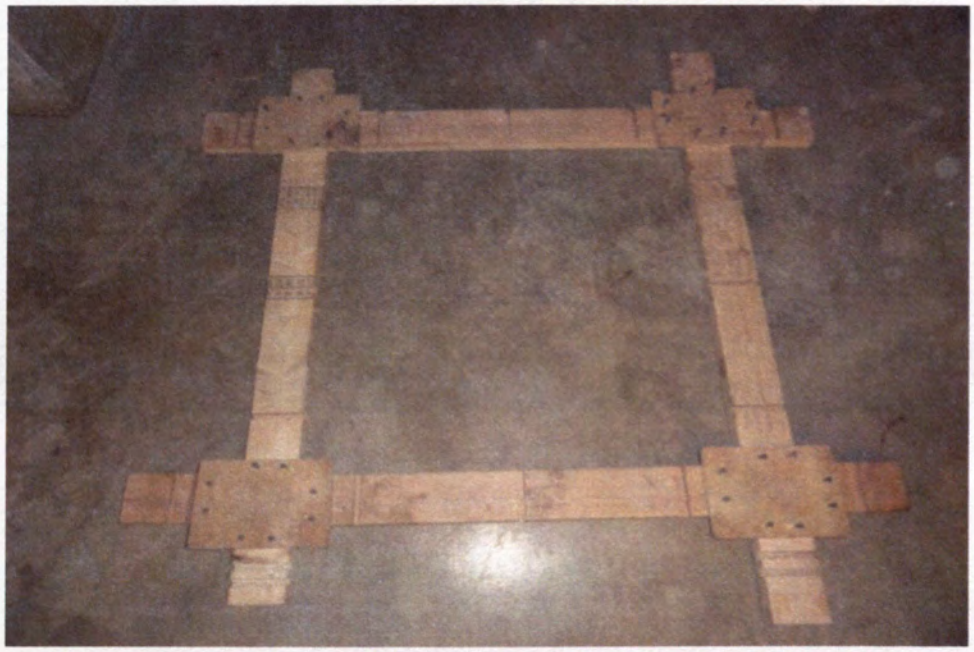

Figure 3.6 – Tying Table

The steel fiber reinforced concrete base layer (i.e. structural concrete) was placed first. The panels were placed in the Missouri S&T SERL. A concrete rotary truck was

ordered for the placement of concrete. Once the truck arrived, the slump was measured and water was added until the slump satisfied the target slump of 130 mm (5.0 in). The steel was then added to the truck at a ratio of 65 kg per every cubic meter (110 lb per 1 yd^3) of concrete, this ratio was selected based upon previous work and recommendations by the manufacturer. The steel fiber was added gradually to the truck and after all the fiber was added, the drum was spun at high speed for five minutes. The concrete was then poured from the truck to the panels to the desired depth, typically 90. mm (3.5 in), and then vibrated and leveled with a screed. A wood board, screed, was slowly pushed across the concrete until a level surface was obtained. For the hybrid panels the concrete was not smooth finished, but instead the finish was just enough to get a fairly even depth throughout while remaining rough on the surface. A trowel was used to finish the panels and after finishing, hooks made from number 3 ASTM bars and the 6.4 mm (0.25 in) stirrups were placed by hand into the panel. **Figure 3.7** illustrates the SFRC placing process. The panels were allowed to cure for at least two days before they were stripped or the sacrificial FA-WF layers were added.

(a) Pouring of SFRC

(b) Vibrating the Concrete

(c) Leveling with Screed

(d) Placing the Stirrups

Figure 3.7 – Concrete Placing

Two different configurations of FA-WF were investigated: a 50 mm (2 in) layer fabricated on top of the structural concrete layer and a 50 mm (2 in) sacrificial FA-WF layer with a 76 mm (3.0 in) gap, referred to as a foam-gap, was filled with Styrofoam insulated sheeting separating the two layers. The foam-gap represents a foam-gap and was used for ease of construction and with the expectation that the Styrofoam insulated sheeting may absorb some of the blast and limit the damage in the SFRC layer. For the

panels with the FA-WF layer placed directly on the structural concrete layer the total depth was 140 mm (5.5 in) and the panels with the foam-gap have a total depth of 220 mm (8.5 in).

The high-volume fly ash-wood fiber layer was batched in a conventional rotary drum mixer in the Missouri S&T Construction Material's Laboratory. **Table 3.7** shows the mix proportions for the FA-WF layer. The units in **Table 3.7** refer to the mass or weight by final volume. For example kg/m^3 means however many kilograms of that material dictated in the table per cubic meter of concrete. Due to the 0.17 m^3 (6 ft^3) capacity of the mixer, the FA-WF layer for one panel was done at a time. The batching process started with adding the majority of the water and then adding all of the wood fiber. The drum was spun slowly at this point and then the fly ash was added gradually ensuring no clumping was occurring. After all the fly ash was added the Portland cement was added gradually. The minimal level of water that was initially withheld was added at the end to improve the mixing process. The mix was watched carefully to ensure no balling occurred. If there was balling the balls were broken up by hand. The drum was watched and spun for about 5 minutes after all the materials were added to ensure consolidation.

Table 3.7 – FA-WF Mix Design

	kgf/m^3	lb/yd^3
Class C fly ash	610.5	1043.955
Portland Cement	367.5	628.425
Wood Fibers	150	256.5
Water	372	636.12

Units are in weight per volume of expected batch

The drum was then emptied into a wheelbarrow and wheeled into the Missouri S&T SERL. The wheelbarrow was then dumped out on top of the panel. The FA-WF was then spread evenly using a trowel. The mixture was not vibrated due to its low workability; instead the sides of the forms were tapped using a rubber mallet. The panel was then smooth-finished with the trowel and then allowed to cure for at least one day before the forms were stripped.

The panels were given at least two weeks to cure under laboratory conditions. After this amount of time the panels were transported to LINE-X in Columbia, MO to coat the panels with the polyurea systems. Four different configurations of polyurea were used: Plain polyurea A (A), polyurea A with glass fibers (A/F), plain polyurea B (B), and polyurea B with glass fibers (B/F). Prior to spraying the panels, the surface was ground using a hand grinder or sand blaster. The grinding created a rough surface for the polyurea to adhere to. The next step was to apply a primer to the panels, which required at least 8 hours but no more than 12 hours to set. The primer was applied to enhance the bond performance of the applied coating systems. After allowing the primer to set the polyurea was applied to the panels until a depth of 6.4 mm (0.25 in) was achieved. A trained professional handled coating the panels; **Figure 3.8** illustrates the polyurea application. The glass fiber was added to the polyurea by attaching a Glasscraft chopper to the polyurea spray gun. The chopping mechanism operated on compressed air and blew the chopped pieces of fiber into the stream of polyurea.

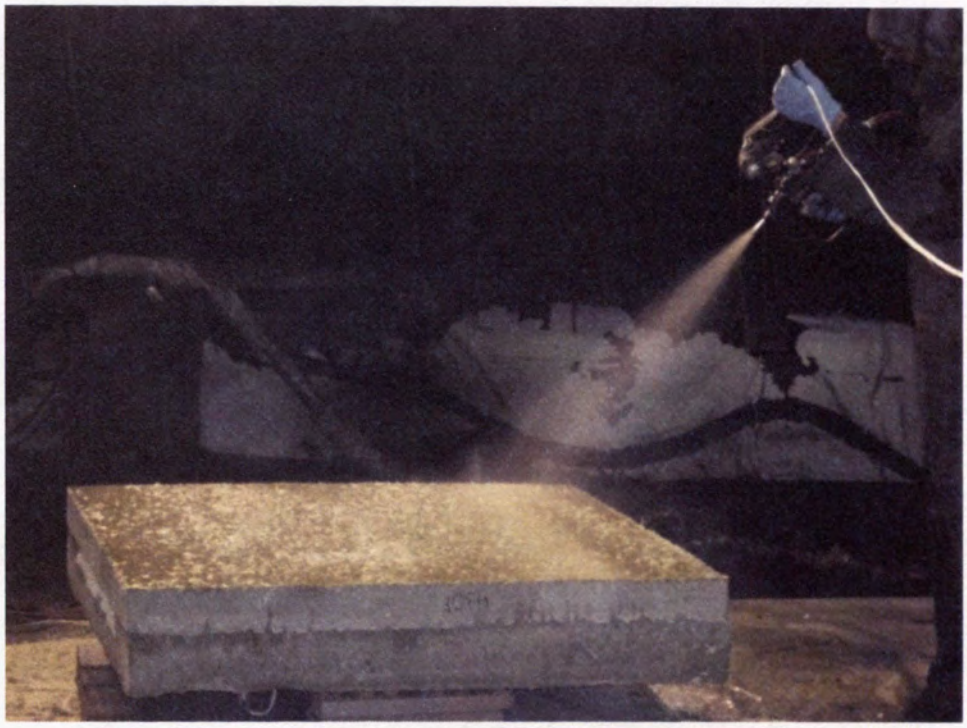

Figure 3.8 – E-Glass DFRP B Application

3.1.3 Blast Test Setup. For the blast testing, the Missouri S&T Experimental Mine was utilized. On their site they have an explosives testing mine, named the Wombat, which was used for this blast testing. The panels were placed in an alcove of the Wombat mine on top of two steel I-beams for support as illustrated in **Figures 3.9a – 3.9b**. Annotated drawings of the test setups are displayed in **Appendix A**. The FA-WF was facing upward and the polyurea layer, when present, was facing downward The typical setup for the foam-gap panels as shown in **Figure 3.9b**, with the supports for the foam-gap running along parallel to the steel supports, was used because this arrangement best represented a panel with a foam-gap that may be found in practice.

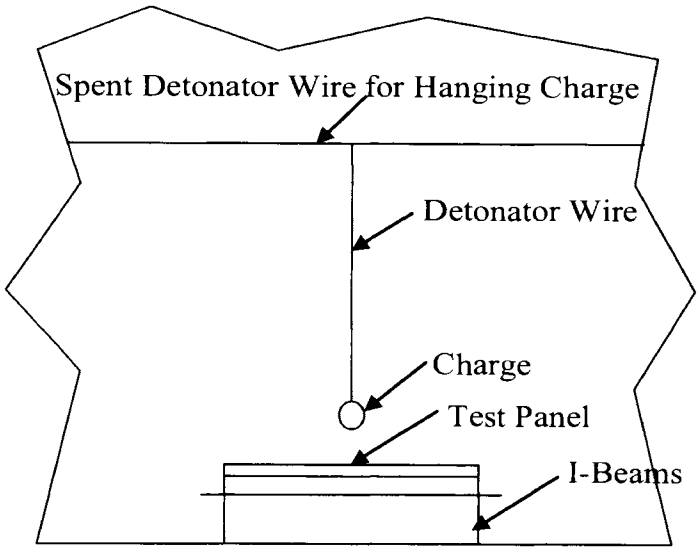

(a) Typical Setup for Hybrid Panels

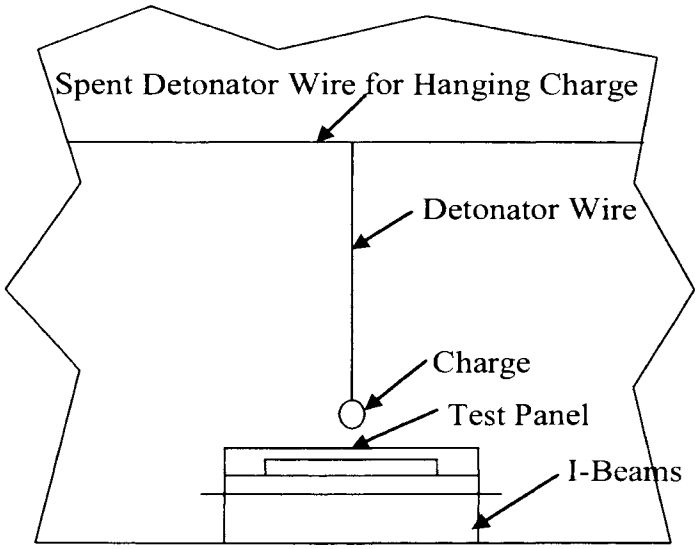

(b) Typical Set up for Hybrid Panels with a Foam-Gap

Figure 3.9 – Typical Blast Setups

The blast testing consisted of an initial blast at a standoff distance of 310 mm (12 in) and then a second blast at a standoff of 150 mm (6.0 in). The first blast event had a

1.4 kg (3.0 lb) C4 charge at a 310 mm (12 in) standoff to remain consistent with the concurrent project by Carey and Myers (2012). Ideally one blast event would have been used; however, two blast events were selected because the first blast event resulted in minimal damage for the majority of the panels. The concern with using two blast events is that the second event tends to build upon the damage from the previous event making it difficult to distinguish the damage for each event and it is difficult to accurately determine what stress level caused the damage level exhibited; however, it was more important to this study that it remain consistent with the concurrent project by Carey and Myers (2012) so comparisons could easily be drawn between both studies. Therefore, a second event was used to achieve more significant and measurable damage.

The estimated peak overpressures were calculated for both events using **Eq. 2.1 and 2.3**. The calculated peak overpressure was 42 MPa (6100 psi) for the 310 mm (12 in) standoff and 340 MPa (49000 psi) for the 150 mm (6.0 in) standoff.

ConWEP version 2.1.0.8 was used to model the blast pressures on the panels given the standoff distances, charge type and weight, and the surface geometry of the panels. ConWEP was not used to model the expected results of the panels but just the surface pressures exhibited on the panels. ConWEP output three dimensional graphs of the surface pressures, which are illustrated in **Appendix B**. ConWEP, calculated the predicted peak pressures to be 108 MPa (15700 psi) for the 310 mm (12 in) event and 280 MPa (41000 psi) for the 150 mm (6.0 in) event. ConWEP also predicts the pressure and impulse time histories which are illustrated in **Figures 3.10 – 3.11** for the 310 mm (12 in) and 150 mm (6.0 in) events, respectively.

The values and graph produced by ConWEP were considerably different than the values and graph calculated with the equations presented earlier. The output from ConWEP is considered a more accurate method of approximating blast pressures and should be used in future studies when drawing comparisons.

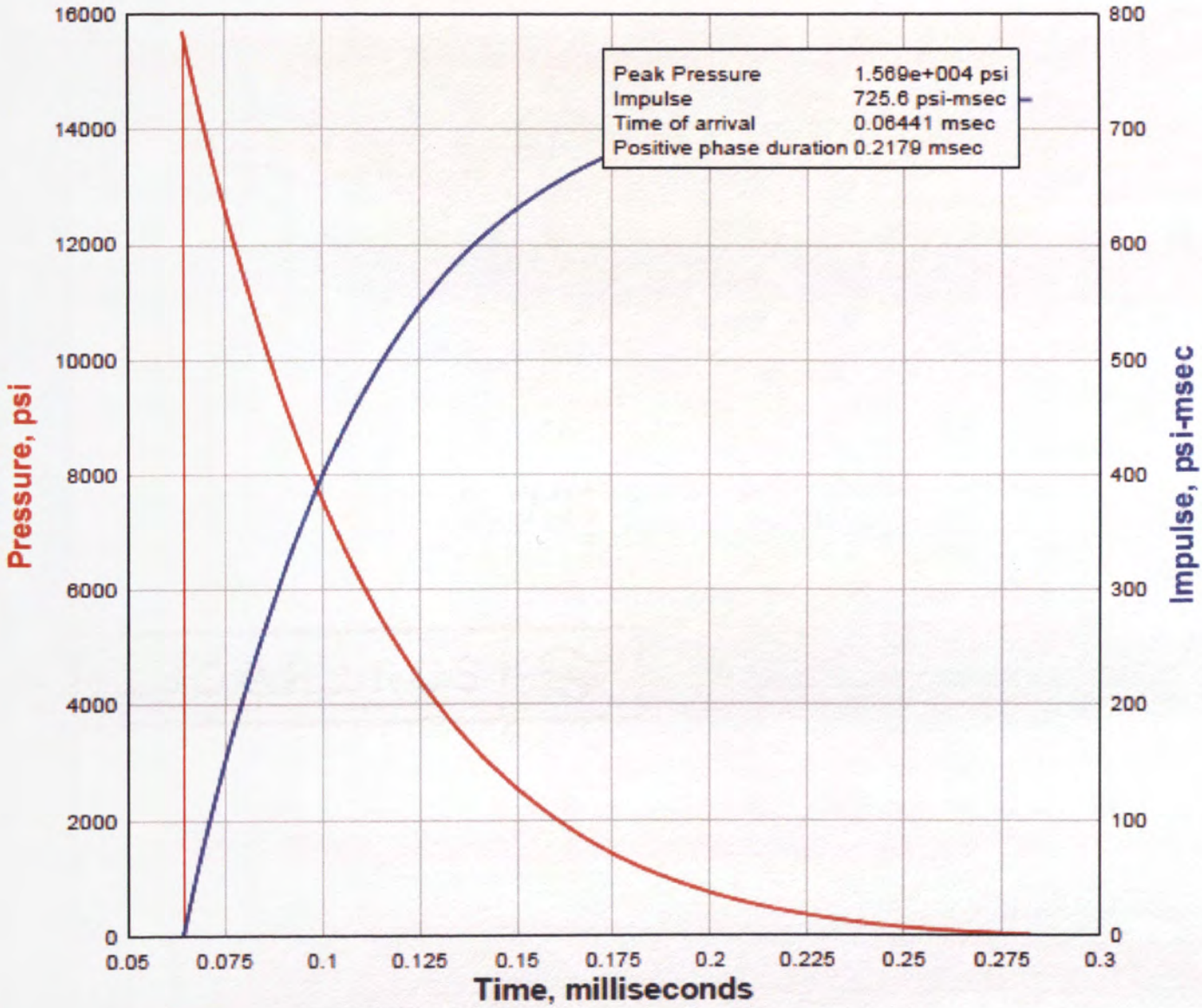

Figure 3.10 – ConWEP Pressure and Impulse Time Histories, 310 mm Standoff

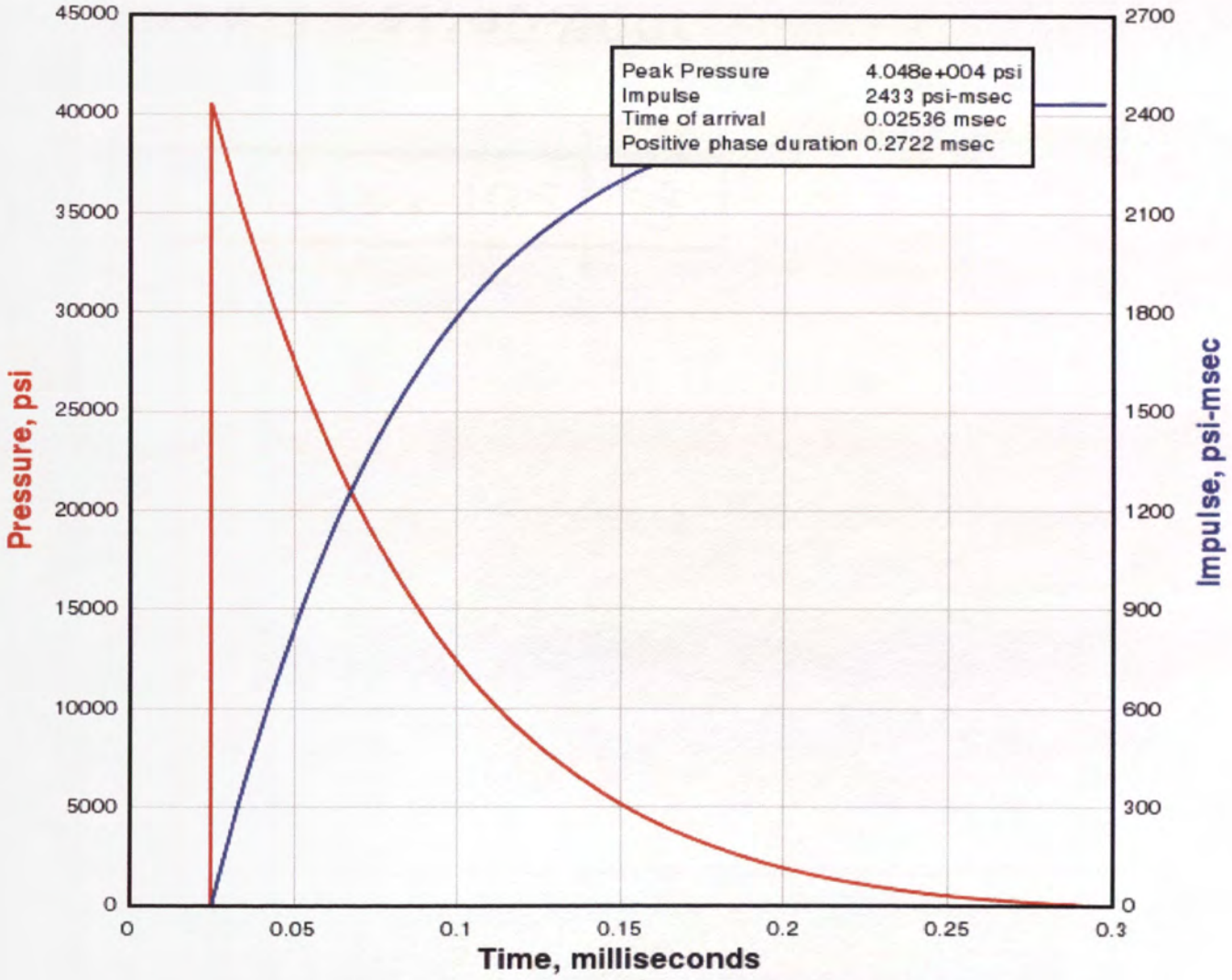

Figure 3.11 – ConWEP Pressure and Impulse Time Histories, 150 mm Standoff

The experimental results in full scale blast testing are often subjective as it is often difficult to get quantitative results from blast testing. This difficulty is due to the damage a full scale blast event does to the test specimens, making using instrumentation costly and unreliable. This was also the case in this study; therefore, numerous photographs were taken prior to the first blast event, after the first blast event, and after the second blast event. These photographs were examined then conclusions were drawn from comparisons. For quantitative data, residual deflections were measured using a

straight edge laid across the panel to represent the original surface of the panel so the gap the straight edge and panel formed represented the residual deflection. A ruler was then used to measure the residual deflections or gap. This process is illustrated in **Figure 3.12.** The residual deflections were taken at the center of the panel and front and back edges of the panel. The residual deflections were taken prior to and after blasting. This proved somewhat difficult with the sacrificial FA-WF layer since it would occasionally break off during the blast event.

Figure 3.12 – Measuring Residual Deflections

Support for the blast testing was provided by personnel from the RMERC at Missouri S&T. The explosive used was 1.4 kg (3.0 lb) of C4 with a lead azide primary to aid detonation for both blast events. The first blast was set up using copper MasterDet wires that hung down from the ceiling until a standoff distance of 310 mm (12 in) was

measured from the center of the panel. The standoff distances were measured from the surface of the panel to the center of the charge using a ruler. The MasterDet wires were then connected to a spool of longer detonator wires that exited the Wombat mine and lead into a blasting machine. The blast was then detonated after allowing everyone to reach cover. After the blast 30 minutes to an hour was given during mine ventilation to allow any toxic chemicals that follow the blast to exit the Wombat mine. After the all clear was given images and residual deflections were taken inside the Wombat mine. After documentation, the panel was readjusted on the two I-beams and the second blast event was set up in the same fashion with the standoff distance changed to 150 mm (6.0 in). After the second blast event the panel was removed from the Wombat mine and additional images of the underside of the panels were documented. The tested panels were then set aside to be disposed of later. This process was repeated for each panel tested.

3.2 MECHANICAL PROPERTIES

Material properties are of great importance. Material properties allow for relating the results of this experiment to future work. They were also important because not all the panels could be cast at the same time so material properties were used to correlate the results from panels cast at different times. The material properties examined in this experiment for the concrete and FA-WF include compressive strength, modulus of rupture, modulus of elasticity, and material density. For the polyurea material the important properties were the tensile strength and the fiber ratio.

3.2.1 Compressive Strength. The compressive strength was determined using 100 x 200 mm (4 x 8 in) cylinders, tested at 7, 14, and 28 days and on the test date. The cylinders were prepared in accordance with ASTM C192/C192M-07. The only deviation with the ASTM was the use of plastic single use molds for more than one use (ASTM C470/C470M-09 2009). To allow the plastic molds to be used multiple times the inside was lightly coated with bar chain oil and a small hole was punctured in the bottom so the cylinder could be extracted with pressurized air. The cylinders were made in two lifts with 25 rods and 25 exterior taps using a 6.4 mm (0.25 in) diameter tamping rod then finished with a trowel. **Figure 3.13** illustrates the cylinders being made. The cylinders were prepared in the lab and then removed from the molds after at least 24 hours. They were then cured next to the panels in the laboratory until testing to match panel curing as closely as possible.

Figure 3.13 – Wet Concrete in Cylinder Molds

To ensure parallel surfaces the SFRC cylinders were capped, at least one day prior to testing, using a sulfur Rediron 9000 Capping Compound in accordance to ASTM C617-11. The capping compound was melted in a 7.57 L (8 qt) Ritehete melting pot then ladled into a beveled plate. The cylinder was then immediately placed into the molten sulfur using an alignment device to center the cap. The cylinder was then removed after giving sufficient time to allow the cap to harden.

The FA-WF cylinders were ground using a Marui & Co. concrete specimen end grinder to ensure parallel surfaces. The machine was set up for grinding 100 mm (4 in) cylinders by placing the proper screen in the machine. The machine requires water so the water to machine was turned on and the outflow hose was placed into the open drainage system in the material's lab. The machine has time and speed inputs that are set to grind the cylinder till you have a flush, fully ground cylinder while also limiting the damage to the grinder. To prevent damage to the grinder, the speed should correlate with the expected strength, the stronger the cylinder the slower the speed. The time input is based on the speed and amount of cylinder that must be ground.

A set of three cylinders were tested in accordance to ASTM C39/C39M-11 at each test date. Prior to testing the diameter of the top and bottom of the cylinder were measured. Once the cylinders were measured the Forney LC-4 was set up for the cylinders by adding steel plates to the bottom platen, to avoid reaching the maximum platen height. The cylinders were then placed into the Forney and wrapped with a cloth for safety. The bottom platen moved and was controlled with a lever switch and throttle to control the loading rate. Initially the lever is set to full advance to quickly raise the bottom until a small load registered on the machine. The full advance can quickly

overload the cylinder causing a premature break in the cylinder so it was important to watch the cylinder and switch the full advance off immediately after a load was recognized. The lever switch was then set to metered advance and the throttle was used to adjust the loading rate. The target loading rate for a 100 mm (4 in) cylinder was 2.3 kN/sec (560 lb/sec). All the cylinders were tested in the Forney LC-4 which has a capacity of 2700 kN (600,000 lb) and is illustrated in **Figure 3.14**.

Figure 3.14 – Forney LC-4

Table 3.8 contains a summary of the compressive strength data from the test date breaks by panel. The strength of some concrete was so low that additional cores were taken out of a panel that was not tested to verify panel compressive strength. The cores were drilled and prepared for testing according to ASTM C42/C42M-11 and then tested in accordance with ASTM C39/C39M-11. Since a 94 mm (3.7 in) core would not allow

for L/D>1 a 43 mm (1.7 in) core was used instead. The target length to diameter ratio was 2 which would result in no correction factor. The cores were drilled in the field and then placed into a bag and transported to the Construction Materials Laboratory, where the ends were sawed to provide parallel surfaces. One specimen required a significant piece be sawed off and thus had an L/D=1.6, which required a correction factor of 0.98. After the specimens were sawed they were placed back into the bag and the following day they were tested in the Forney LC-4. Measurements were taken of the diameter and length prior to testing. **Table 3.9** contains the results of the core testing. The values were divided by 0.85 to adjust for the lower compressive strength from cores. The adjusted values of the compressive strength from the cores did not vary much from the cylinder compressive strength which confirmed that the cylinders were representative of the actual strength.

Table 3.8 – Mechanical Properties of Concrete Based Products at Test Age

	Compressive Strength (MPa)		MOE (MPa)		MOR (MPa)
	RC	FA-WF	RC	FA-WF	RC
SFRC-3.5	26.47	N/A	21240	N/A	3.51
SFRC-5.5	28.36	N/A	26060	N/A	
1-RC	30.26	N/A	25430	N/A	
2-RC	30.26	N/A	25430	N/A	
1-H	16.78	11.64	21750	6980	2.47
2-H	28.36	10.74	26060	4870	
H-A	29.75	10.77	26710	7190	3.18
H-A/F	29.75	10.77	26710	7190	3.18
H-B	16.78	11.76	21750	6980	2.47
H-B/F	16.78	10.82	21750	6980	2.47
H-FG	29.75	10.77	26710	7190	3.18
H-FG-A/F	29.75	10.77	26710	7190	3.18
H-FG-B/F	29.75	10.77	26710	7190	3.18

Unit Conversion: 1.00 MPa=145 psi

Table 3.9 – Core Data

	Core 1	Core 2	Core 3
L/D	1.6	1.94	1.87
f'c (Mpa)	18.25	17.81	16.73
Average (Mpa)	17.60		

Unit Conversion 1.00 MPa=145 psi

3.2.2 Modulus of Elasticity. The same 100 mm by 200 mm (4 in x 8 in) cylinders were used to determine the modulus of elasticity (MOE). This test was performed at 28 days and on the test date. For this test ASTM C 469/C469M-10 was followed. A manually recorded compressometer and the Forney LC-4 were used for all the MOE tests.

The comprsessometer that was used consists of 2 yokes with a digital dial gage set up in the direction of compression connecting the yokes along with spring and pivot rod opposite the dial gage. The pivot rod was used to maintain a constant distance while the allowing only the side with the dial gage to move thus causing the deflection seen by the dial gage to be twice the actual deflection, a correction that is calibrated in the dial gage. **Figure 3.15** illustrates the compressometer attached to a cylinder in the Forney LC-4. The ultimate strength of the cylinders was necessary to determine where data points would be taken so to determine the ultimate strength a cylinder was tested to failure in compression prior to determining MOE. The two remaining cylinders that make up a complete test for compressive strength were used to determine the MOE before they were tested to failure in compression. Each specimen was fitted with the compressometer and then loaded at a 2.3 kN/sec (560 lb/sec) rate until 40% of ultimate strength then unloaded

with no recording of data. After this initial loading the cylinder was then loaded with data points taken at .5%, 1% and 1.5% strain then at 20%, 30% and 40% of ultimate strength. Several data points were taken to develop an elastic stress-strain relationship as a check on the accuracy of the calculations. This was found for the SFRC and WFFA and the procedure did not differ for either material. The MOE was found by taking the difference of the first and last stress points divided by the difference of the first and last strain points as illustrated in **Equation 3.1**.

$$E = \frac{s_2 - s_1}{\varepsilon_2 - \varepsilon_1} \tag{3.1}$$

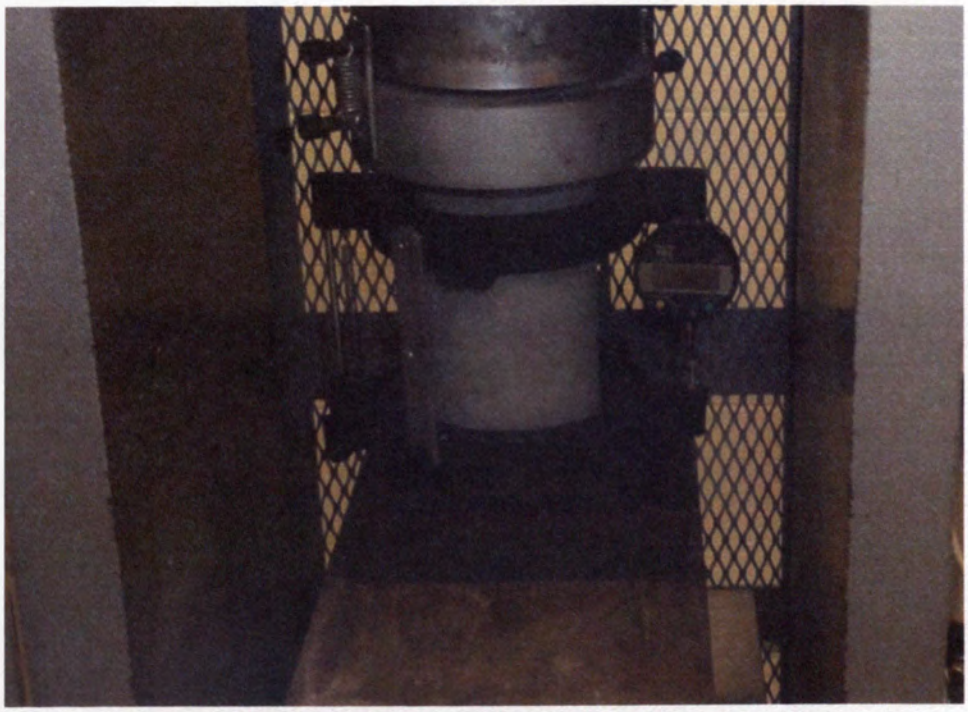

Figure 3.15 – Compressometer for Determining MOE

The MOE's for each panel are recorded in **Table 3.8.** The values found during testing were close to the ACI 318-08 8.5.1 approximation for concrete with the exception of the FA-WF material. FA-WF is a non-concrete based material so the lack of correlation with the ACI code is expected. A large disparity was noticed in the MOE values for the FA-WF material which suggest an error in the measurements as the mix proportions and materials did not vary.

3.2.3 Modulus of Rupture. The modulus of rupture (MOR) was determined using two 605 x 150 x 150 mm (24 x 6 x 6 in) samples tested at 28 days and on the test date. The test specimens were fabricated according ASTM C192/C192M-07 and tested according to ASTM C78/C78M-10. The beams were placed in two lifts with 50 rods after each lift, using a 16 mm (0.63 in) tamping rod, and were hammered 25 times with a rubber mallet. The beams were stripped after 1 day and then allowed to cure next to the panels until testing.

A Tinius Olsen testing machine was used for testing MOR beams, which were loaded in a three point loading configuration. To center the beam, lines were drawn around the beam at the loading locations. The two base loads were placed approximately 76 mm (3.0 in) from each end of the beam, while the two interior action loads were located on the top of the beam 150 mm (6.0 in) inward from the base loads leaving 150 mm (6.0 in) between the two loads. The beam was set into place on the Tinius Olsen and then the software was configured for MOR testing using an existing file on the computer. The beam was then loaded at 2.25 kN/sec (50 lb/sec) until fracture. As long as the fracture was in the middle third the test satisfied the standard, the lines drawn around the beam allowed easy verification of this. All the MOR specimens tested were acceptable.

Table 3.8 shows the values of MOR for the test age specimens. Only the first two batches were tested for MOR. No FA-WF specimens were made or tested for MOR as the material was used as a sacrificial layer. The values from this were similar to the empirical model predicted values found with equation 9-10 from ACI 318-08.

3.2.4 Material Density. The material density was determined by using the 100 x 200 mm (4 x 8 in) compressive cylinders. The density was determined with two different methods, using volume and mass and using water displacement method. The volume and mass is a very simplistic method but can also be inaccurate. For this method the diameter of a cylinder was measured twice at the top, middle and bottom of the cylinder to the nearest 0.025 mm (0.001 in). The height of the cylinder was also measured at four different locations to the nearest 0.025 mm (0.001 in). After all the dimensional measurements were recorded, a dry mass was found for the cylinder by taking a dry specimen and massing it on a scale. From the dimensional measurements the volume was calculated and then once the volume was calculated the material density was calculated by dividing the dry mass by the volume.

The second method uses a scale with an under-mount hook attachment. The scale was placed on a table with a hole in it, and the hook was attached to the bottom of the scale and hung down through the hole in the table and the hook supported a platform that extended into a water bath. To determine the density the dry and wet mass must be found. The dry mass was found in the last method leaving the wet mass, which is found by placing the specimen on the platform so that it is submerged. Volume is calculated with **Eq. 3.2** by taking the difference of the dry mass (M) and wet mass (M_s) divided by the density of the water (ρ_w), which was taken as 997 kg/m^3 (1.93 slug/ft^3), which is the

density of water at 25°C (77°F). The testing setup for the second method is illustrated in **Figure 3.16** and the values for the densities of the SFRC and FA-WF are displayed in **Table 3.10**. The values found using both methods were very similar, which adds confidence to the values found.

$$V = \frac{M - M_s}{\rho_w} \tag{3.2}$$

Table 3.10 – Material Densities

	Material Density (kg/m^3)	
Material	Method 1	Method 2
SFRC	2276.2	2274.2
FA-WF	1497.0	1508.3

Unit Conversion: 1.00 kg/m^3=0.00194 slug/ft^3

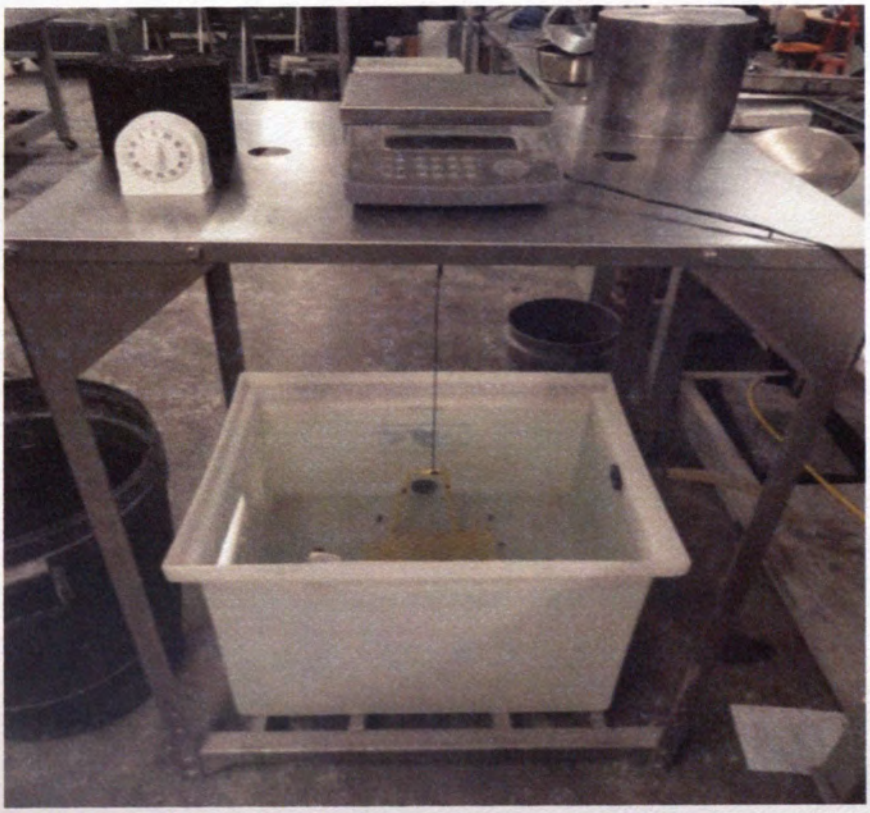

Figure 3.16 – Water Bath Setup for Density

3.2.5 Tensile Capacity of Polyurea. The tensile capacity and fiber ratio of the polyurea were the two properties determined for that material. These properties allowed for comparison to an earlier study done on the characterization of the polyurea. The tensile capacity was found using a combination of ASTM D3039/D3039M-08 and ASTM D7565/D7565M-10. The samples were constructed by spraying the polyurea on a greased metal sheet. Upon cooling and solidifying of the polyurea, the polyurea was peeled off the metal sheet. The polyurea sheets were then cut into 40 mm (1.6 in) by 230 mm (9.0 in) coupons. One of the variations from the ASTM was the specimen size; the ASTM however, does state that the geometry of the specimens and gripping mechanisms are in large part an art due to a lack of industrial consensus. An approximately 130 mm (5.0 in) gage length was marked on the specimens for installation in the Instron 4485 available at the Missouri S&T. The polyurea specimens were tested without end tabs as recommended by Carey and Myers (2010). The Instron was programmed with a data acquisition software for testing, and was set up for testing a metal coupon. The e-glass DFRP specimens and the plain polyurea A specimens were loaded until failure while the plain polyurea B specimens were loaded past yielding but not till failure. The plain polyurea B samples did not fracture even when allowing the Instron to reach its maximum displacement.

Table 3.11 shows a summary of the results from coupon tests. Polyurea B with discrete E-glass fibers resulted in the highest tensile yield strength in the set from this project. There was great variance in the values for the tensile yield strength in the E-glass DFRP specimens. This was due in part to air pockets that developed during the specimen fabrication. The air pockets only affected some specimens and resulted in quick tearing of

the specimen through the air pockets. Also since the glass fiber is blown into the polyurea as the polyurea is applied to the panel, it is impossible to achieve a perfect distribution of fiber. To help account for the variance in the results, the fiber ratio of each coupon specimen was determined.

Table 3.11 – Polyurea Test Results

Polyurea		Yield Strength (Mpa)	Strain @ Yield (%)	MOE (MPa)	Stress @ Break (Mpa)	Elongation (%)	Fiber Ratio (%)
XS-100 (A)	Average	1.421	1.021	284.354	4.213	91.423	N/A
	Std. Dev.	0.185	0.374	48.265	0.197	5.243	
	COV	0.130	0.366	0.170	0.047	0.057	
XS-100F (A/F)	Average	1.643	0.707	457.299	4.519	8.528	19.0096
	Std. Dev.	0.380	0.523	229.728	0.823	3.005	1.9276
	COV	0.231	0.739	0.502	0.182	0.352	0.1014
XS-430 (B)*	Average	1.565	1.589	106.665	5.040	355.187	N/A
	Std. Dev.	0.263	0.403	21.658	0.215	9.597	
	COV	0.168	0.254	0.203	0.043	0.027	
XS-430F (B/F)	Average	2.563	1.329	288.005	4.639	23.018	6.527265
	Std. Dev.	0.675	0.473	257.018	0.912	15.483	1.410193
	COV	0.263	0.355	0.892	0.196	0.673	0.216047

Unit Conversion: 1.00 MPa=145 psi

*The XS-430 (B) sample did not reach failure so the stress at break and elongation are from the last point recorded

3.2.6 Fiber Ratio. Another important property is the fiber ratio of the glass fiber polyurea. To determine the fiber ratio a burn-off test, also referred to as the ignition loss test, was run in accordance to ASTM D3171/D3171M-11 procedure G. After the discrete fiber specimens were tested in the Instron 4485 they were then cut into 40 mm (1.6 in) by 50 mm (2 in) specimens in preparation for the burn-off test. These specimens were cut from the coupon specimens after they were tested. The initial mass of the specimen, and

specimen plus glass slide was recorded then the samples were placed in a muffle furnace which was set to 600°C (1112°F) for 2 hours to melt down the polyurea and leave behind the glass fibers. After allowing the specimens to cool the mass of the glass slide plus remnants (glass fibers), and the glass slide by itself were recorded. The muffle furnace, a sample before the ignition loss and that sample after the ignition loss are displayed in **Figure 3.17**. The fiber ratio was then found as a simple mass ratio of the mass of the glass fibers to the initial mass of the specimen. These values are reported in **Table 3.11**.

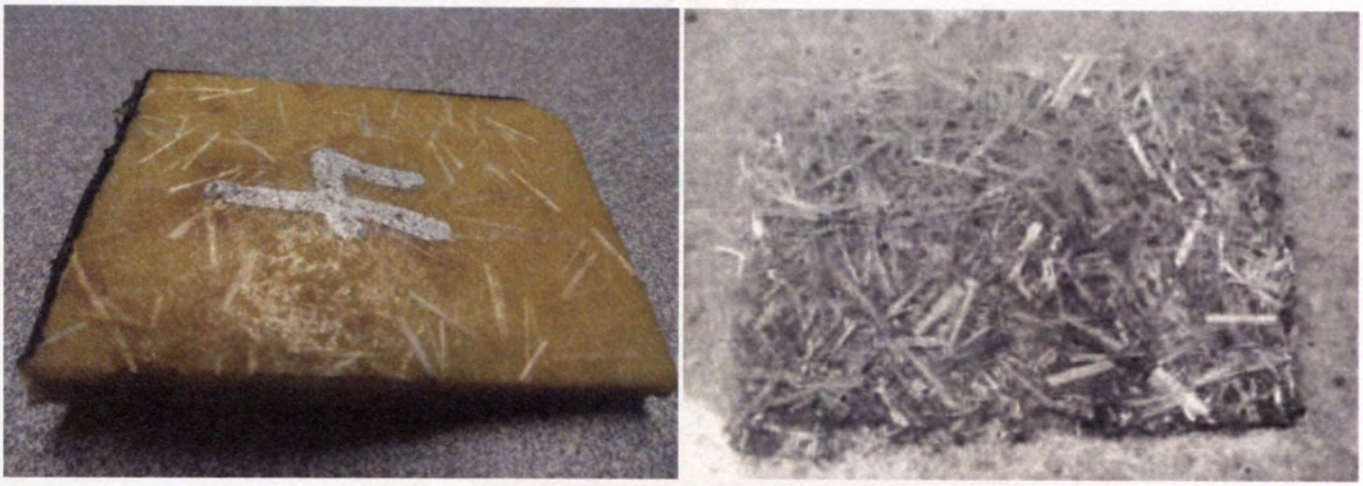

(a) Specimen Before (b) Specimen After

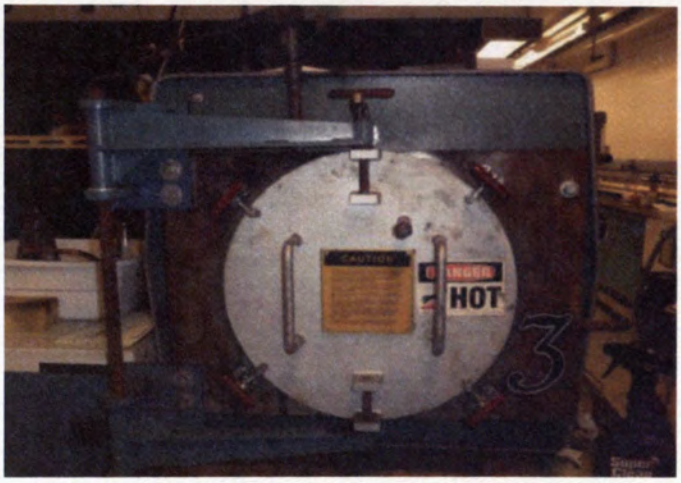

(c) Muffle Furnace

Figure 3.17 – Ignition Loss Testing

The high fiber ratio in the discrete fiber polyurea A specimens help explain the low elongation values recorded for those specimens. The ignition loss and tensile data for the DFRP specimens are reported in **Appendix C**, and graphs of the tensile data are reported in **Appendix D**.

4. EXPERIMENTAL TEST RESULTS

This study evaluated the performance of FA-WF, e-glass DFRP, and steel fiber reinforced concrete as a composite panel under blast loading. The test procedure was reported in Section 3.1. The following is an evaluation of the blast mitigation performance based primarily on visual inspection. The crack widths reported in the later sections were measured by using images of the cracks and AutoCAD to measure the crack widths. The images with AutoCAD annotations are located in **Appendix E**. The sides of the panel are referred to as top face or compression face for the surface that faces the ceiling of the alcove and the bottom face or tension face for the surface that faces the floor of the alcove. The rest of the faces are described as if you were standing at the entry of the alcove and looking at panel. **Figure 4.1** displays how the faces of the panel were named. **Figure 4.1** was captured looking into one of the alcoves of the Wombat mine.

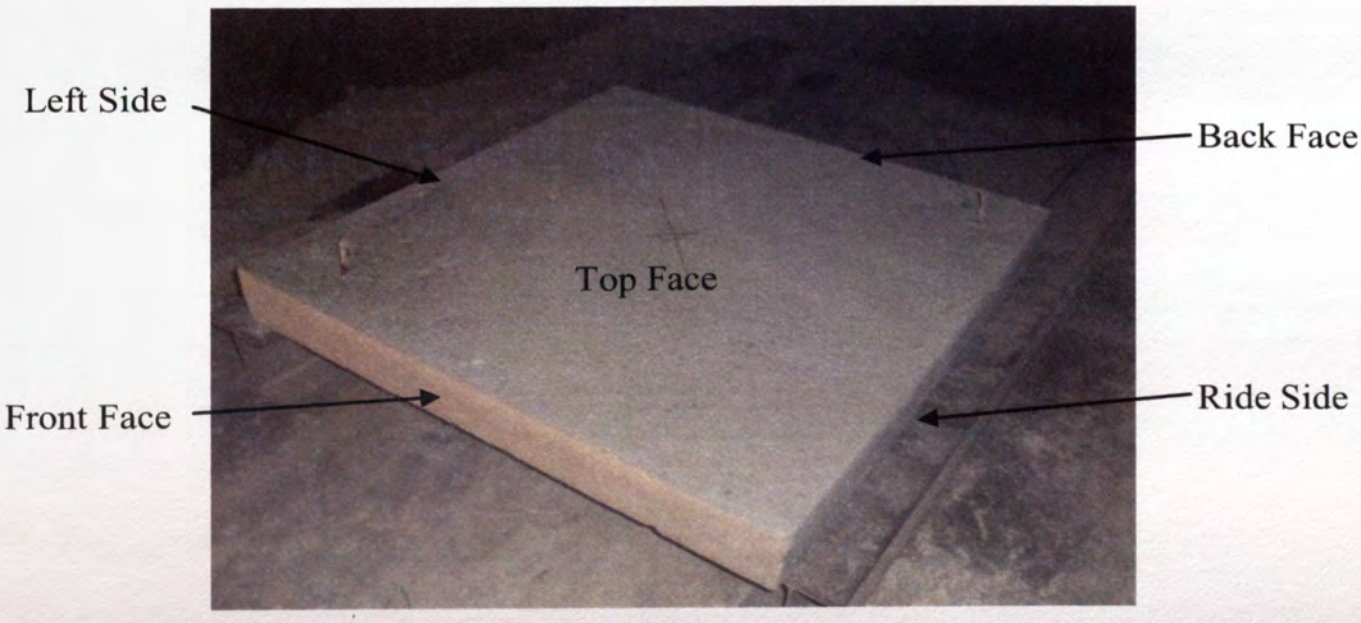

Figure 4.1 – Configuration of Typical Panel

4.1 3.5" SFRC CONTROL PANEL (SFRC-3.5)

The SFRC-3.5 panel consisted of a 90. mm (3.5 in) thick layer of steel fiber reinforced concrete. The panel was tested with only one blast event of 1.4 kg (3.0 lb) charge at 310 mm (12 in). This panel was to examine how beneficial the FA-WF layer is and will later be compared to the 2-H panel. The initial pre blast images are illustrated in **Figure 4.2**.

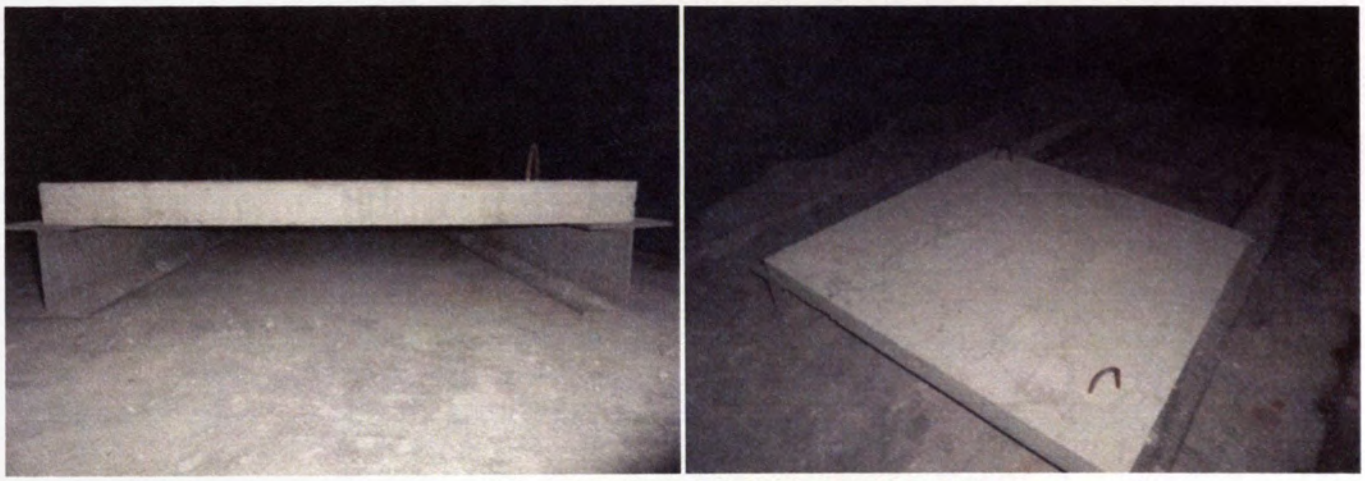

(a) Front Profile View (b) Isometric View

Figure 4.2 – Panel SFRC-3.5 Prior to Blast Event

The blast event resulted in significant damage to the panel. A large 10. mm (0.39 in) wide flexural crack illustrated in **Figures 4.3b and 4.3c**, extended along the bottom of the panel and resulted in spalling in the center of the panel (**Figure 4.3c**). Evidence of concrete crushing was observed on the compression and is illustrated in **Figure 4.3a**. This damage indicates that the panel failed structurally and at containing the blast.

(a) Concrete Crushing on Compression Face (b) Flexural Cracks on Front Face

(c) Flexural Crack and Spalling on Tension Face

Figure 4.3 – Panel SFRC-3.5 After Blast Event, 1.4 kg at 310 mm

4.2 5.5" SFRC CONTROL PANEL (SFRC-5.5)

The SFRC-5.5 panel consisted of a 140 mm (5.5 in) thick layer of steel fiber reinforced concrete. This panel test was to evaluate how beneficial the FA-WF layer was as a sacrificial layer. This panel will later be compared to panel 2-H. The initial pre-blast images are illustrated in **Figure 4.4**.

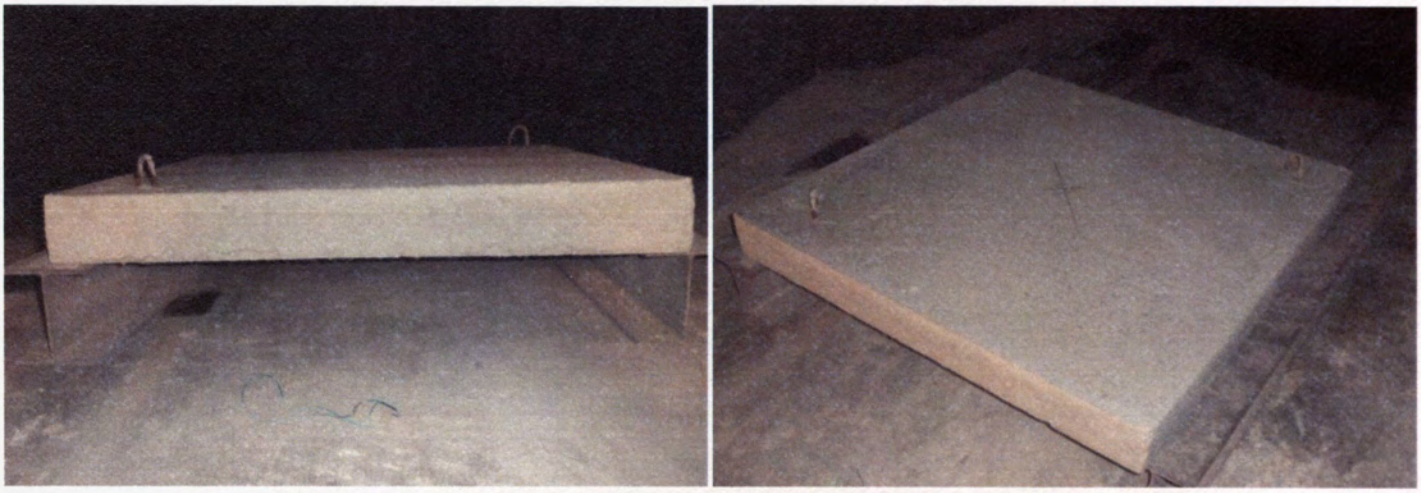

(a) Front Profile View (b) Isometric View

Figure 4.4 – Panel SFRC-5.5 Prior to Blast Events

After the first blast event of 1.4 kg (3.0 lb) at a 31 mm (12 in) standoff, very little damage was identified. In fact residual deflection and cracking was unnoticeable. The only evident damage was scarring on the top of the panel from the blast wires (**Figure 4.5b and 4.5c**) and a small tensile crack in the center of the tension face of the panel (**Figure 4.5 d**).

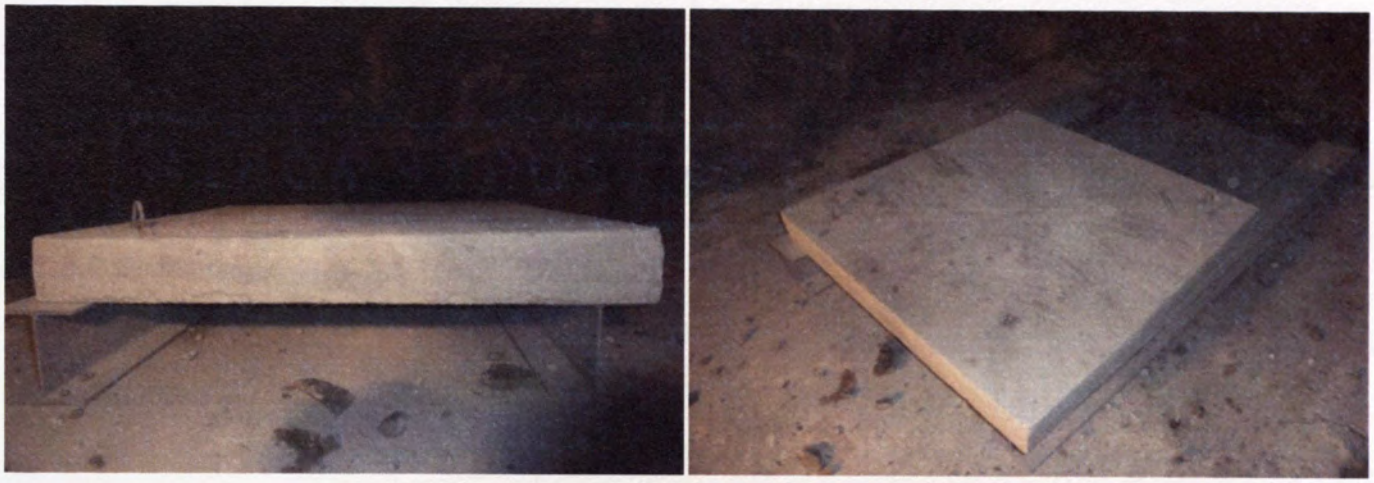

(a) Front Profile View (b) Isometric View

(c) Compression Face from Right (b) Tension Face from Back

Figure 4.5 – Panel SFRC-5.5 After First Blast Event, 1.4 kg at 310 mm

The second blast event—a 1.4 kg (3.0 lb) charge at 150 mm (6.0 in) standoff—resulted in an increase in observed damage; however the damage was not very significant. The primary damage was a few flexural cracks in the front face, with the largest crack being 3.4 mm (0.13 in) wide (**Figure 4.6c and 4.6d**) and it continued across the bottom contributing to spalling (**Figure 4.6d**) on the tension face. The residual deflection observed in this panel was minimal, but recordable. Overall the panel was able

to withstand the blast without losing significant integrity. However, given the objective of this research is to contain the blast, this panel failed because some spalling occurred, which could cause damage or injury if it occurred in practice.

(a) Back Profile View

(b) Isometric View

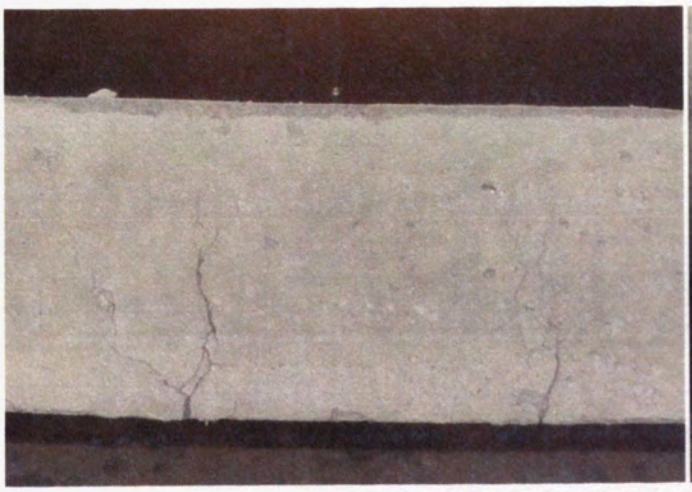

(c) Flexural Cracks on Back Face

(d) Spalling on Tension Face

Figure 4.6 – Panel SFRC-5.5 After Second Blast Event, 1.4 kg at 150 mm

4.3 PLAIN RC CONTROL PANEL 1 (1-RC)

The first plain reinforced concrete control panel consisted of a 90. mm (3.5 in) thick layer of plain reinforced concrete. This panel was subjected to a single blast event with the standoff distance being 150 mm (6.0 in). This panel was to compare the different stand-off distances and will later be compared to 2-RC. Images of the initial setup and panel condition are illustrated in **Figure 4.7**.

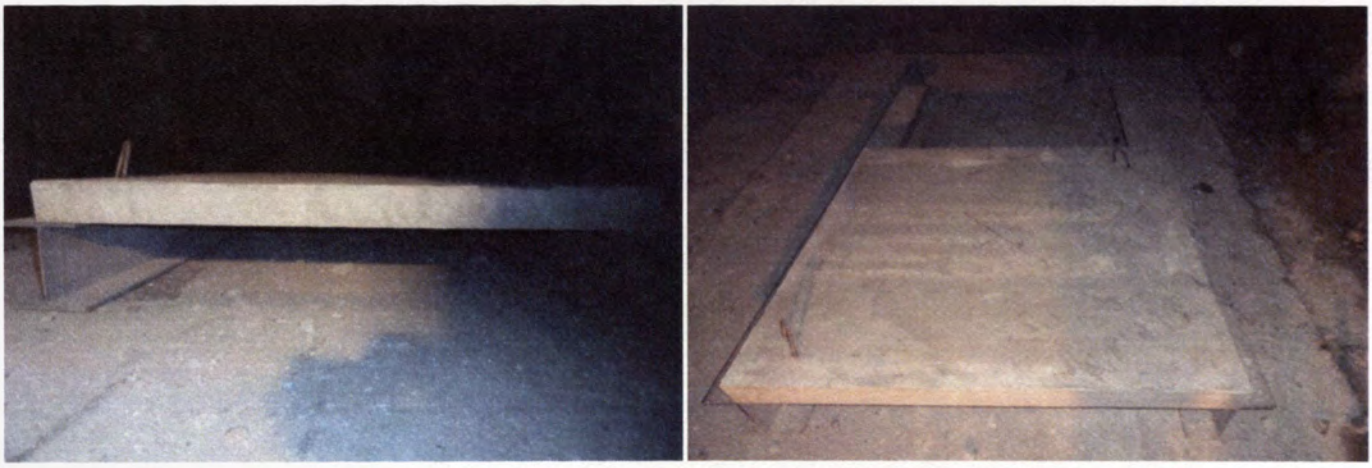

(a) Front Profile View (b) Compression Face From Front

Figure 4.7 – Panel 1-RC Prior to Blast Event

The blast event consisting of 1.4 kg (3.0 lb) charge at a 150 mm (6.0 in) standoff caused tremendous damage to this panel resulting in several shear failures including a large hole that developed due to shear punching and a large shear crack near the support. The large hole is illustrated in **Figures 4.8b, 4.8e, and 4.8f**. The large hole also resulted in unbonded rebar and a large amount of rubble to be ejected from the panel. This means that this panel performed poorly at containing the blast. **Figure 4.8c** illustrates the large shear cracks that opened up resulting in significant residual deflections. While shear

attributed to the most of the damage **Figures 4.8d – 4.8e** illustrates some flexural cracks which were all less than 0.60 mm (0.024 in) wide. Also, some patterned cracking in the form of an X shape developed on the surface of the panel and is illustrated in **Figure 4.8b**. The x-pattern cracking is a result of the reflected blast wave. First a compression wave hits the center of the panel then it radiates toward the edges where some of the wave is reflected back as a tension wave toward the center of the panel due to the difference in density between the air and panel. The lines where these stresses meet form the x-pattern cracking.

(a) Front Profile View

(b) Compression Face From Front

(c) Shear Crack in the Front Face

(d) Flexural Cracks in the Back Face

(e) Hole From Above the Panel

(f) Debris and Tension Face

Figure 4.8 – Panel 1-RC After Blast Event, 1.4 kg at 150 mm

4.4 PLAIN RC CONTROL PANEL 2 (2-RC)

The second plain reinforced concrete control panel (2-RC) consisted of a 90. mm (3.5 in) thick layer of plain reinforced concrete and was identical to the first plain reinforced control panel (1-RC). Both the 1-RC and 2-RC panels were tested to compare the different stand-off distances. A comparison between 1-RC and 2-RC is presented later in this section. The 2-RC panel was tested with one blast event with a 310 mm (12 in) stand-off. Images of the initial setup and panel condition are illustrated in Figure 4.9.

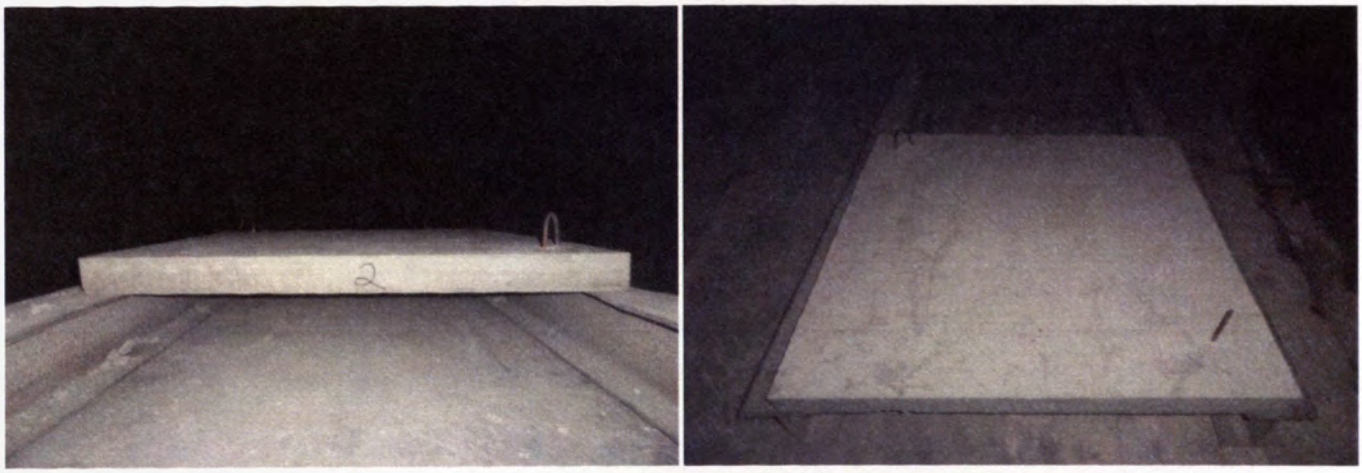

(a) Front Profile View (b) Compression Face From Front

Figure 4.9 – Panel 2-RC Prior to Blast Event

The 1.4 kg (3 lb) charge at 310 mm (12 in) blast event resulted in significant damage to the panel including substantial flexural cracking which resulted in large residual deflections. The largest flexural crack observed in the 2-RC panel was 1.2 mm (0.047 in) wide. **Figure 4.10c** shows these flexural cracks did propagate vertically through the panel and **Figure 4.10d** shows, one crack extended across the bottom of the panel. Also **Figure 4.10d** shows a large chunk has spalled off the panel. This indicates

that the panel did not sufficiently contain or mitigate the blast event and allowed some material to be ejected and fragment from the panel. The overall damage is relatively large for the blast event tested.

(a) Front Profile View

(b) Compression Face From Front

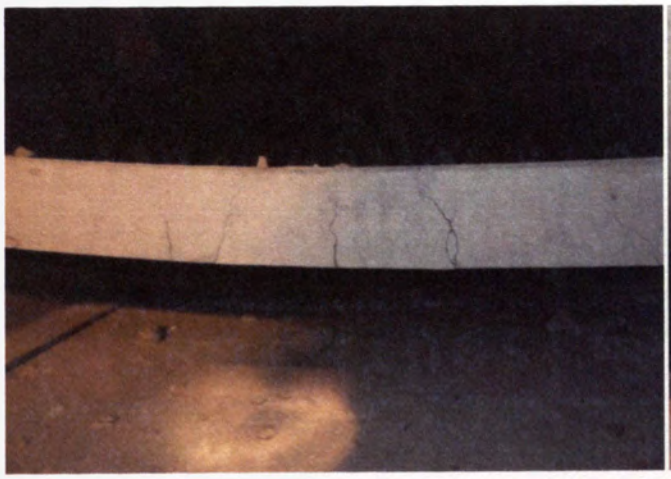

(c) Flexural Cracks in the Front Face

(d) Tension Face From Front

Figure 4.10 – Panel 2-RC After Blast Event, 1.4 kg at 310 mm

Comparing the panels 1-RC and 2-RC it can be observed that the level of damage in 1-RC is significantly greater. The residual deflections are greater and the loss of

material is substantially larger in 1-RC. It is important to note how the majority of the damage in 2-RC was flexural damage and in panel 1-RC it was shear damage. The shear damage in panel 1-RC is likely due to a more concentrated and higher magnitude load from the shorter stand-off distance; whereas, in panel 2-RC the larger stand-off distance allowed the load to be distributed over a greater area and also decreased the magnitude of the distributed load—the 3D-models from ConWEP that predicted the pressure distribution illustrate this theory and are presented in **Appendix B**. This would mean that the two blast events tested in this study work in two different fashions suggesting that while sequential blast events will have a tendency to build upon the damage from the previous event in this case significant damage can be distinguished as unique to a certain event.

4.5 FA-WF CONTROL PANEL 1 (1-H)

The first FA-WF control panel contains a 90. mm (3.5 in) layer of SFRC and then a 50 mm (2 in) sacrificial layer of FA-WF. This panel corresponds to the atypical concrete strength from batch 2. Test age compressive strengths for all the panels were reported in **Table 3.8**. This panel will be compared to panels 2-H, H-B and H-B/F, later in their respective sections. Initial images of the pre-blast condition of this panel are illustrated in **Figure 4.11**.

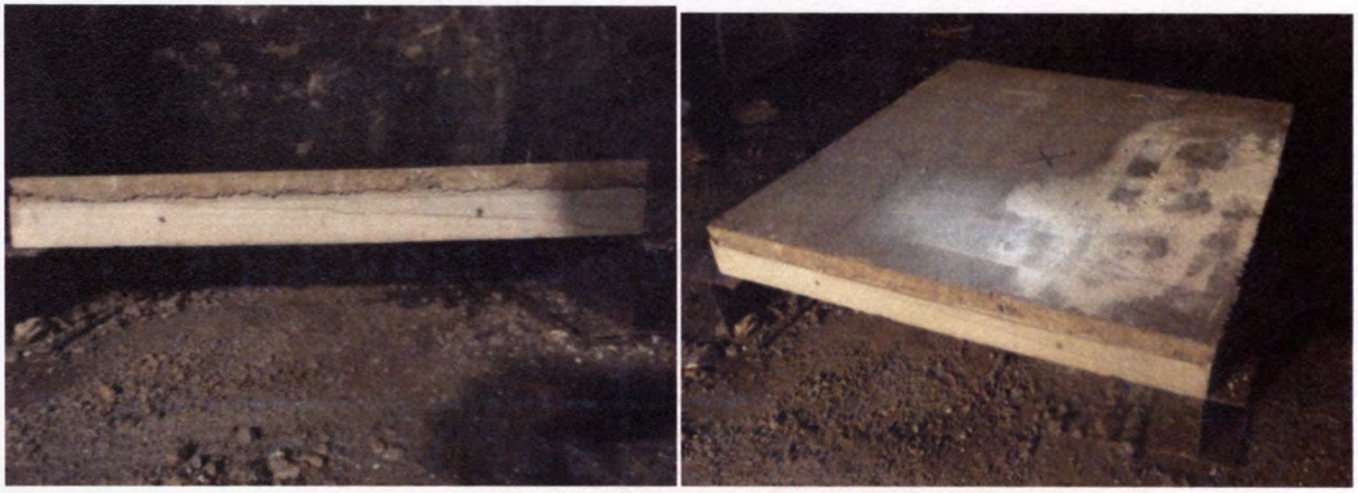

(a) Front Profile View (b) Isometric View

Figure 4.11 – Panel 1-H Prior to Blast Events

After the first blast event, which was a 1.4 kg (3.0 lb) charge at a 310 mm (12 in) standoff, some slight damage was noticed on the compression face and a crack developed through the panel. Scarring and cratering developed on the compression face of this panel is illustrated in **Figure 4.12b**. A 0.36 mm (0.14 in) wide flexural crack developed during the blast and runs along one of the rails from the rebar chairs, which is illustrated in **Figure 4.12d**. The crack propagated all the way through to the extreme compression fiber of the front face of the SFRC layer and is illustrated in **Figures 4.12a and 4.12c**. Several other much less significant cracks also developed during the blast event. There was some spalling, cratering and cracking that developed in the center of the panel indicating that a punching failure may occur at higher threat levels.

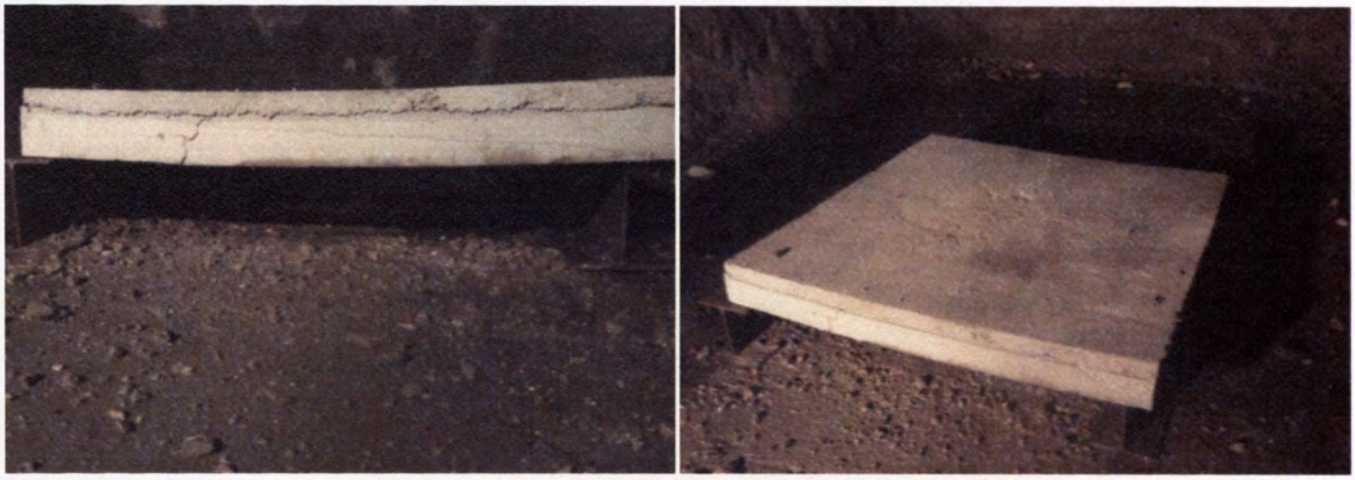

(a) Front Profile View (b) Isometric View

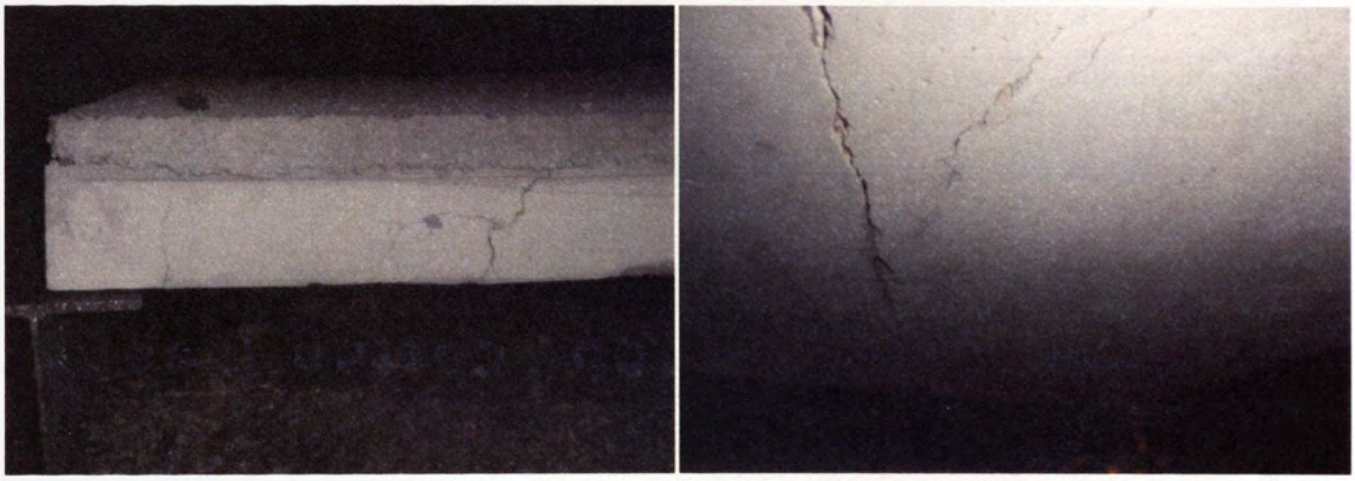

(c) Flexural Crack in the Front Face (d) Flexural Crack in the Tension Face

Figure 4.12 – Panel 1-H After First Blast Event, 1.4 kg at 310 mm

After the second blast, which was a 1.4 kg (3.0 lb) charge at 150 mm (6.0 in) standoff, a combined flexural and punching failure was observed. The crack that developed after the first event opened up exposing the debonded rebar. A large 330 mm (13 in) diameter hole was also punched through the center of the panel. The second blast event caused tremendous damage and ejected many fragments of concrete through the back of the panel. **Figures 4.12a and 4.12b** illustrate this damage. Although the damage

was great, the rebar prevented the panel from full separation and limited the fragmentation of the panel. The debonded rebar in the center of the panel and in the large crack are illustrated in **Figures 4.13c and 4.13d,** respectively. Also **Figure 4.13c** illustrates the FA-WF and SFRC layers separated indicating delamination occurred between the layers. **Figure 4.13e** illustrates the large 110 mm (4.4 in) wide flexural-shear crack and some of the debris that was ejected from the panel. The large crack appears to be an expansion of the flexural crack from the first event with a shear action as many new diagonal cracks developed. Overall the panel performed poorly as it did not contain the second blast event, and instead allowed a significant amount of material to be ejected.

(a) Front Profile View

(b) Isometric View

(c) Punching Failure

(d) Flexural-Shear Crack in the Back Face

(e) Crack and Debris From Front

Figure 4.13 – Panel 1-H After Second Blast Event, 1.4 kg at 150 mm

4.6 FA-WF CONTROL PANEL 2 (2-H)

The second FA-WF control panel is the same geometrically, 90. mm (3.5 in) SFRC layer and 50 mm (2 in) FA-WF sacrificial layer, as the 1st control. The only difference is the concrete strength is the typical strength, 27.6 MPa (4000 psi), found in most of the panels. This panel was compared to SFRC-3.5 and SFRC-5.5 to determine the impact of the FA-WF layer. The 2-H panel will be compared to 1-H to determine the impact of the strength of the SFRC layer later in this section. The 2-H panel will also be compared to H-FG, H-B and H-B/F in their respective sections. Images of the initial setup and panel condition are illustrated in **Figure 4.14**.

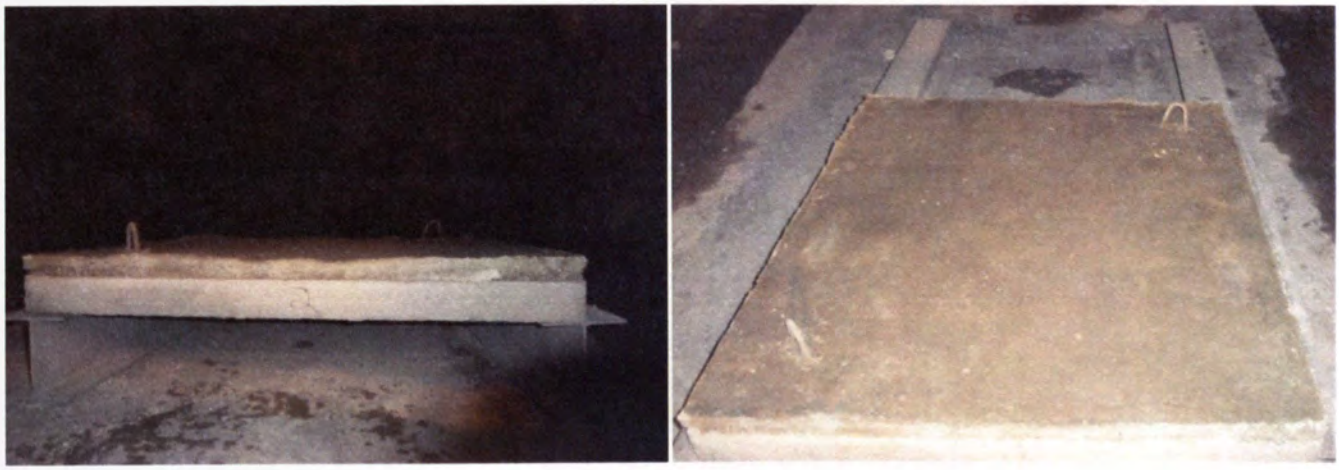

(a) Front Profile View (b) Compression Face From Front

Figure 4.14 – Panel 2-H Prior to Blast Events

The 1.4 kg (3.0 lb) charge at 310 mm (12 in) standoff blast event resulted in significant residual deflections and cracking. **Figures 4.15c and 4.15d** illustrate a 2.5 mm (0.098 in) wide flexural crack running across the bottom of the panel and also up the panel vertically respectively. Similarly to the 1-H panel this panel appears to have a

major flexural crack run along one of the chair legs. The compression face of the panel experienced some scarring and cratering (**Figure 4.15b**) and minimal cracking. Overall the panel performed very well against the first blast event.

(a) Back Profile View

(b) Compression Face From Back

(c) Flexural Crack in the Tension Face

(d) Flexural Crack in the Back Face

Figure 4.15 – Panel 2-H After First Blast Event, 1.4 kg at 310 mm

The 1.4 kg (3.0 lb) charge at 150 mm (6.0 in) standoff blast event resulted in a punching shear failure along with continued propagation of the flexural crack. A small

152 mm (6 in) diameter hole was punched through the FA-WF layer and expanded to a 310 mm (12in) diameter hole once it reached the extreme tension fiber in the SFRC layer as illustrated in **Figures 4.16c and 4.16d**. The flexural crack expanded slightly from 2.5 mm (0.098 in) to 2.6 mm (0.10 in), but did not open up significantly until it neared the center of the panel as illustrated in **Figures 4.16e and 4.16f**. A large shear crack and delamination between the FA-WF and SFRC layers is illustrated in **Figure 4.16e**. The impact of the delamination of the two layers is illustrated in the **Figure 4.16b** by the pieces of the sacrificial FA-WF layer that broke off. The hole that punched through the panel was the most significant damage and resulted in a pile of debris that was ejected from the panel and is illustrated in **Figure 4.16f**. The panel performed poorly in containing the blast and, with all the cracking and the puncture, the panel has lost most of its structural integrity.

(a) Back Profile View

(b) Compression Face From Back

(c) Hole in the Compression Face

(d) Hole in the Tension Face

(e) Flexural Cracks in the Back Face

(f) Tension Face from Back

Figure 4.16 – Panel 2-H After Second Blast Event, 1.4 kg at 150 mm

In comparison to 1-H, 2-H performed much better with much less significant damage. The panels performed similarly after the first blast event with 2-H performing slightly better in residual deflections and exhibiting smaller flexural cracking. The major difference was seen in damage from the second blast event. A larger hole developed in 1-H and the cracking and residual deflections were much more severe in 1-H. This suggests that the higher strength SFRC performs better under blast loading. This was the expected result and allows for later panels to be compared to each other despite the disparity in compressive strengths.

The 2-H panel performed much better than the SFRC-3.5 panel. The residual deflections and cracking observed in panel 2-H were less severe than the residual deflections and cracking observed in the SFRC-3.5 panel. This indicates that adding the FA-WF layer does reduce damage. The extra layer adds a significant improvement in blast mitigation over the plain SFRC panel. Comparing 2-H to SFRC-5.5 the level of damage is dramatically different. A hole punched all the way through the center of 2-H, while only spalling occurred on the bottom of SFRC-5.5. Also the residual deflection in 2-H was significantly greater than SFRC-5.5. Overall the SFRC-5.5 outperformed the 2-H panel.

4.7 FA-WF FOAM-GAP CONTROL PANEL (H-FG)

The FA-WF foam-gap control panel has a 50 mm (2 in) FA-WF layer and 90. mm (3.5 in) SFRC base separated by a 76 mm (3.0 in) foam gap. This panel was compared with the 1-H and 2-H panels and will be later compared to the H-FG-A/F and H-FG-B/F panels. Images of the initial setup and panel condition are illustrated in **Figure 4.17a**. The

first image, **Figure 4.17a**, was captured outside the Wombat mine, while the other image, **Figure 4.17b,** was captured inside the Wombat mine.

(a) Back Profile View (b) Compression Face From Front

Figure 4.17 – Panel H-FG Prior to Blast Event

The 1.4 kg (3 lb) charge at 310 mm (12 in) standoff blast event resulted in significant damage and resulted in most of the sacrificial FA-WF layer being removed. Upon first inspection the panel H-FG appears to be mostly intact as although the blast event fragmented the FA-WF layer into many pieces, the pieces remained on the panel as illustrated in **Figure 4.18b. Figure 4.18e** illustrates that after removing the detached FA-WF pieces, only limited amounts of the sacrificial FA-WF layer remains. A large 2.9 mm (0.11 in) wide flexural crack developed through the midline of the panel and is illustrated in **Figures 4.18c and 4.18d.** The damage was so extensive that a second blast was deemed unnecessary. Since nearly all the FA-WF layer was removed from the first blast event, the damage from a second blast would be unrepresentative of damage on this panel type.

Comparing panel H-FG to panels 1-H and 2-H the damage is similar with more damage observed in the H-FG panel. They all exhibited flexural damage after the first event. One major difference in damage between the panels was the residual deflection observed after the first blast event in the H-FG panel was much greater than the residual deflections observed in 1-H and 2-H panels. Another major difference was that the FA-WF remained intact with the exception of a few pieces in the 1-H and 2-H panels, but was nearly completely removed from the H-FG panel. This is a result of the FA-WF layer collapsing into the foam-gap. The H-FG panel was expected to perform better than the 1-H and 2-H panels because the foam-gap increases the stand-off distance to the base panel and as standoff distance increases the blast pressure reduces exponentially. Overall the H-FG panel performed slightly worse than the 1-H and 2-H panels.

(a) Front Profile View

(b) Isometric View

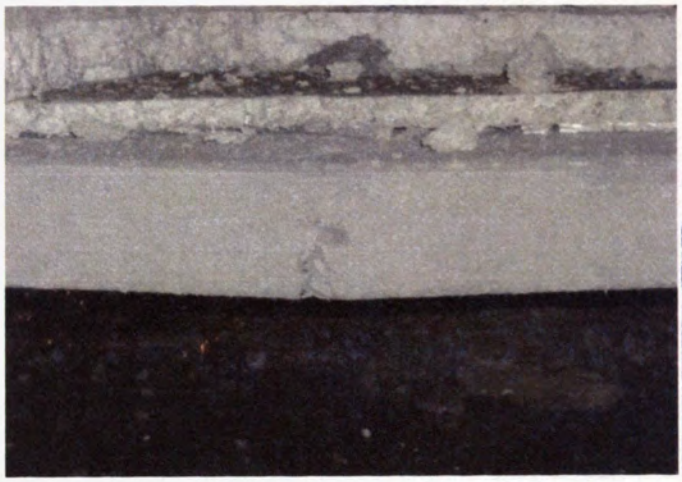

(c) Flexural Crack in the Back Face

(d) Flexural Crack Tension Face

(e) Compression Face After FA-WF Pieces were Cleared Off

Figure 4.18 – Panel H-FG After the Blast Event, 1.4 kg at 310 mm

4.8 FA-WF XS100 PANEL (H-A)

The H-A panel has a 50 mm (2 in) FA-WF layer, 90. mm (3.5 in) SFRC base, and a 5 mm (0.25 in) XS100 plain polyurea coating. This panel was constructed in the first batch and consisted of concrete which is the typical strength or 27.5 MPa (4000 psi). This panel was compared to 2-H panel, and will later be compared to the H-B, H-A/F, and H-FG-A/F panels. The initial setup and panel condition are illustrated in **Figure 14.19**.

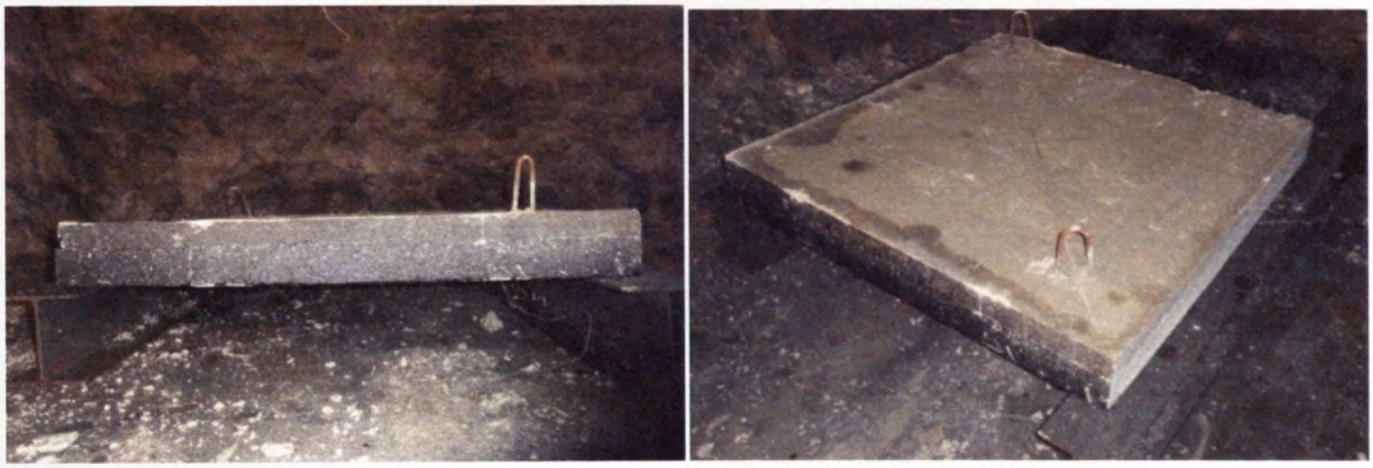

(a) Front Profile View (b) Isometric View

Figure 4.19 – Panel H-A Prior to Blast Events

The first blast event—a 1.4 kg (3 lb) charge at a 310 mm (12 in) standoff—created minor damage. Some scarring and cracking was noticed but nothing that indicated the panel was close to failure. Due to the sides being partially coated with the polyurea it was difficult to detect any cracking. Some cracking was found in the sacrificial FA-WF layer and a small piece of the corner detached completely as illustrated in **Figure 4.20c**. The compression face showed scarring near the center below where the charge was placed (**Figure 4.20d**) and several small cracks developed in the FA-WF layer but there was no indication of imminent punching failure. The residual deflection

was minor showing that the composite acted elastically to the blast. This is the ideal outcome and indicates the panel sufficiently absorbed the blast without significant damage or fragmentation. **Figure 4.20a** illustrates the left side of the panel fell from the support which indicates the panel moved rather significantly during the blast event. The piece of FA-WF that chipped off may be contributed to the action of the panel falling on the ground or directly to the explosion.

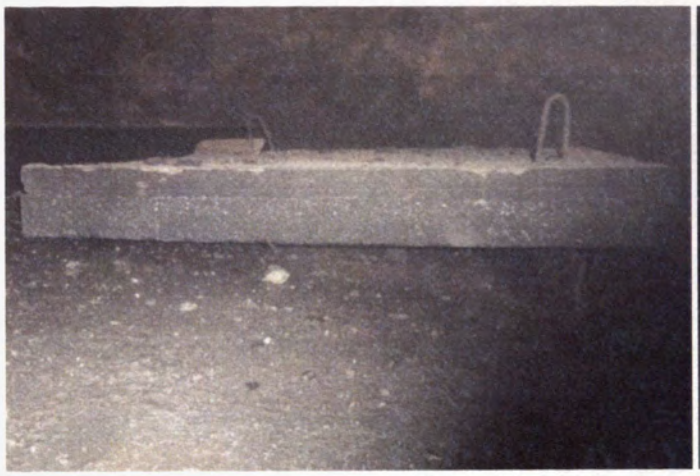

(a) Front Profile View

(b) Isometric View

(c) Detached FA-WF Piece

(d) Compression Face from Right

Figure 4.20 – Panel H-A After First Blast Event, 1.4 kg at 310 mm

The second blast event—a 1.4 kg (3.0 lb) charge at a 150 mm (6.0 in) standoff—significantly increased the damage, but the panel system still contained the blast. The residual deflections increased dramatically and the cracking in the SFRC and FA-WF also increased. Several large pieces of the sacrificial FA-WF layer detached from the panel, which is illustrated in **Figures 4.21b, 4.21d, and 4.21e**. This suggests that the bond between the SFRC and FA-WF layers is rather weak. A large bulge, which is illustrated in **Figure 4.21c**, developed in the polyurea under the panel indicating that the SFRC fragmented and attempted to punch through the polyurea layer. However, there was no tearing in the polyurea layer, so the panel adequately sustained the blast without allowing any material to penetrate through the other side of the panel. If this had been a non-structural wall or floor panel it would have been considered successful in containing the specific blast pressure tested. The FA-WF layer above the bulge in the center of the panel did not show any signs of punching, as illustrated in **Figure 4.21b**, suggesting that the two layers delaminated. **Figure 4.21f** illustrates a location where there was significant delamination between the SFRC and sacrificial FA-WF layers. A 1.7 mm (0.067 in) wide flexural crack is illustrated in **Figure 4.21e**. The large residual deflection, cracks, and large bulge indicate the panel failed in the traditional sense of strength design. The cracks and residual deflection indicate a flexural failure, where the steel likely exceeded its yielding stress and while the panel still has some capacity it would probably have a dramatic failure upon further loading. The bulge suggests a complete shear failure at that section of the panel, meaning the panel has little to no capacity for further loading in the center of the panel.

(a) Front Profile View

(b) Isometric View

(c) Large Bulge in Tension Face

(d) FA-WF Pieces Compression Face

(e) Large Crack Back Face of Panel

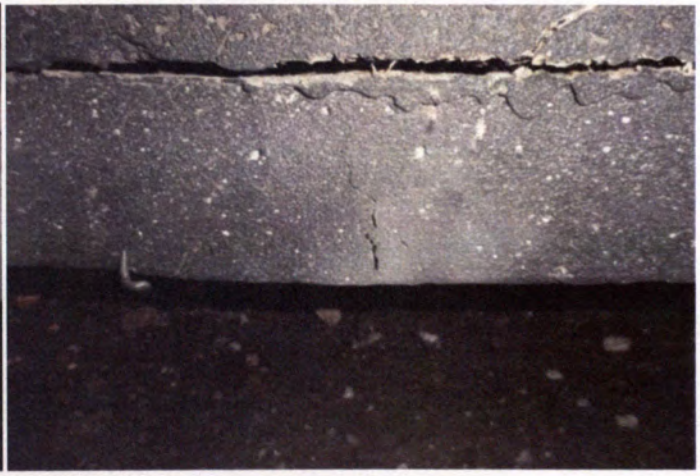

(f) Crack and Delamination Front Face

Figure 4.21 – Panel H-A After Second Blast Event, 1.4 kg at 150 mm

The damage seen in the H-A panel was much less significant than the damage seen in the 2-H panel. The modes of damage and failure were similar in the two panels as each exhibited flexural cracking and shear punching. The 2-H panel had a large hole punch through the panel which allowed debris to be ejected from the panel, which resulted in the panel unsuccessfully containing the blast. The H-A panel contained the blast event allowing only pieces of the FA-WF to fragment and an apparent punching failure where the rubble was contained in the bulging polyurea layer. The H-A panel deflected a little more than the 2-H panel suggesting the polyurea layer may increase residual deflections by containing the material. This can be understood with momentum. The 2-H panel was able to dissipate a tremendous amount of momentum through jetting fragments, whereas the H-A panel contained the fragments causing the momentum to spread through the panel increasing residual deflections. The polyurea layer contained a large amount of material but that caused increased residual deflection.

4.9 FA-WF XS100F PANEL (H-A/F)

The H-A/F panel has a 50 mm (2 in) FA-WF layer, 90. mm (3.5 in) SFRC base, and a 6.4 mm (0.25 in) XS100 polyurea coating with discrete glass fibers. The panel was compared with the 2-H and H-A, and will later be compared to the H-FG-A/F and H-B/F. The initial pre-blast images are illustrated in **Figure 4.22**.

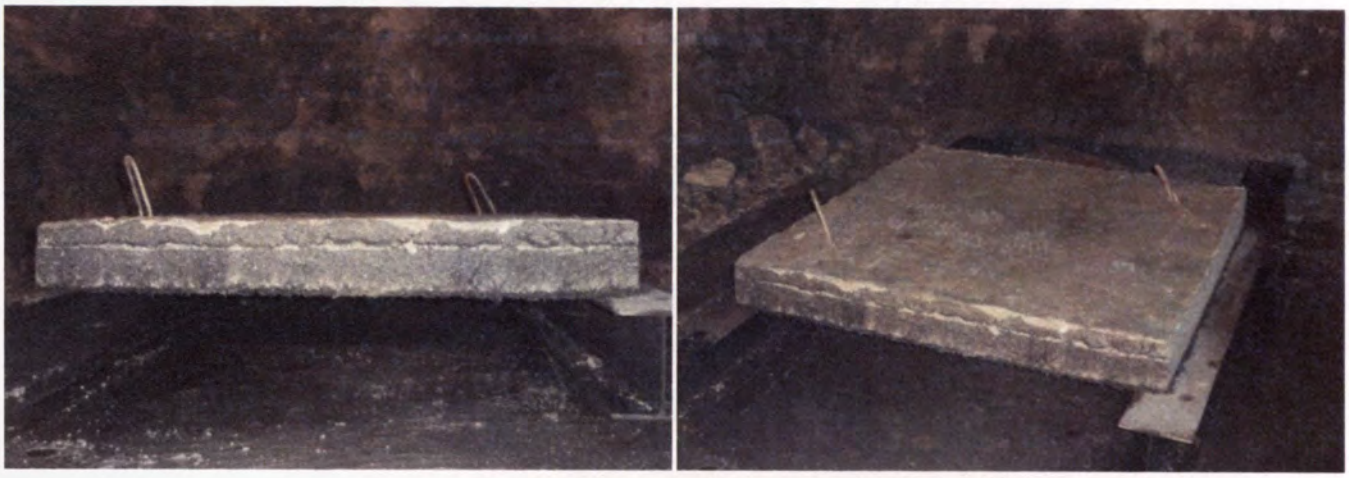

(a) Front Profile View (b) Isometric View

Figure 4.22 – Panel H-A/F Prior to Blast Events

The first blast event, which was a 1.4 kg (3.0 lb) charge at a 310 mm (12 in) standoff, resulted in very minimal changes in the panel. The residual deflection was slight and though cracking was observed in the FA-WF on the compression face, this was the only location where cracking could be observed. Again scarring was found directly below where the charge was placed and is illustrated in **Figure 4.23c**. **Figures 4.23c and 4.23d** illustrates the cracks in the top sacrificial FA-WF layer and in **Figure 4.23d** the cracks were outlined with a permanent marker so they would show up better when photographed. A few less than 0.5 mm (0.02 in) wide flexural cracks also developed in the panel though none propagated all the way through the panel suggesting elastic behavior in the panel. Overall the panel performed very well against this first blast event, with little recordable damage. In **Figures 4.23a and 4.23b** some debris appears to have gathered on the top of the panel, but this debris was fragments of rock that fell from the ceiling of the Wombat mine.

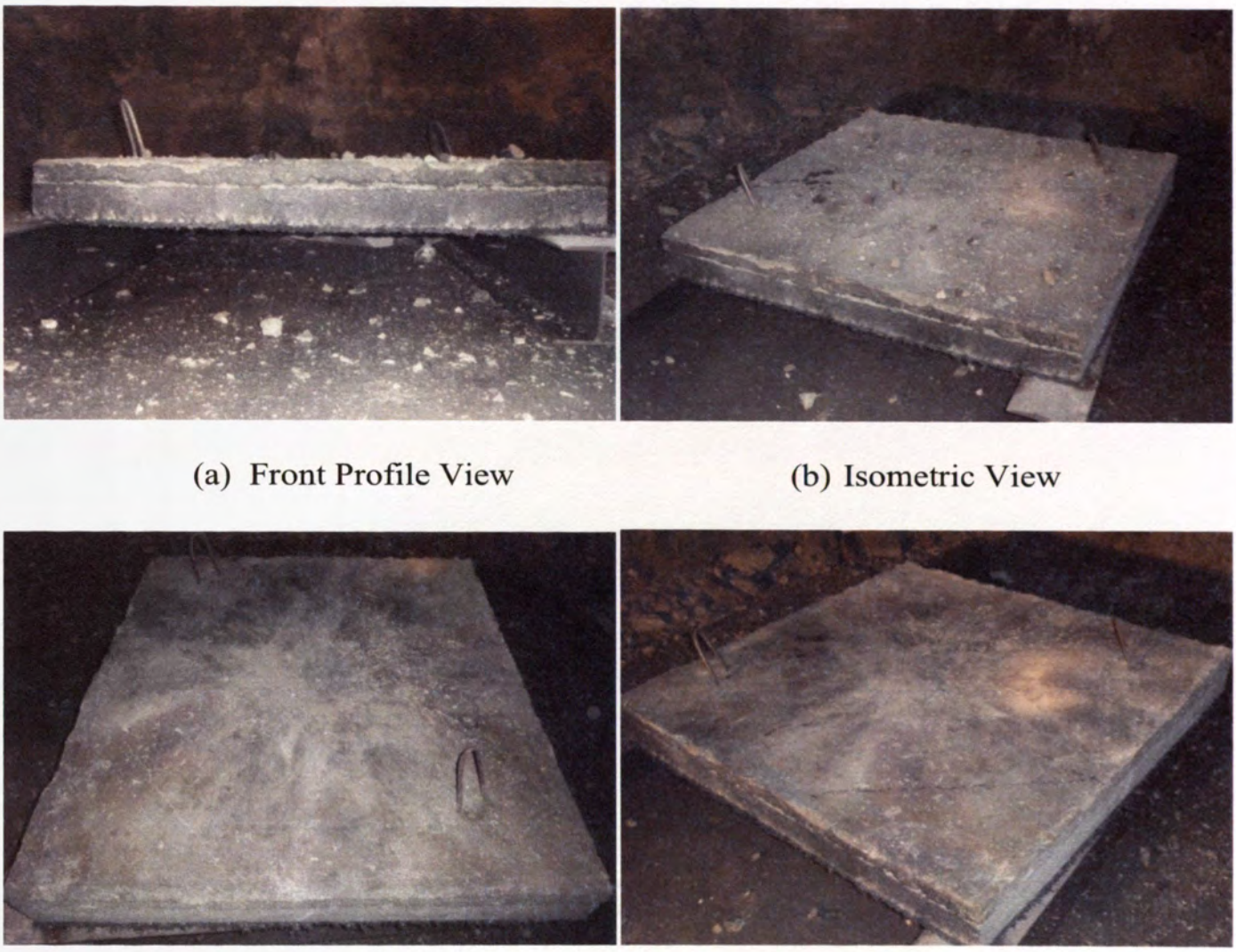

(a) Front Profile View (b) Isometric View

(c) Right Side Top View (d) Isometric View Cracks Outlined

Figure 4.23 – Panel H-A/F After First Blast Event, 1.4 kg at 310 mm

The second blast event, which was a 1.4 kg (3 lb) charge at a 150 mm (6.0 in) standoff, resulted in significant damage and tearing in the polyurea layer. The tearing in the polyurea layer is illustrated in **Figure 4.24e** and means the panel failed its purpose, to contain the blast. **Figure 4.24e** was captured inside the Wombat and shows the tearing in the polyurea layer and a large amount of debris that punched through the panel, while **Figure 4.24f** was captured outside the Wombat and shows the bottom of the panel and

the exposed rebar and chair. A large 6.5 mm (2.6 in) flexural crack expanded upon the crack formed from the first blast event. The surface cracking also expanded upon cracks formed during the first blast event. A couple of pieces of the sacrificial FA-WF layer that detached are illustrated in **Figures 4.24b and 4.24c** and delamination was also observed (**Figure 4.24d**) between the two layers. The panel failed through shear punching but did not appear to fail in flexure. So the E-glass DFRP system seemed to strengthen the panel against flexure; however, because of the decreased ductility when adding the E-glass fibers to the polyurea, the E-glass DFRP layer tore.

(a) Front Profile View (b) Isometric View

(c) Right Side Top View (d) Back Face Crack and Delamination

(e) Polyurea Tear and Rubble Tension Face {f) Exposed Rebar and Chair Tension Face

Figure 4.24 – Panel H-A/F After Second Blast Event, 1.4 kg at 150 mm

This panel performed better than the 2-H panel in all respects but due to the tearing in the polyurea layer it performed worse than the H-A panel. Since both the 2-H and H-A/F panels ejected some debris they were compared by estimating amount of debris and also by comparing residual deflections and the crack sizes/extent. In all of these categories the H-A/F panel performed better or nearly the same. From this it can be concluded that the e-glass DFRP layer provided some flexural strengthening to the panel. The H-A/F panel had the smallest residual deflections of the three panels being compared. This is likely due to the additional strengthening from adding glass fibers to the polyurea.

One of the main objectives of this research is to develop a material that can contain a blast without having any particles ejected. Given this the H-A/F panel has to be viewed as a failure. Also since the polyurea tore it is difficult to determine to what extent the glass fibers may have improved the strength, but it does indicate that the addition of the glass fibers decreased the ductility of the polyurea significantly enough to allow it to tear. The H-A panel was able to contain the second blast and thus gave better results than the H-A/F panel, according to the objectives of this research.

4.10 FA-WF XS100F FOAM-GAP PANEL (H-FG-A/F)

The H-FG-B/F panel has a 50 mm (2 in) FA-WF layer, 76 mm (3.0 in) foam-gap formed with stryofoam insulated sheeting, and a 90. mm (3.5 in) SFRC base with a 6.4 mm (0.25 in) XS100 polyurea coating with discrete glass fibers applied to the tension face. This panel was compared to H-FG, H-A/F and H-A. This panel will later be

compared to H-FG-B/F. Images of the initial setup and panel are illustrated in **Figure 4.25**.

(a) Front Profile View (b) Isometric View

Figure 4.25 – H-FG-A/F Prior to Blast Events

The 1.4 kg (3.0 lb) charge at 310 mm (12 in) standoff blast event resulted in a considerable amount of cosmetic damage to the panel and great damage to the FA-WF layer but the residual deflection and cracking noticed in the SFRC layer was negligible. Several large pieces of the FA-WF broke off the panel as illustrated in **Figures 4.26b and 4.26c**. It appeared as though the FA-WF layer also cracked along the thicker support areas, suggesting end action, and along the steel reinforcement lines, suggesting a need for more reinforcement spaced closer together. In the SFRC layer it was difficult to observe cracking due to some polyurea on the sides, and with close examination no cracking was observed. While the damage appears to be dramatic this was a great result, because the FA-WF layer is intended as a sacrificial layer and there was no significant damage found in the SFRC layer.

(a) Front Profile View

(b) Isometric View

(c) Compression Face From Back

Figure 4.26 – H-FG-A/F After First Blast Event, 1.4 kg at 310 mm

The second blast event resulted in even more dramatic cosmetic damage but once again little damage to the SFRC and polyurea. This time almost the entire FA-WF and Styrofoam layer was blasted off the panel, only a small piece of FA-WF remained and it was only attached to the rebar. The dramatic damage makes the panel appear to be nearly destroyed, but in actuality the SFRC layer has some significant cracking but no punching meaning the SFRC layer still has strength. A 3.3 mm (0.13 in) flexural crack is illustrated

in **Figure 4.27c** and indicates the panel may have failed in flexural strength meaning the reinforcement has yielded. However, the flexural cracks in **Figure 4.27c** do not appear to propagate through the member. This and rough surface of the SFRC in **Figure 4.27d** make it difficult to determine if there is any surface cracking on the SFRC but the large residual deflection suggests there was significant cracking. **Figure 4.27e** shows the tension face of the panel and as it is apparent there was no bulging. **Figure 4.27f** illustrates that there was no cratering or sign of shear punching near the center of the panel. As mentioned before much of the reason for limited damage in these panels is due to the increased stand-off distance from the air-gap. The decreased damage may be additionally attributable to shock impedance mismatch between the layers. Overall, this panel system performed very well and the best of the hybrid systems.

(a) Front Profile View

(b) Isometric View

(c) Flexural Crack Back Face

(d) Rough Top Surface From Back

(e) Tension Face View

(f) Compression Face From Back

Figure 4.27 – Panel H-FG-A/F After Second Blast Event, 1.4 kg at 150 mm

The H-FG-A/F panel performed the best of the panels tested so far. Most of the damage occurred in the sacrificial FA-WF, allowing the base SFRC to be exhibit only minor damage including, small residual deflection and limited cracking. When comparing this panel to the control (H-FG) the first event was used. Comparing **Figures 4.1c and 4.26b** the level of damage to the FA-WF layers is dramatically different. In the control there was nearly no FA-WF left on the panel. The FA-WF layer held up much better in the H-FG-A/F indicating that the polyurea layer added to the panel's flexural strength.

When comparing this panel to the H-A and H-A/F the most important thing to note is that there was no punching failure or apparent punching failure in the SFRC layer. This means that the H-FG-A/F panel was more than adequate at containing the blast. Some of the decreased damage may also be attributable to dissipation in the blast wave energy caused by having the foam-gap and from strengthening provided by the polyurea layer.

4.11 FA-WF XS430 PANEL (H-B)

The H-B panel has a 50 mm (2 in) FA-WF layer, 90. mm (3.5 in) SFRC base, and a 6.4 mm (0.25 in) XS430 plain polyurea coating. This panel was compared to 1-H and H-A. The panel will be compared to H-B/F and H-FG-B/F in their respective sections. The initial setup and panel condition are illustrated in **Figure 4.28**.

(a) Front Profile View (b) Isometric View

Figure 4.28 – Panel H-B Prior to Blast Events

After the first blast—a 1.4 kg (3.0 lb) charge at a 310 mm (12 in) standoff—the damage was very minimal and most of the noticeable damage was a FA-WF piece breaking off. In this panel some small less than 0.61 mm (0.024 in) wide shear cracks developed near the supports as illustrated in **Figure 4.29c**. The lack of flexural cracking may be attributed to the lower strength higher ductility SFRC and Polyurea layers found in this panel. Several surface cracks were observed in the FA-WF layer then they were outlined with permanent marker to show up better when photographed, as illustrated in **Figure 4.29d**. The residual deflection was minimal in this panel and overall the panel performed well against the first blast event.

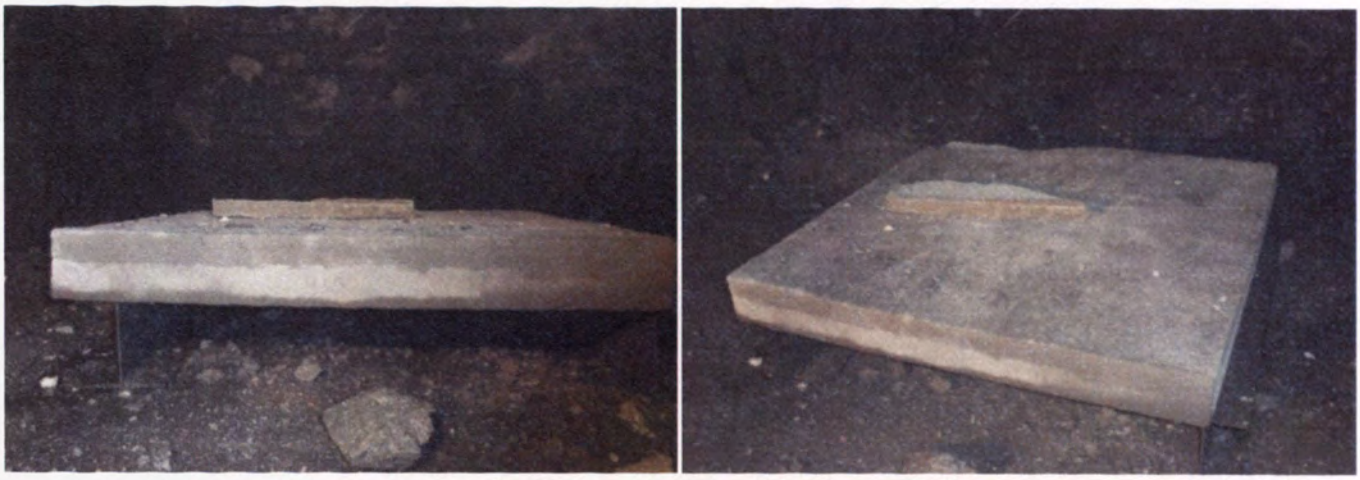

(a) Front Profile View (b) Isometric View

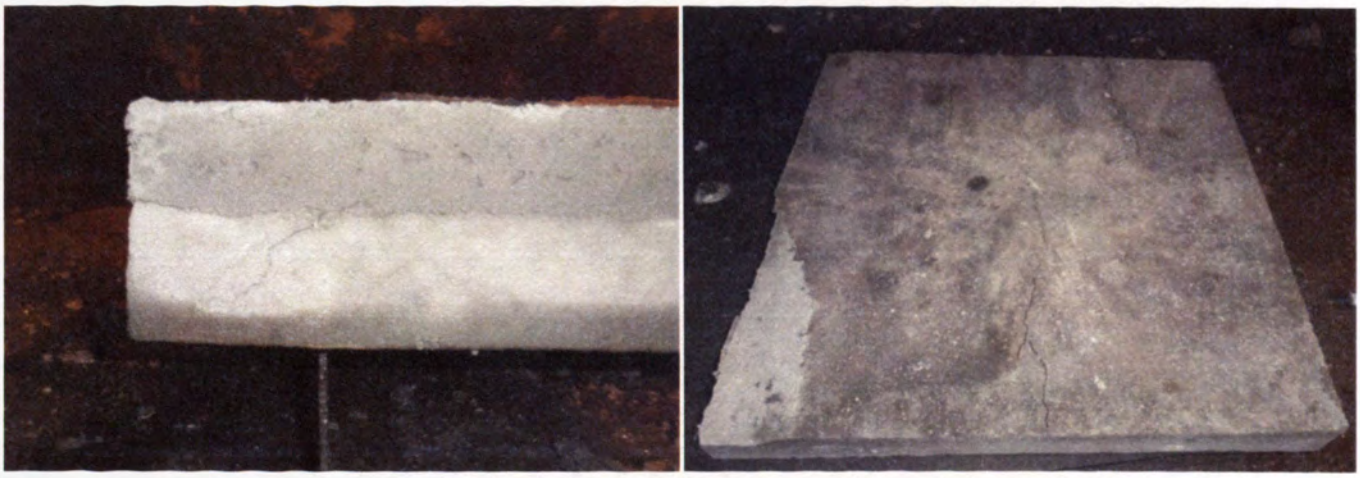

(c) Shear Cracking Front Face (d) Compression Face From Left Side

Figure 4.29 – Panel H-B After First Blast Event, 1.4 kg at 310 mm

The second blast brought a significant increase in damage. The shear cracks that formed in the initial blast opened up to 4.5 mm (0.18 in) wide and propagated through the FA-WF layer (**Figure 4.30c**). Although the shear cracking was significant there was no apparent flexural cracking. For this panel shear was of much greater concern, including a large crater in the center of the panel indicating a shear punching failure occurred and is

illustrated in **Figure 4.30d**. **Figure 4.30e** illustrates the bulge that resulted from the shear punching failure. Although the bulge was very large no tearing was noticed in the polyurea layer. This means that the panel may have failed in regards to strength but for the purpose of containing the blast it was adequate. Overall the panel performed well and the highly ductile materials that made up the panel allowed it to deflect considerably without considerable flexural cracking.

The H-B panel performed much better than panel 1-H. The 1-H panel exhibited significant shear cracking and shear punching failure that punctured through the panel after the second event. The H-B panel exhibited similar damage with less significant cracking than 1-H panel and instead a full puncture, which was present in the 1-H panel, the H-B exhibited bulging in the polyurea layer that indicates shear punching. This shows the one of the significant benefits of polyurea is containing spalling and fragmentation.
In the H-B panel, the first event did not result in any visible flexural damage, which may be due to flexural strengthening from the polyurea layer. However, when comparing to the H-A panel, only the H-A panel exhibited visible flexural cracking after the first blast event. A possible explanation may be that polyurea B in combination with the lower strength concrete was a more elastic system allowing the panel to flex more without cracking. In addition to the lack of flexural cracks after the first event the H-B panel also exhibited better results in regards to overall residual deflection. This means that the H-B panel was able to better contain the blast while maintaining more residual structural integrity than the H-A panel

(a) Back Profile View

(b) Isometric View

(c) Shear Cracking Front Face

(d) Cratering in Compression Face

(e) Bulge in Tension Face

Figure 4.30 – Panel H-B After Second Blast Event, 1.4 kg at 150 mm

4.12 FA-WF XS430F PANEL (H-B/F)

The H-B/F panel has a 50 mm (2 in) FA-WF layer, 90. mm (3.5 in) SFRC base, and a 6.4 mm (0.25 in) XS430 polyurea coating with discrete glass fibers. This panel was compared to the 1-H, H-A/F, and the H-B panels and will later be compared to the H-FG-B/F panel. The initial pre-blast images are illustrated in **Figure 4.31**.

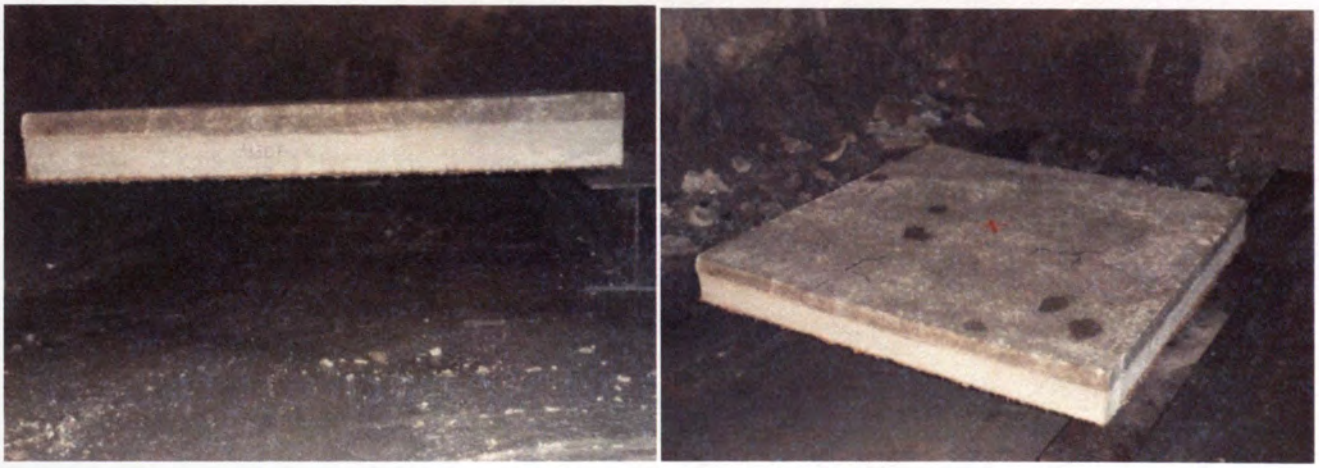

(a) Front Profile View (b) Isometric View

Figure 4.31 – Panel H-B/F Prior to Blast Events

The first blast event, which was a 1.4 kg (3.0 lb) charge at a 310 mm (12 in) standoff, resulted in little damage. A small piece of the FA-WF broke off of the corner and several surface cracks also developed, which is illustrated in **Figure 4.32b and 4.32d**. Several small less than 0.5 mm (0.02 in) flexural cracks did develop in this panel and are illustrated in **Figure 4.32c**. The small flexural cracks indicate that while the concrete exceeded its tensile strength the flexural steel did not yield. The flexural and surface cracks were outlined with permanent marker so they would show up when photographed. Scarring developed under the charge and is illustrated in **Figure 4.32 d**.

The residual deflections were insignificant and overall the panel contained the first blast event very well.

(a) Front Profile View (b) Isometric View

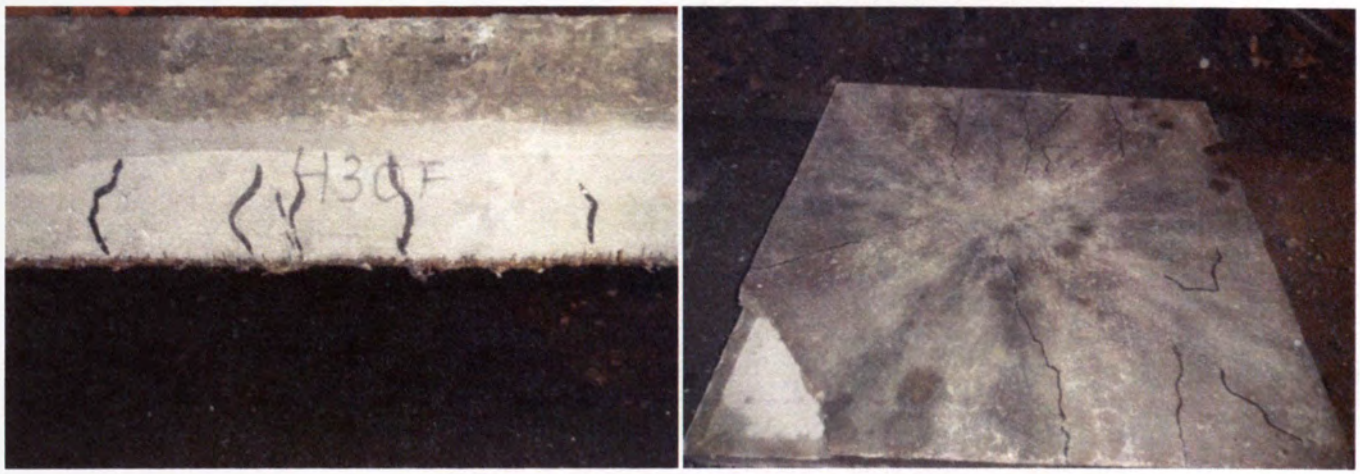

(c) Flexural Cracking in the Front Face (d) Compression Face From Left

Figure 4.32 – Panel H-B/F After First Blast Event, 1.4 kg at 310 mm

The second blast event, which was 1.4 kg (3.0 lb) charge at a 150 mm (6.0 in) standoff, increased the damage, but the panel was still able to contain the blast. Several additional flexural cracks developed, which are illustrated in **Figure 4.33c**, the ones

outlined in black are from the first even while the rest is new. Despite additional flexural cracks developing, all the flexural cracks observed were still less than 0.5 mm (0.02 in) wide. In addition to the flexural cracks a significant 3.5 mm (0.14 in) wide shear crack also developed propagating through the top of the SFRC layer (**Figure 4.33d**). A slight bulge developed in the tension face (**Figures 4.33f and 4.33g**) and the compression face exhibited a small crater (**Figure 4.33 e**), indicating a punching failure occurred. The panel exhibited both flexural and shear damage; however, it appears that the panel failed in shear only. While the SFRC layer may have failed with regards to strength the panel system adequately contained the blast.

(a) Front Profile View (b) Isometric View

Figure 4.33 – Panel H-B/F After Second Blast Event, 1.4 kg at 310 mm

(c) Shear Crack in the Front Face

(d) Flexural Cracks in the Front Face

(e) Compression Face From Left

(f) Bulge in Tension Face

(g) Bulge in Tension Face

Figure 4.33 cont. – Panel H-B/F After Second Blast Event, 1.4 kg at 150 mm

This panel was able to contain the blast and exhibit the least amount of damage of all the non-foam-gap panels. When comparing to both the 1-H and H-A/F it is easy to determine this panel system outperformed them because it was not punctured. The lower strength more ductile polyurea B gives some understanding to why the H-B/F panel was not punctured and the H-A/F panel was. In addition to no presence of punctures, the H-B/F panel had smaller residual deflections than either the 1-H or H-A/F panels. This panel however performed very similar to the H-B panel with a smaller bulge from the second blast event. Flexural cracking was not very prevalent in either the H-B/F than the H-B panel, which was unexpected as the two panels had the same strength SFRC layer and the intention of adding the discrete E-glass fibers to the polyurea was in part to improve the flexural strength of the composite. Both the H-B/F and H-B panels exhibited better flexural performance than any of the other panels.

4.13 FA-WF XS430F FOAM-GAP PANEL (H-FG-B/F)

The H-FG-B/F panel has a 50 mm (2 in) FA-WF layer, 76 mm (3.0 in) air-gap formed with stryofoam, and a 90. mm (3.5 in) SFRC base with a 6.4 mm (0.25 in) XS430 polyurea coating with discrete glass fibers applied to the tension face. This panel will be compared to the H-FG, H-FG-A/F, H-B, and H-B/F panels later in this section. Images of the initial setup and panel are illustrated in **Figure 4.34**.

(a) Front Profile View (b) Isometric View

Figure 4.34 – Panel H-FG-B/F Prior to Blast Events

The 1.4 kg (3.0 lb) charge at a 310 mm (12 in) standoff blast event did significant damage to the sacrificial FA-WF layer. **Figure 4.35c** shows where a piece has broken off and all the other surface cracks. The FA-WF layer cracked along the line of thicker supports indicating end action was present. It was noted from the shape and location of the cracks present in the FA-WF layer, that the layer would not be able to withstand additional loading. The SFRC panel appeared to have no significant damage as there was no visible cracking and the residual deflections were measured on the FA-WF layer so they appear more significant than the actual situation present in the SFRC layer.

(c) Back Profile View

(d) Isometric View

(c) Compression Face From Right

Figure 4.35 – Panel H-FG-B/F After First Blast Event, 1.4 kg at 310 mm

The 1.4 kg (3.0 lb) charge at a 150 mm (6.0 in) standoff blast event resulted in nearly all the FA-WF layer detaching from the panel and a significant flexural crack. Similarly to panel H-FG-A/F the damage is aesthetically very substantial but most of the damage was to the sacrificial FA-WF layer. Only a couple pieces of the FA-WF layer remained but even they were only attached to the reinforcement bars as illustrated in **Figure 4.36b**. The 1.2 mm (0.047 in) wide flexural cracks visible in **Figure 4.36c**

contributed to the residual deflection and suggest the rebar has yielded, meaning the panel has failed in flexure. As illustrated in **Figure 4.36d** one of the flexural cracks continued along the surface. **Figure 4.36e** displays that despite the significant damage to the panel no bulging or tearing was exhibited in the polyurea layer.

This panel and the H-FG-A/F panel performed the best at containing the blast while allowing the least amount of damage to the SFRC layer. The control H-FG lost most of its sacrificial layer during the first blast and while little damage was found in the SFRC layer, of the H-FG panel, the damage was similar to the damage found in the H-FG-A/F and H-B/F-AG after the second blast event. The E-glass DFRP-foam-gap panels only saw significant damage to the sacrificial layer and flexural cracking in the SFRC layer while the rest of the panels saw significant shear punching damage that reduced the panels to being structurally unsound. This means that the foam-gap panels were the best at containing the blast events tested. As mentioned earlier this limited damage is likely due to the increased stand-off distance provided by the presence of the foam-gap.

Comparing H-FG-A/F and H-FG-B/F it is a little more difficult but the only important measurable difference is the residual deflections. From this the H-FG-B/F panel was slightly better at containing the blast.

(a) Front Profile View

(b) Isometric View

(c) Flexural Cracks Front Face

(d) Crack in the Compression Face

(e) Tension Face

Figure 4.36 – Panel H-FG-B/F After Second Blast Event, 1.4 kg at 150 mm

4.14 RESIDUAL DEFLECTIONS

The residual deflections were found to provide some quantitative data. The process of obtaining the deflections can be found in Section 3.1.3. The results from the residual deflection data were used in the comparisons of panels present the earlier sections of Chapter 4. To better visualize the data, bar graphs were created for each blast event. **Figures 4.37** and **4.38,** and **Table 4.1** display the residual deflection data for the first and second blast event. Some panels do not have data for a certain event, which is a result of either that blast event was not tested on that panel, or the damage of some of the panels made it difficult or impossible to accurately measure the residual deflections. The panels with missing data were notated with either a NT for not tested, or UM for un-measureable.

Table 4.1 – Residual Deflection Data

	Residual Deflections (in)			
	First Event		Second Event	
Panel	Mid	Spans	Mid	Spans
SFRC-3.5	38.0	UM	NT	NT
SFRC-5.5	0.8	1.6	24.6	18.3
1-RC	34.9	60.3	NT	NT
2-RC	28.6	31.0	NT	NT
1-H	10.3	12.3	NT	108.0
2-H	5.6	6.0	50.8	23.8
H-FG	21.4	25.4	NT	NT
H-A	6.4	6.4	62.6	27.8
H-A/F	3.2	7.1	58.8	23.4
H-FG-A/F	UM	10.3	20.4	17.2
H-B	2.4	3.2	UM	10.7
H-B/F	1.3	1.6	UM	9.5
H-FG-B/F	11.1	14.3	8.0	7.1

Unit conversion 1.00 mm=0.0394 in

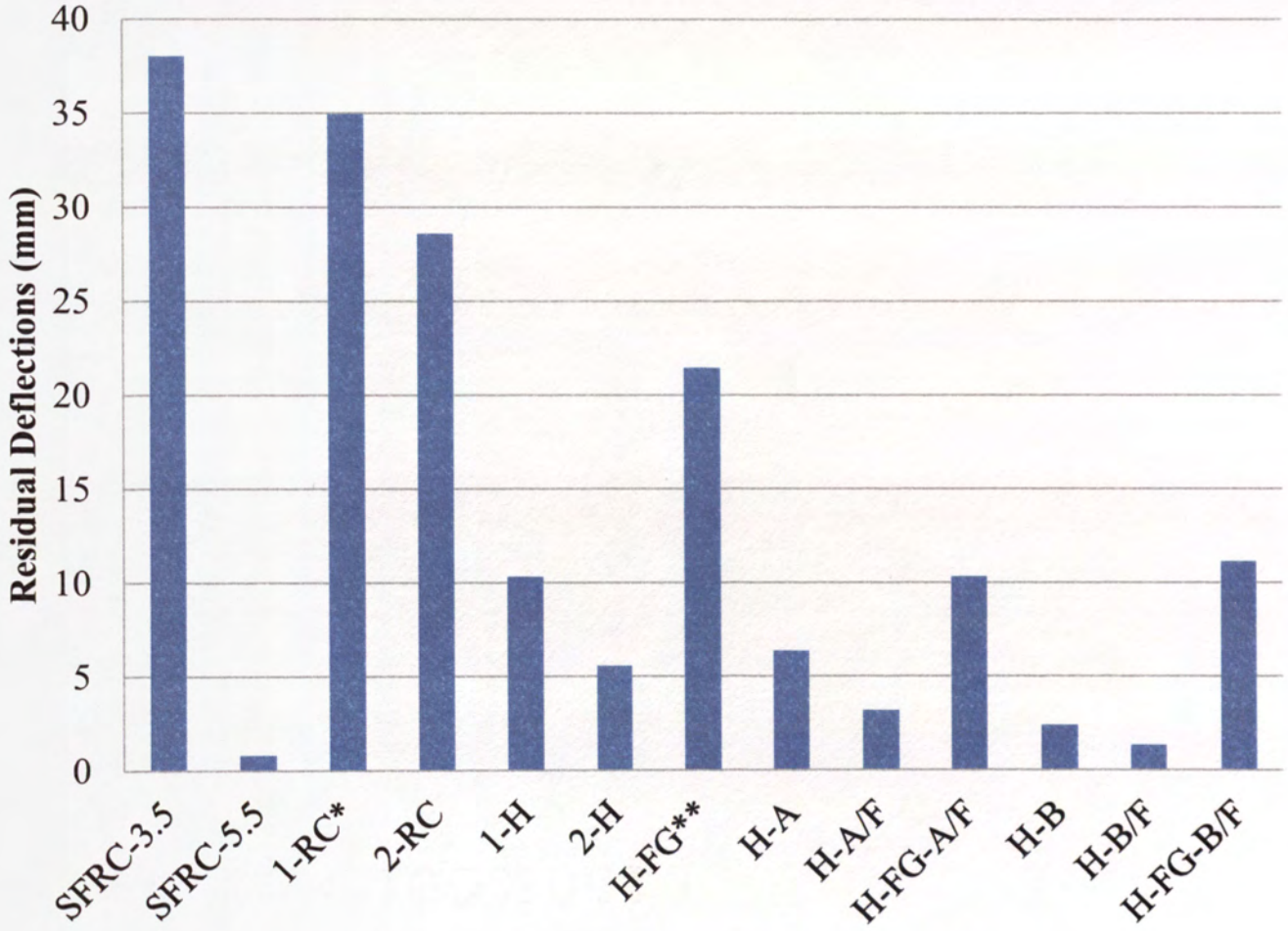

* The blast event was 1.4 kg with a 150 mm standoff
**Measured on the SFRC layer after the FA-WF layer was cleared off

Figure 4.37 – Residual Deflection Data for the First Event

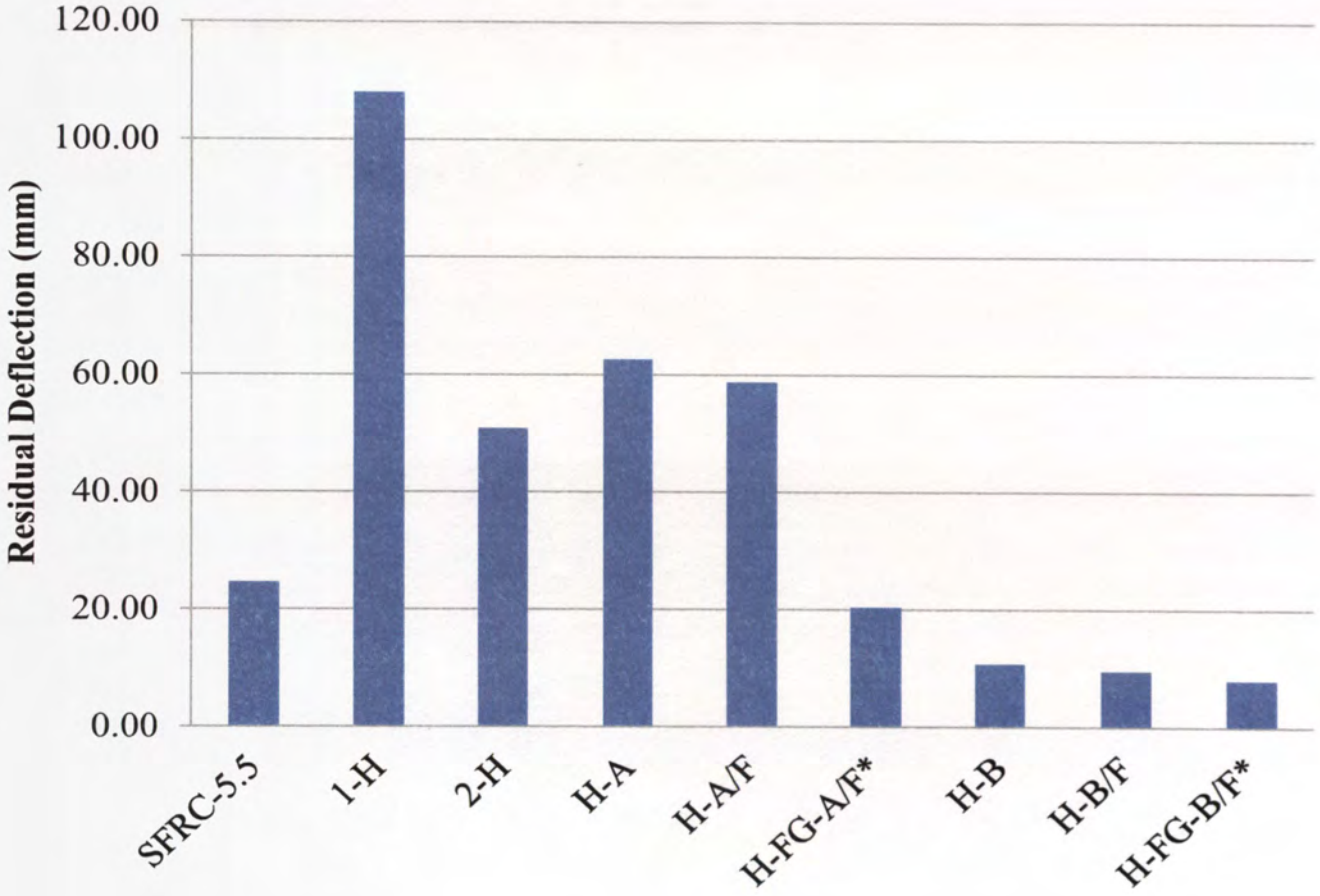

* Measured on the SFRC layer after the FA-WF layer was cleared off

Figure 4.38 – Residual Deflection Data for the Second Event

The residual deflection data showed the polyurea B panels performed the best with the SFRC-5.5 panel shortly behind. The residual deflections for the H-FG-B/F panel get smaller in the second event, which happened because the residual deflections taken after the first event were measured on the FA-WF and the residual deflections after the second event were measured on the SFRC layer because the FA-WF layer was nearly completely removed. The only two panels that had no bulging or hole after two blast events were the H-FG-A/F and H-FG-B/F panels, which indicates that these panels withstood the two blast events while maintaining structural integrity in the SFRC layer.

4.15 MASS LOSS

Another source of quantitative data is estimated mass loss. The mass loss was estimated with the use of images and AutoCAD. A visual method was selected due to the complexity of determining a representative mass loss for a panel. Part of the complexity in finding the mass loss stemmed from the multiple layers. If a panel loses 26% of its original mass but it is all in the sacrificial layer, as is the case in the H-FG-A/F panel, the damage to the panel is insignificant but stating that the panel lost 26% of its mass indicates very significant damage. This meant that measuring the physical mass of the panel before and after blast testing was not representative of the actual damage. Another issue was the difficulty in measuring the physical mass at the Missouri S&T Experimental Mine. Even if the physical mass would have been taken visual methods would have had to have been used to differentiate the mass loss anyways.

To determine the estimated mass loss an image that best showed the compression face of the panel was copied into AutoCAD. Then a polygon was drawn tracing the outside of the panel and additional polygons were drawn tracing the areas of damage. The areas of damage were then broken down into 3 area damage categories: Penetrating damage, sacrificial damage, contained damage. Once the area was drawn, the hatch feature in AutoCAD, which allows the drawer to fill in polygons with patterns, was used to differentiate the categories of damage. The area of damage described as contained damage were developed by drawing lines along the cracking on the top surface or estimated based on other images of the panel and is a very rough estimate. The other areas of damage were based on tracing the fracture lines. An area calculation tool in AutoCAD was utilized to determine the drawn areas. The area from the polygon that

traced the outside of the panel was compared to the calculated area of a typical panel which is 1.395 m^2 (2162 in^2) to develop a scale for damage found in the center of the panel. If the damage was not in the center of the panel then a line was drawn from side to side through the center of the damage. Then the length of the line drawn through the damage was compared to the length of the panel 1180 mm (46.5 in) to develop a scale. The appropriate scale was then multiplied with its corresponding area of damage to develop the scaled areas of damage. These scaled areas of damages were then multiplied by the depth of the layer they were in to develop a volume. The volume was then multiplied by the densities established in Section 3.2.4 to determine the mass of the area of damage. This value was compared to a calculated mass of the original panel to determine a percentage of damage. The data for estimated mass loss broken down by category is displayed in **Figure 4.39, and Table 4.2**.

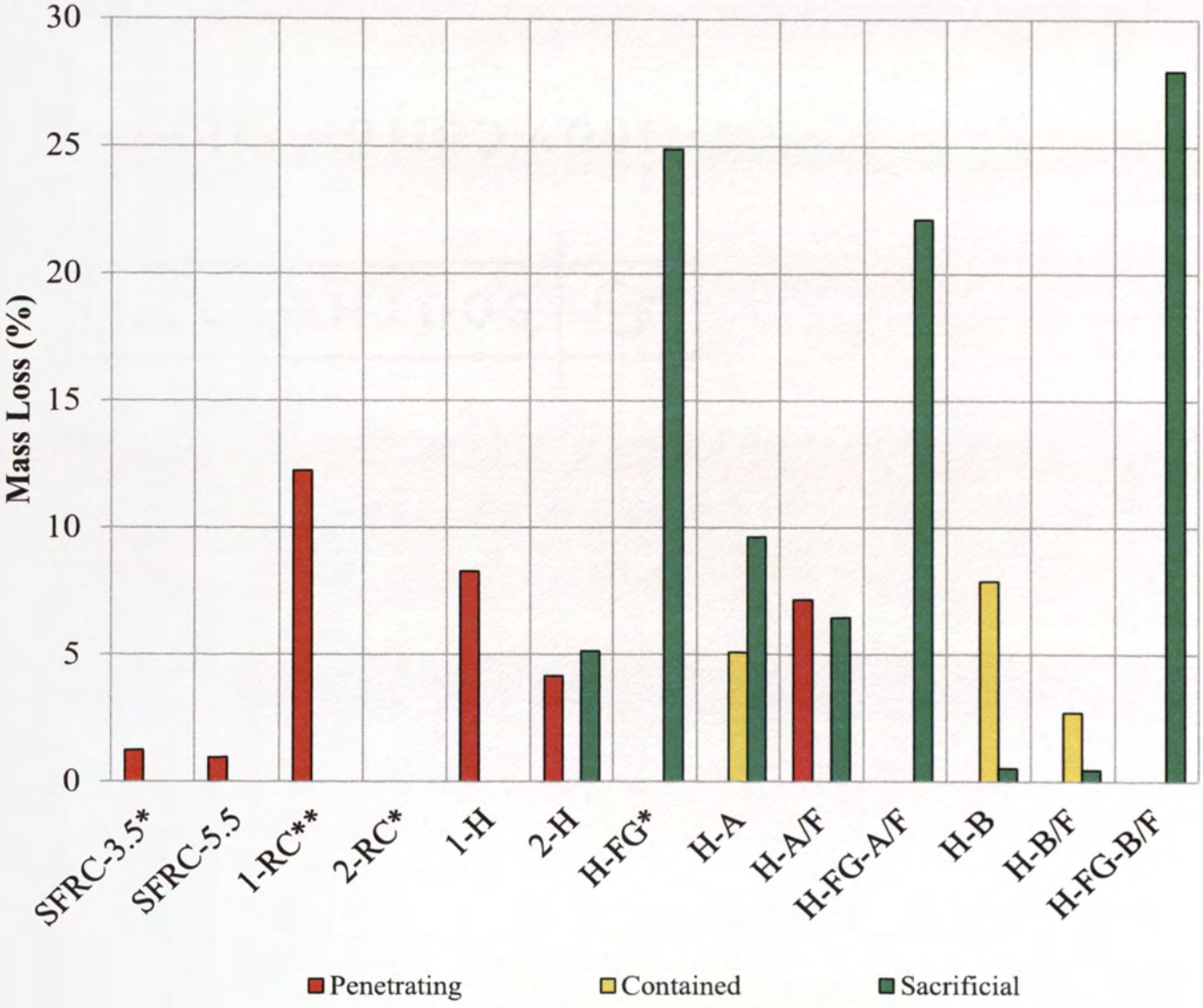

* Indicates one blast event at 310 mm standoff tested
** Indicates one blast event at 150 mm standoff tested

Figure 4.39 – Estimated Mass Loss–By Category

Table 4.2 – Estimated Mass Loss–By Category

	Estimated Mass Loss							
	Penetrating		Sacrificial		Contained		Total	
Panel	(kg)	(%)	(kg)	(%)	(kg)	(%)	(kg)	(%)
SFRC-3.5	0	0	N/A	N/A	N/A	N/A	0	0
SFRC-5.5	4.195	0.947	N/A	N/A	N/A	N/A	4.195	0.947
1-RC**	34.53	12.25	N/A	N/A	N/A	N/A	34.53	12.25
2-RC*	0	0	N/A	N/A	N/A	N/A	0	0
1-H	32.25	8.274	0	0	0	0	32.25	8.274
2-H	16.18	4.152	20.03	5.14	0	0	36.22	9.293
H-FG*	0	0	111.7	24.89	0	0	111.7	24.89
H-A	0	0	37.54	9.632	19.8	5.082	57.34	14.71
H-A/F	27.89	7.155	25.17	6.458	0	0	53.05	13.61
H-FG-A/F	0	0	99.25	22.13	0	0	99.25	22.13
H-B	0	0	2.026	0.52	2.026	0.52	4.053	1.04
H-B/F	0	0	1.769	0.454	10.55	2.706	12.32	3.16
H-FG-B/F	0	0	276.6	27.97	0	0	276.6	27.97

* Indicates one blast event at 310 mm standoff tested
** Indicates one blast event at 150 mm standoff tested
Unit Conversion 1.0 kg=2.2 lb

The penetrating damage mass loss is the worst damage as it is an estimation of the material to penetrate through the panel creating shrapnel or fragmentation that can greatly contribute to injuries and loss of life. Comparing the penetrating damage bars it was obvious that the polyurea panels are much better at preventing this damage. Only one panel that contains polyurea, the H-A/F panel, had any penetrating damage and this was the result of a significant tear in the e-glass DFRP layer.

The contained damage indicates a loss of strength in the base panel from fragmented pieces that are trapped in the bulging polyurea layer. This damage is the second most harmful as it does indicate a loss in strength, and could cause the structure to

collapse, if it occurs in a structural component. Comparing this damage indicates that the two foam-gap panels with DFRP performed the best as they ended up with no contained damage, meaning the base SFRC layer was more intact and less likely to contribute to a collapse.

The sacrificial damage is from pieces of the sacrificial FA-WF layer breaking off. The sacrificial damage is the least harmful because it occurs on the exterior of the structural component making the chance this damage causing any additional harm unlikely. When comparing this damage the foam-gap panels had significantly more damage than rest of the panels, which was expected.

Overall the panels that performed the best according to mass loss were the foam-gap panels with e-glass DFRP. The reason why the H-FG, SFRC-3.5, and 2-RC panels do not rank better is they were only tested with one blast event. A good indicator of the damage of the second event can be determined by comparing the damage between 1-RC and 2-RC. The 1-RC was subjected to only the 150 mm (6.0 in) blast event and has over 12% mass loss where the 2-RC was subjected to only the 310 mm (12 in) blast event and has no recordable mass loss. This shows that despite the lack of damage in the H-FG, SFRC-3.5, and 2-RC panels they would have significant damage from the second event. Also only the 1-RC panel had any damage beyond just sacrificial damage after one blast event.

5. FINDINGS, CONCLUSIONS AND FURTHER RECOMMENDATIONS

This study consisted of the blast testing of 13 composite concrete panels. Testing was performed at the Missouri S&T Experimental Mine and consisted of two 1.4 kg (3 lb) charges of an RDX based C-4 explosive at two different stand-off distances. The objective of this research was to determine the performance of FA-WF in combination with SFRC and E-glass DFRP at resisting blast damage. The following is the findings, conclusions and further recommendations drawn from this investigation:

- The sacrificial high volume fly ash-wood fiber (FA-WF) material provided an improvement over no additional layer. The 1-H, 2-H panels saw less significant residual deflections and cracking after the first blast event than the SFRC-3.5 panel.
- The control panels with the FA-WF layer (1-H and 2-H) did not perform as well as the SFRC-5.5 panel. This indicates that an additional 50 mm (2 in) of SFRC is a more effective way resisting blast damage compared to a sacrificial layer alone.
- An investigation considering cost would be useful. The additional 50 mm (2 in) of SFRC proved to be better at resisting blast than 50 mm (2 in) of FA-WF. However, the FA-WF material is significantly less expensive than the SFRC material so if cost was considered it may find that FA-WF is a more cost effective way to resist blast. However, the FA-WF may also present some aesthetic concerns for architects.

- An investigation comparing using SFRC and FA-WF as a retrofitting layer would allow for a better comparison between the two materials. In the SFRC-5.5 panel, one lift of 140 mm (5.5 in) is not comparative to two separate lifts, which is present in the hybrid panels.
- The foam-gap significantly reduced the damage in the base layer. The foam-gaps present some issues though, they create a large amount of fragments on the blast side of the panel that may contribute to damage and injuries experienced outside the structure, although it is unlikely the fragmented pieces will cause significant damage beyond the blast wave effects to humans. Another related issue is that if a missile or two blast events are used the impact of the missile or first blast event is likely to reduce the sacrificial layer to rubble exposing the base layer.
- Future research should include a way to improve the foam-gap system. This could be achieved by using SFRC instead of FA-WF or by using mesh reinforcement in the layer on top of the foam-gap. Also the construction of the foam-gap can be improved by using a form that has a sturdy removable sheet to form the foam-gap or by using sheet metal.
- Future research should include a plain control panel tested with a standoff distance that would be equivalent to the standoff distance to the base layer in the foam gap panels. In other words a plain SFRC panel should be tested at a standoff of 430 mm (17 in) which is equivalent to the 310 mm (12.0 in) standoff in the foam gap panel after adding the 75 mm (3.0 in) styrofoam layer and 50 mm (2 in) FA-WF layer. After comparing the damage in the two

panels you could better determine if the reason for the decreased damage in the foam gap panels is due to increasing the standoff distance or if it is contributable to shock impedance mismatch.

- Future research should include a way to improve the bond between the SFRC and FA-WF to improve the FA-WF material's resiliency. The bond between the SFRC and FA-WF layers was very weak and may have resulted in some of the poor results.
- The panels with polyurea, in general, performed better than those without. The only two exceptions are the H-A/F and SFRC-5.5 panel. For all the panels except the H-A/F panel, the polyurea layer contained fragmented pieces, not allowing any material to penetrate the panel. This indicates that polyurea may be a lifesaving material, when used on walls of structures that are prone to explosive attacks.
- The e-glass DFRP had mixed results. The H-A/F panel tore allowing a significant amount of material to penetrate the panel. This was due mostly to the high fiber ratio present in the e-glass DFRP A, which resulted in a stiffer material that tore at a low elongation. The rest of the panels (H-B/F, H-FG-A/F, and H-FG-B/F) all showed signs that the polyurea layer added stiffness to the panel system. This was evident by the lower residual deflection values for these panels compared to the control and plain polyurea panels.
- Future research should include a better mechanism of integrating the glass fiber into the polyurea. One possibility is a better chopping and spraying mechanism like what is used in the fiberglass industry or using a mesh and

rolling it on and covering it with polyurea. A better mechanism of integrating fiber may also allow for other fiber type to be used, such as aramid and carbon.

- Future research should investigate the use of discrete fiber polyurea on a wall system. In other words a full scale test including either a concrete panel wall or concrete masonry unit wall.
- Future research should include multiple test panels of the same configuration. Multiples of each type of specimen add to the confidence in the final data.

6. BIBLIOGRAPHY

Ameren Corporation. "Chemical Composition, MRT Labadie, Silo C, sample date 3/4/11, sample ID #11MRSM037." Labadie Power Plant, 2011.

American Coal Ash Association. *Coal Combustion Products Production & Use Statistics.* ACAA Advancing the Management & Use of Coal Combustion Products. 2012. http://acaa.affiniscape.com/displaycommon.cfm?an=1&subarticlenbr=3 (accessed January 27, 2012).

American Coal Ash Association. "Fly ash Facts for Highway Engineers." Technical Report, Federal Highway Administration, 2003.

American Society for Testing and Materials (ASTM A370/A370M-11a). "Standard Test Methods and Definitions for Mechanical Testing of Steel Products." Standard, West Conshohocken, PA, 2011.

American Society for Testing and Materials (ASTM A370-11a). "Standard Test Methods and Definitionfor Mechanical Testing of Steel Products." Standard, West Conshohocken, PA, 2011.

American Society for Testing and Materials (ASTM A615/A615M-09b). "Standard Specification for Deformed and Plain Carbon-Steel Bars for Concrete Reinforcement." Standard, West Conshohocken, PA, 2009.

American Society for Testing and Materials (ASTM C150/C150M-11). "Standard Specification for Portland Cement." Standard, West Conshohocken, PA, 2011.

American Society for Testing and Materials (ASTM C192/C192M-07). "Standard Practice for Making and Curing Concrete Test Specimens in the Laboratory." Standard, West Conshohocken, PA, 2007.

American Society for Testing and Materials (ASTM C39/C39M-11a). "Standard Test Method for Compressive Strength of Cylindrical Concrete Specimens." Standard, West Conshohocken, PA, 2011.

American Society for Testing and Materials (ASTM C42/C42M-11). "Standard Test Method for Obtaining and Testing Drilled Cores and Sawed Beams of Concrete." Standard, West Conshohocken, PA, 2011.

American Society for Testing and Materials (ASTM C470/C470M-09). "Standard Specification for Molds for Forming Concrete Test Cylinders Vertically." Standard, West Conshohocken, PA, 2009.

American Society for Testing and Materials (ASTM C618-08a). "Standard Specificatoin for Coal Fly Ash and Raw or Calcined Natural Pozzolan for Use in Concrete." Standard, West Conshohocken, PA, 2008.

American Society for Testing and Materials (ASTM C78/C78M-10). "Standard Test Method for Flexural Strength Concrete (Using Simple Beam with Third-Point Loading)." Standard, West Conshohocken, PA, 2010.

American Society for Testing and Materials (ASTM D3039/D3039M-08). "Standard Test Method for Tensile Properties of Polymer Matrix Composite Materials." Standard, West Conshohocken, PA, 2008.

American Society for Testing and Materials (ASTM D412-06a). "Standard Test Methods for Vulcanized Rubber and Thermoplastic Elastomers-Tension." Standard, West Conshohocken, PA, 2006.

American Society for Testing and Materials. "Standard Test Method for Determining Tensile Properties of Fiber Reinforced Polymer Matrix Composites Used for Strengthening Civil Structures." Standard, West Conshohocken, PA, 2010.

Applied Research Associates, Inc. "Protecting the Protectors." 2004.

Argwal, Jai Prakash. *High Energy Materials: Propellants, Explosives and Pyrotechnics.* Weinheim: Wiley-VCH, 2010.

Baker, W E. *Explosions in Air.* Austin, TX: University of Texas Press, 1973.

Bulson, P S. *Explosive Loading of Engineering Structures.* London: E & FN Spon, 1997.

Carey, N. L., and J. J. Myers. "Discrete Fiber Reinforced Polymer Systems for Repair of Concrete Structures: Polyurea-fiber Characterization Results." 2010.

Carey, N., and J. J. Myers. "Blast and Impact Resistance of Hybrid System fo Barrier and Wall Panel Applicaitons." MS Thesis, Missouri University of Science and Technology, Rolla, MO, 2009.

Chock, Jeffrey M. K., and Rakesh K. Kapania. "Review of Two Methods for Calculating Explosive Air Blast." *The Shock and Vibration Digest* 33, no. 2 (2001): 91-102.

Coatanlem, Pascale, Raoul Jauberthie, and Frank Rendell. "Lightweight Wood Chipping Concrete Durability." *Construction and Building Materials* 20, no. 9 (2006): 776-781.

Cooper, Paul W. *Explosive Engineering.* Toronto: Wiley-VCH, 1996.

Crawford, John E., and Shengrui Lan. "Blast Barrier Design and Testing." *Karagozian and Case.* 2006. http://www.kcse.com/pdfs/P-06-1_add.pdf (accessed February 28, 2011).

Davidson, J. S., J. R. Porter, R. J. Dinan, M. I. Hammons, and J. D. Connell. "Explosive Testing of Polymer Retrofit Masonry Walls." *Journal of Performance of Constructed Facilities* 18, no. 2 (2004).

Durisol Building Systems, Inc. "Durisol Wall Form System." Technical Guide, 2006.

Durisol Building Systems, Inc. *The Durisol Material.* 2011. http://durisolbuild.com/material-shtml/ (accessed January 27, 2012).

Gonchar, Joann. "Greatest Hurdle is Securing Existing Federal Buildings." *Building for a Secure Future: Government.* Engineering News-Record. March 25, 2002. http://enr.construction.com/features/Buildings/archives/020325d.asp (accessed March 12, 2012).

Greene, C., and J. J. Myers. "Glass Fiber-Reinforced Polyurea Strengthening of Reinforced Concrete." MS Thesis, Missouri University of Science and Technolgy, 2010.

Halstead, Woodrow J. *Use of Fly Ash in Concrete.* Washington, D.C.: Transportation Research Board, National Research Council (U.S.), 1986.

Hill, John. "Changing Place/Changing Times." *Invisible Insurrection*, 2004.

Episode 176: Drain Disater. Directed by Pete Rees. Performed by Jamie Hyneman, Adam Savage, Tory Belleci, Kari Byron, & Grant Imahara. 2011.

HyperPhysics. *Amines.* 2010. http://hyperphysics.phy-astr.gsu.edu/hbase/organic/amine.html (accessed March 13, 2012).

Joshi, N., and J. J. Myers. "Investigation of an Alternative Wood Fiber-Fly Ash Material for Infill Wall Systems (CIES 06-60)." Center for Infrastructure Engineering Studies, University of Missouri, Rolla, MO, 2005.

LINE-X Protective Coatings Corp. *H.P. White Certification.* September 2007. http://www.linex.com/pages/2010/military/test_results/white_certification.php (accessed March 12, 2012).

LINE-X Protective Coatings Corp. *U.S. Air Force Approves Line-X for Bomb Blast Mitigation.* 2004. http://www.linex.com/pages/2010/military/test_results/air_force_test_results.php (accessed March 12, 2012).

Mazarak, Oleg, Claude Martins, and John Amanatides. "Animating Exploding Objects." Department of Computer Science, York University, 1999.

Michel, Lou, and Dan Herbeck. *American Terrorist: Timothy McVeigh and the Oklahoma City Bombing.* Manhattan: ReganBooks, 2001.

Nadel, Barbara A. "High-risk Buildings Placed in a Class All Their Own." *Building for a Secure Future: Environmental Design.* Engineering News-Record. March 25, 2002. http://enr.construction.com/features/Buildings/archives/020325c.asp (accessed March 12, 2012).

National Counterterroism Center. *TNT Equivalents for Various Explosives and Fuel-Air Mixtures.* 2011. http://www.nctc.gov/site/technical/tnt.html (accessed January 30, 2012).

Occupational Safety & Health Administration. *Isocyanates.* 2008. http://www.osha.gov/SLTC/isocyanates/index.html (accessed March 13, 2012).

Owens Corning. *BMC Chopped Strands.* 2012. http://www.ocvreinforcements.com/product-families/BMC_Chopped_Strands.aspx (accessed January 31, 2012).

PAXCON. *PAXCON Spray on Spall Lining.* 2011. (accessed March 12, 2012).

PAXCON. *What is Paxcon.* 2011. http://www.paxcon.co.uk/what-is-paxcon®.html (accessed March 12, 2012).

Polyurea Development Association. *What is Polyurea.* 2010. http://www.pda-online.org/whatispolyurea.asp (accessed March 13, 2012).

Propex Concrete Systems. "Novocon 1050." Product Data Sheet, Chattanooga, TN, 2007.

Security Management Consulting. "Safeguarding Buiding Perimeters for Bomb Attacks." *Security Articles & Tips.* May 12, 2010. http://www.secmgmt.com/safeguarding-building-perimeters-for-bomb-attacks/ (accessed March 12, 2012).

The Monarch Cement Company. *Mill Tests: Monarch Portland Cement Type I.* 2011. http://www.monarchcement.com/Products/portland.html (accessed January 9, 2012).

Tinsley, M, and J. J. Myers. "Investigation of High-Volume Fly Ash-Wood Fiber Material Subjected to Low Velocity Impact and Blast Loads (CIES 07-74)." MS Thesis, Center for Infrastructure Engineering Studies, University of Missouri-Rolla, Rolla, MO, 2007.

United States General Services Adminstration. "GSA Finalizes Site Security Design Guidelines." September 17, 2007. http://www.gsa.gov/portal/content/102765 (accessed March 12, 2012).

Wright, Andrew G., and Tom Ichniowski. "As Terror War Expands, Money Flows at Home." *Building For a Secure Future.* Engineering News-Record. March 25, 2002. http://enr.construction.com/features/Buildings/archives/020325a.asp (accessed March 2012, 2012).

APPENDIX A: TEST SETUP DRAWINGS

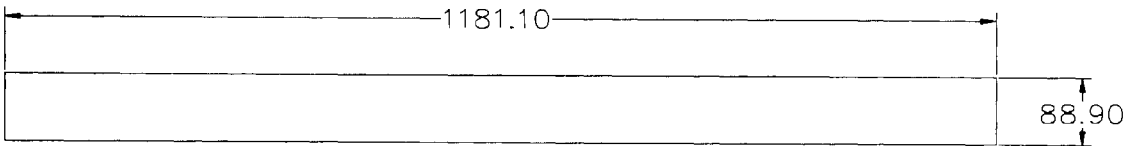

Unit conversion 1.0 mm=0.039 in

Figure A.1 – Panels SFRC-3.5, 1-RC, and 2-RC Profile in mm

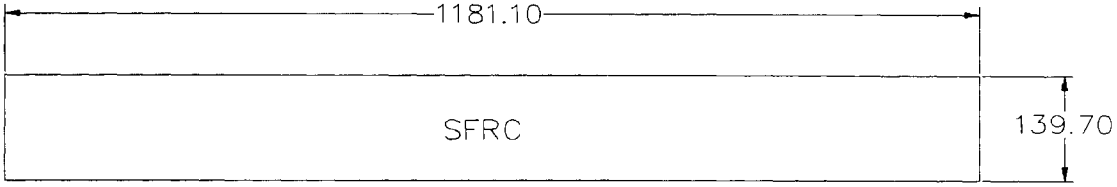

Unit conversion 1.0 mm=0.039 in

Figure A.2 – Panel SFRC-5.5 Profile in mm

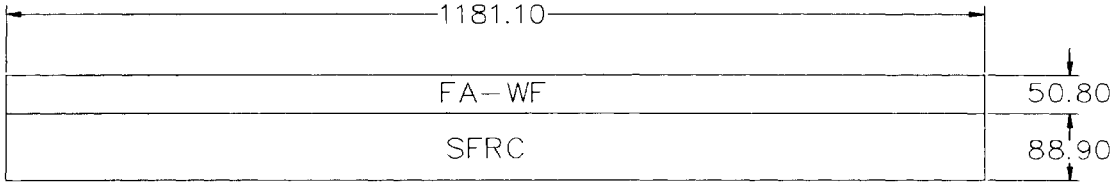

Unit conversion 1.0 mm=0.039 in

Figure A.3 – Panels 1-H, 2-H, H-A, H-A/F, H-B, H-B/F Profile in mm

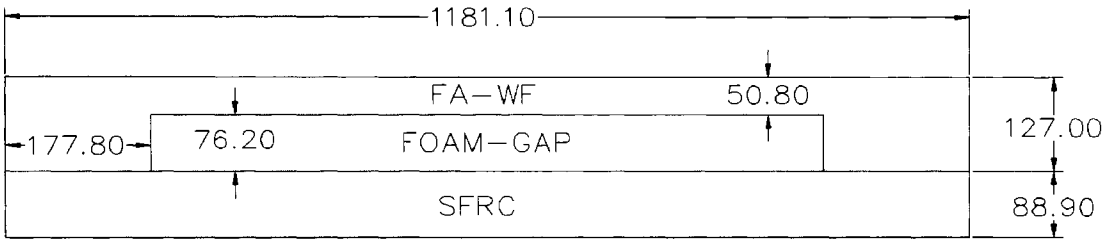

Unit conversion 1.0 mm=0.039 in

Figure A.4 – Panels H-FG, H-FG-A/F, H-FG=B/F Profile in mm

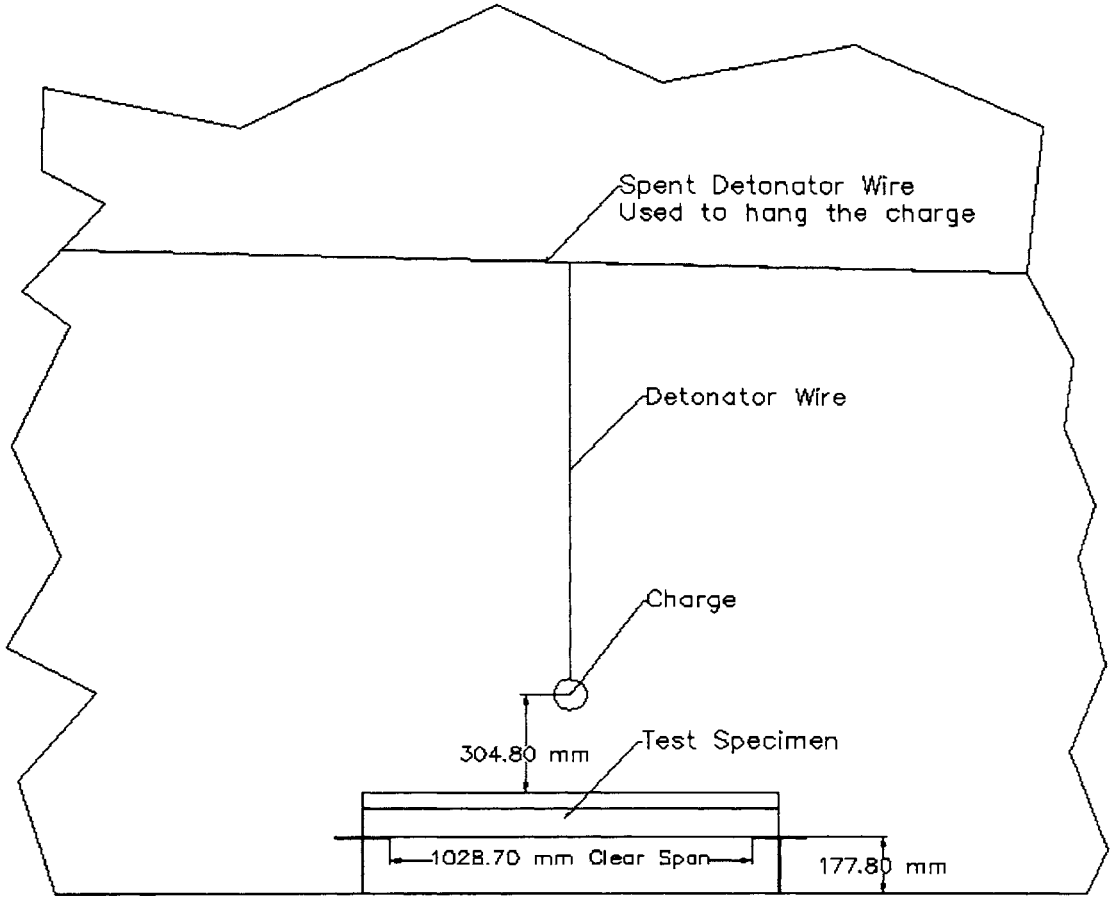

Unit conversion 1.0 mm=0.039 in

Figure A.5 – Blast Test Setup for 310 mm Standoff or First Event

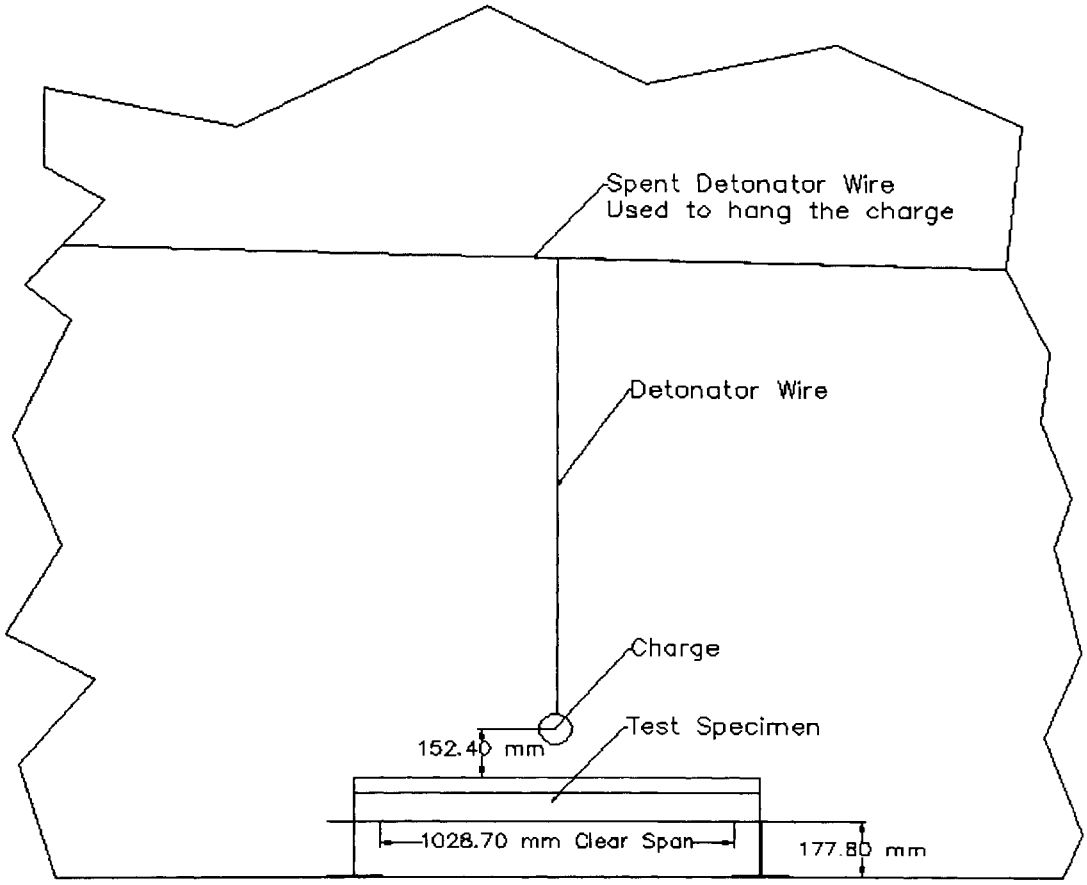

Unit conversion 1.0 mm=0.039 in

Figure A.6 – Blast Test Setup for 150 mm Standoff or Second Event

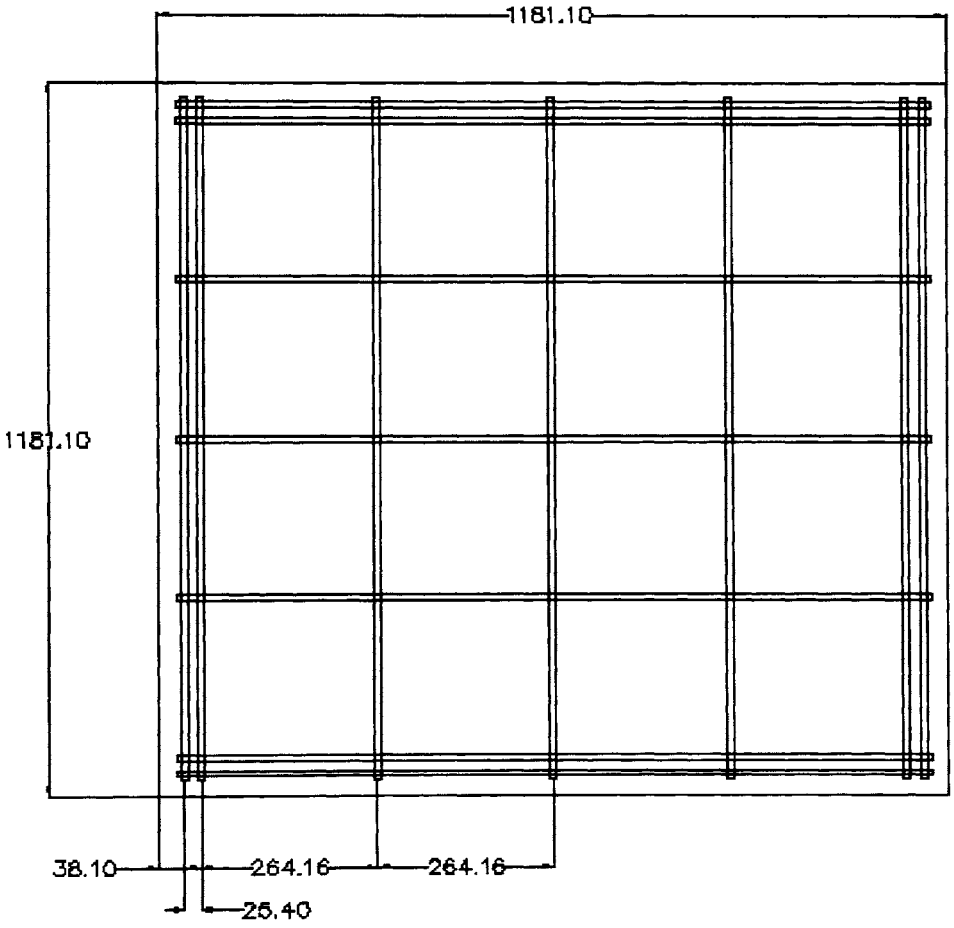

Unit conversion 1.0 mm=0.039 in

Figure A.7 – Rebar Layout in mm

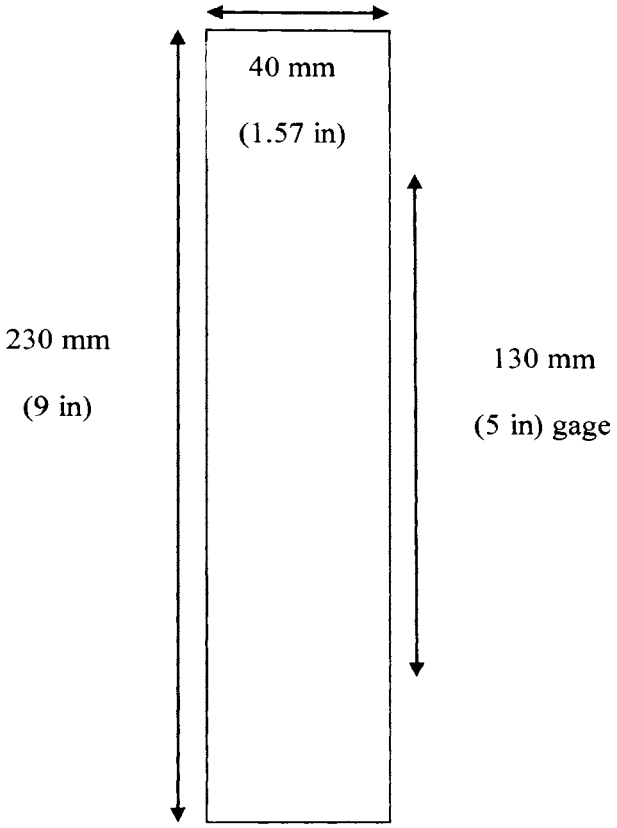

Figure A.8 – Coupon Test Specimen

APPENDIX B: CONWEP GRAPHS

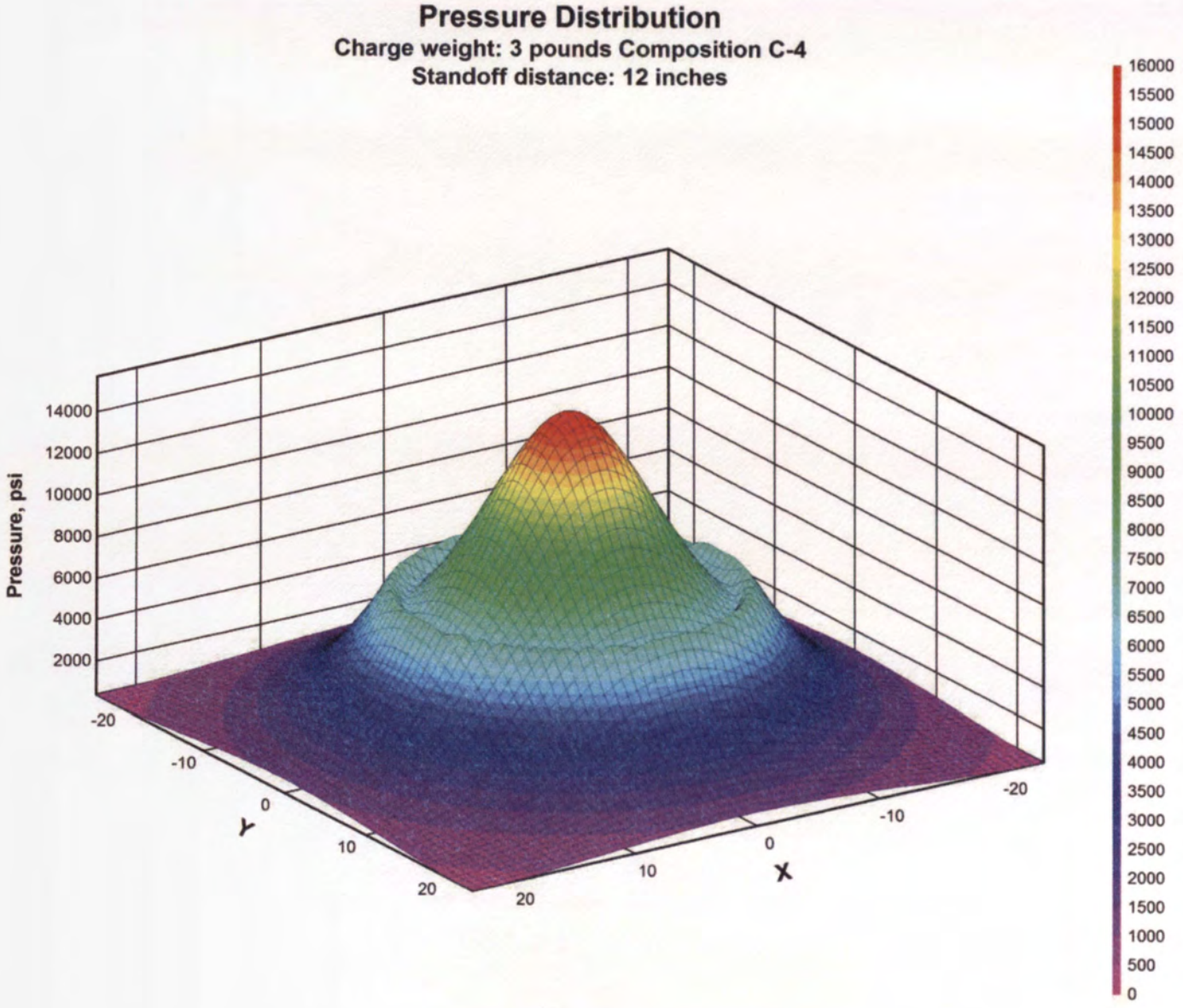

Unit conversions: 1.0 psi=6.9 KPa, 1.0 in=25 mm

Figure B.1 – Incident and Reflected Pressures for 1.4 kg C-4 at 310 mm

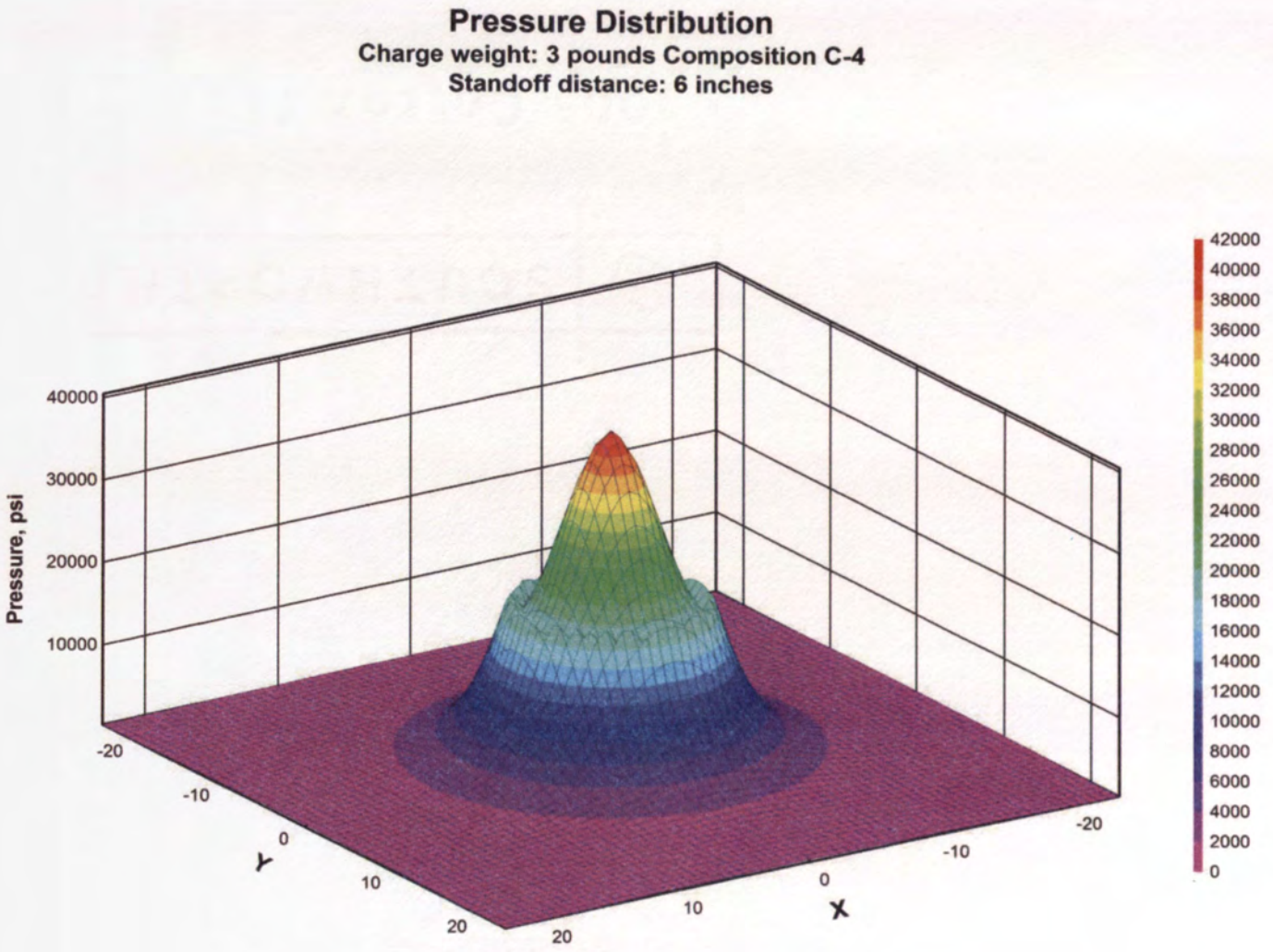

Unit conversions: 1.0 psi=6.9 KPa, 1 in=25 mm

Figure B.2 – Incident and Reflected Pressures for 1.4 kg C-4 at 150 mm

APPENDIX C: DFRP TENSILE DATA

Table C.1 – Coupon Test for Polyurea A with Discrete E-glass Fibers

	Yield Stress (MPa)	Strain @ Yield (%)	MOE (MPa)	Stress @ Break (MPa)	Strain @ Break (%)	Quality of Test
A/F-1	1.751241037	0.76	297.111142	3.461114175	4.04	Very Poor-Grips
A/F-2	1.3858246	0.45	507.549641	4.474627689	14.26	Good
A/F-3	2.592388307	2.52	190.237176	3.805846663	4.66	Poor-Bubbles
A/F-4	1.482349697	0.35	862.610314	4.488416988	6.22	Good
A/F-5	1.027302813	0.55	266.347215	2.985383343	8.33	Poor-Bubbles
A/F-6	1.833976834	1.28	164.285714	5.136514065	14.65	Good
A/F-7	1.640926641	0.63	375.013789	4.116105902	6.78	Poor-Bubbles
A/F-8	1.592664093	0.58	396.594043	4.619415334	7.81	Poor-Bubbles
A/F-9	1.39271925	0.51	419.105074	3.833425262	5.2	Poor-Bubbles
A/F-10	1.634031991	0.57	414.761445	4.943463872	11.59	Good
A/F-11	2.158025372	0.63	475.130998	5.894925538	8.07	Good
A/F-12	1.820187534	0.49	601.896029	5.074462217	8.11	Good
A/F-13	1.578874793	0.39	753.957529	4.543574186	9.03	Good
A/F-14	1.289299504	0.42	534.418092	4.902095974	10.46	Poor-Bubbles
A/F-15	1.151406509	0.55	297.262824	3.440430226	7.04	Poor-Bubbles
A/F-16	1.578874793	0.36	967.932984	5.467457253	8.45	Poor-Bubbles
A/F-17	2.027027027	0.98	249.862107	5.632928847	10.27	Good
Average	1.643360047	0.70705882	457.298595	4.518834561	8.52764706	
Std. Dev.	0.379549852	0.52269452	229.727654	0.823077453	3.00469119	
COV	1.592385854	0.73925181	3.46358316	1.255817331	0.35234704	

Table C.2 – Coupon Test for Polyurea B with Discrete E-glass Fibers

	Yield Stress (MPa)	Strain @ Yield (%)	MOE (MPa)	Stress @ Break (MPa)	Strain @ Break (%)	Quality of Test
B/F-1	2.275234418	0.64	489.8235	5.701875345	12.97	Poor-Bubbles
B/F-2	3.792057363	2.06	206.281	3.936845008	3.08	Poor-Bubbles
B/F-3	2.033921677	1.31	174.9173	4.074738003	17.37	Poor-Bubbles
B/F-4	2.619966906	0.35	1206.019	4.198841699	1.38	Very Poor-Grips
B/F-5	2.551020408	1.18	251.0411	4.612520684	16	Poor-Bubbles
B/F-6	2.516547159	1.06	282.9426	4.805570877	11.13	Poor-Bubbles
B/F-7	2.523441809	1.61	170.8081	4.336734694	37.27	Good
B/F-8	3.764478764	1.51	277.2339	5.108935466	3.93	Poor-Bubbles
B/F-9	2.426916713	1.46	183.4322	4.881412024	44.82	Good
B/F-10	1.241036955	0.87	170.3392	1.95118588	25.36	Poor-Bubbles
B/F-12	2.151130723	1.35	177.4821	4.43325979	25.33	Good
B/F-13	3.536955323	1.9	211.5003	5.384721456	26.08	Poor-Bubbles
B/F-14	2.557915058	1.78	153.9162	4.805570877	56.74	Good
B/F-15	3.006067292	0.86	444.0017	6.10176503	13.21	Poor-Bubbles
B/F-16	1.647821291	1.64	109.356	5.467457253	24.72	Poor-Bubbles
B/F-17	2.564809708	1.87	149.9035	4.357418643	33.49	Good
B/F-18	2.364864865	1.15	237.0794	4.702151131	38.43	Good
Average	2.563187437	1.329412	288.0045	4.63888258	23.018235	
Std. Dev.	0.674604262	0.472579	257.0185	0.911526528	15.483116	
COV	1.814600072	0.35548	6.152863	1.354778019	0.6726457	

APPENDIX D: DFRP TENSILE GRAPHS

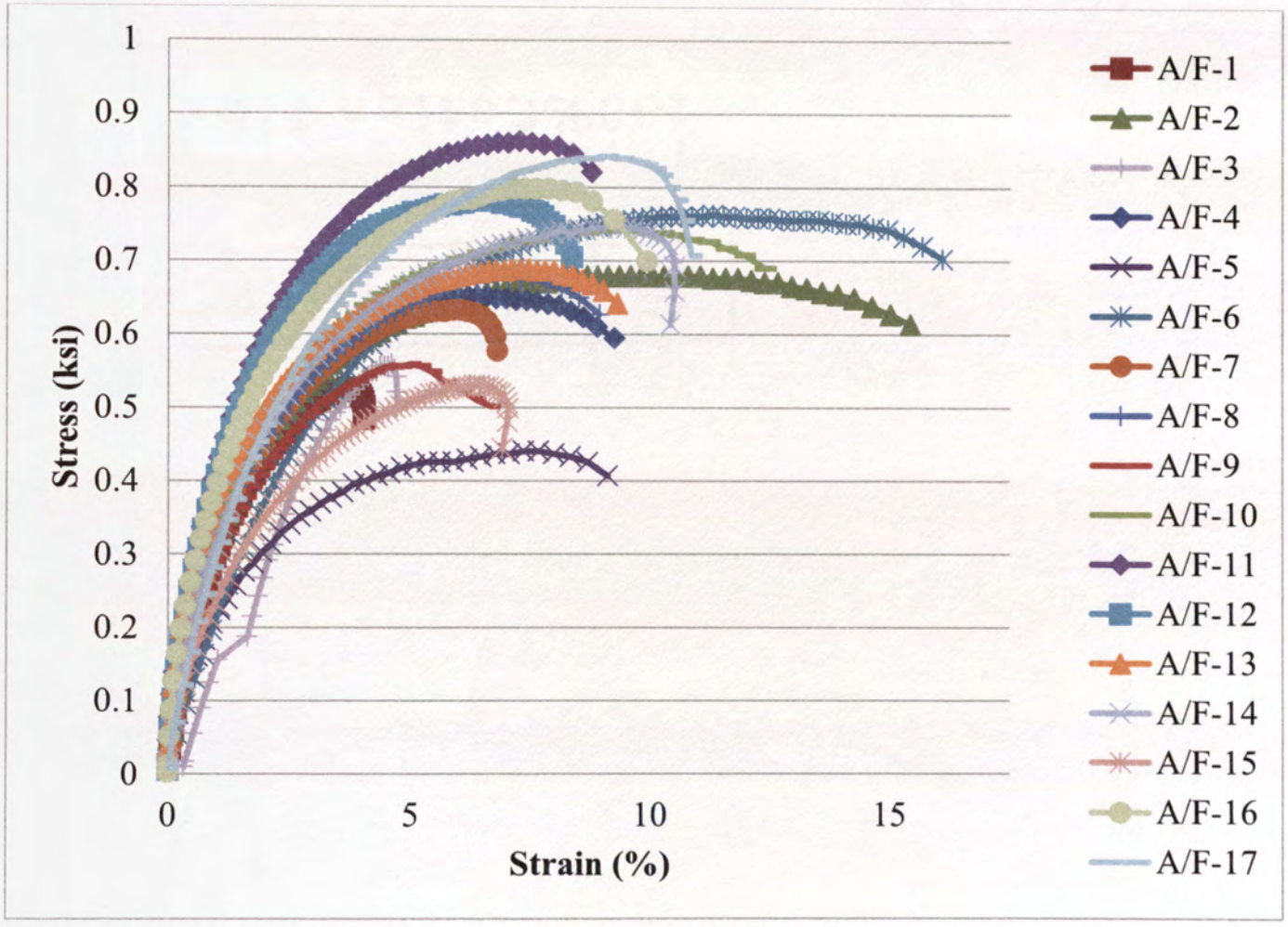

Unit conversion 1 ksi=6.895 MPa

Figure D.1 – Coupon Test for Polyurea A with Discrete E-glass Fibers

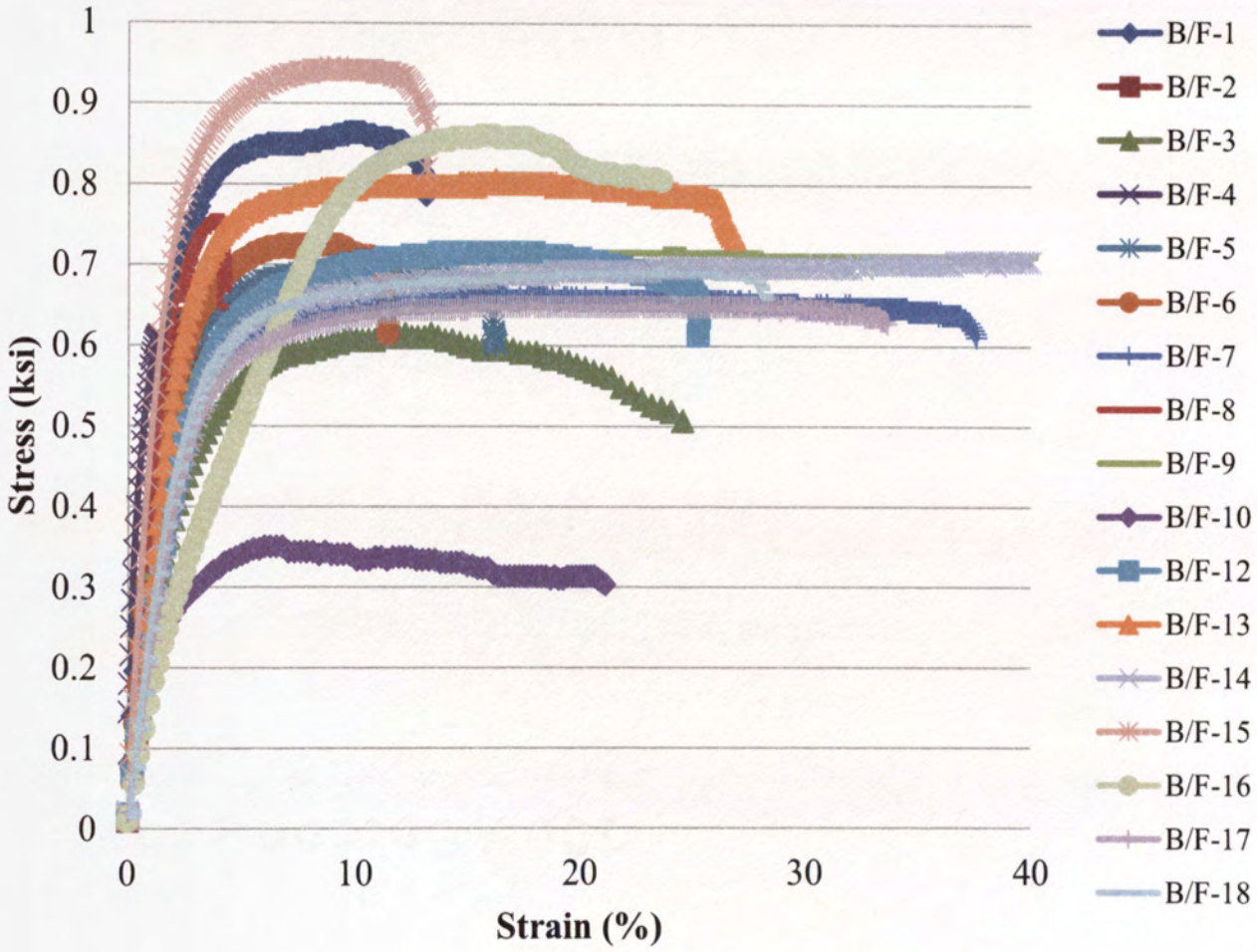

Unit conversion 1 ksi=6.895 MPa

Figure D.2 – Coupon Test for Polyurea B with Discrete E-glass Fibers

APPENDIX E: CRACK WIDTH ESTIMATION FIGURES

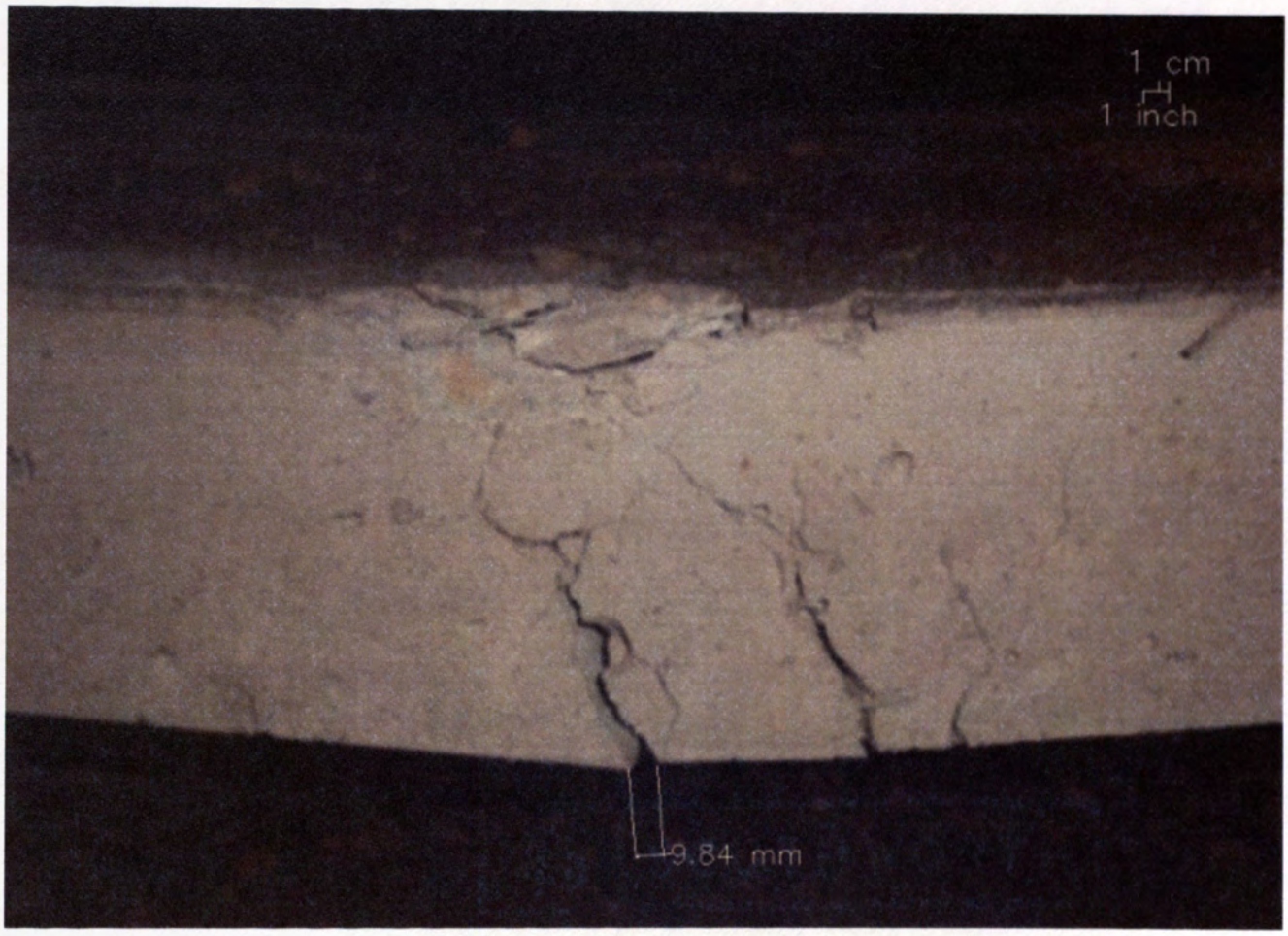

Figure E.1 – Flexural Cracks in the Front Face of SFRC-3.5

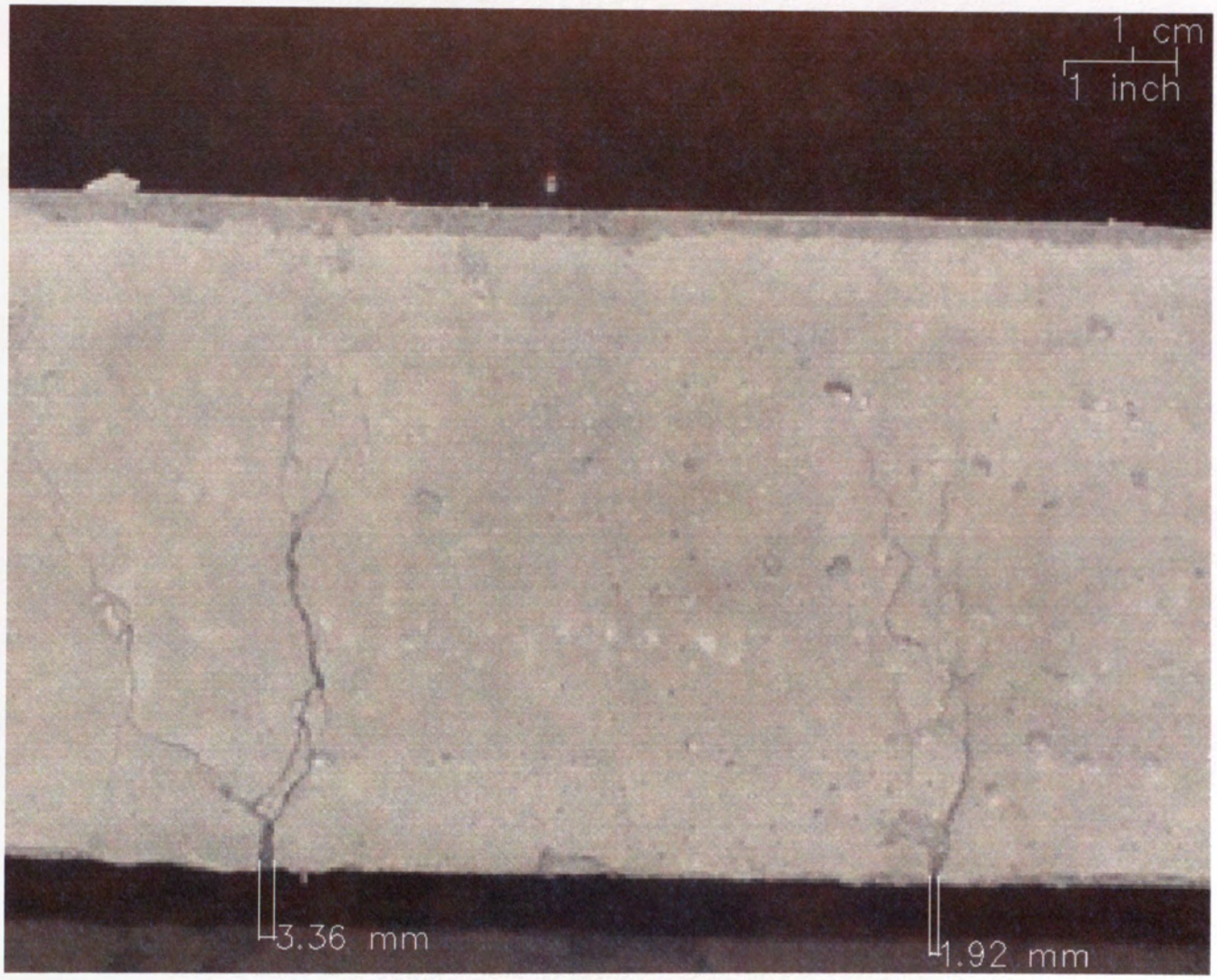

Figure E.2 – Flexural Cracks in the Back Face of SFRC 5.5, 2nd Event

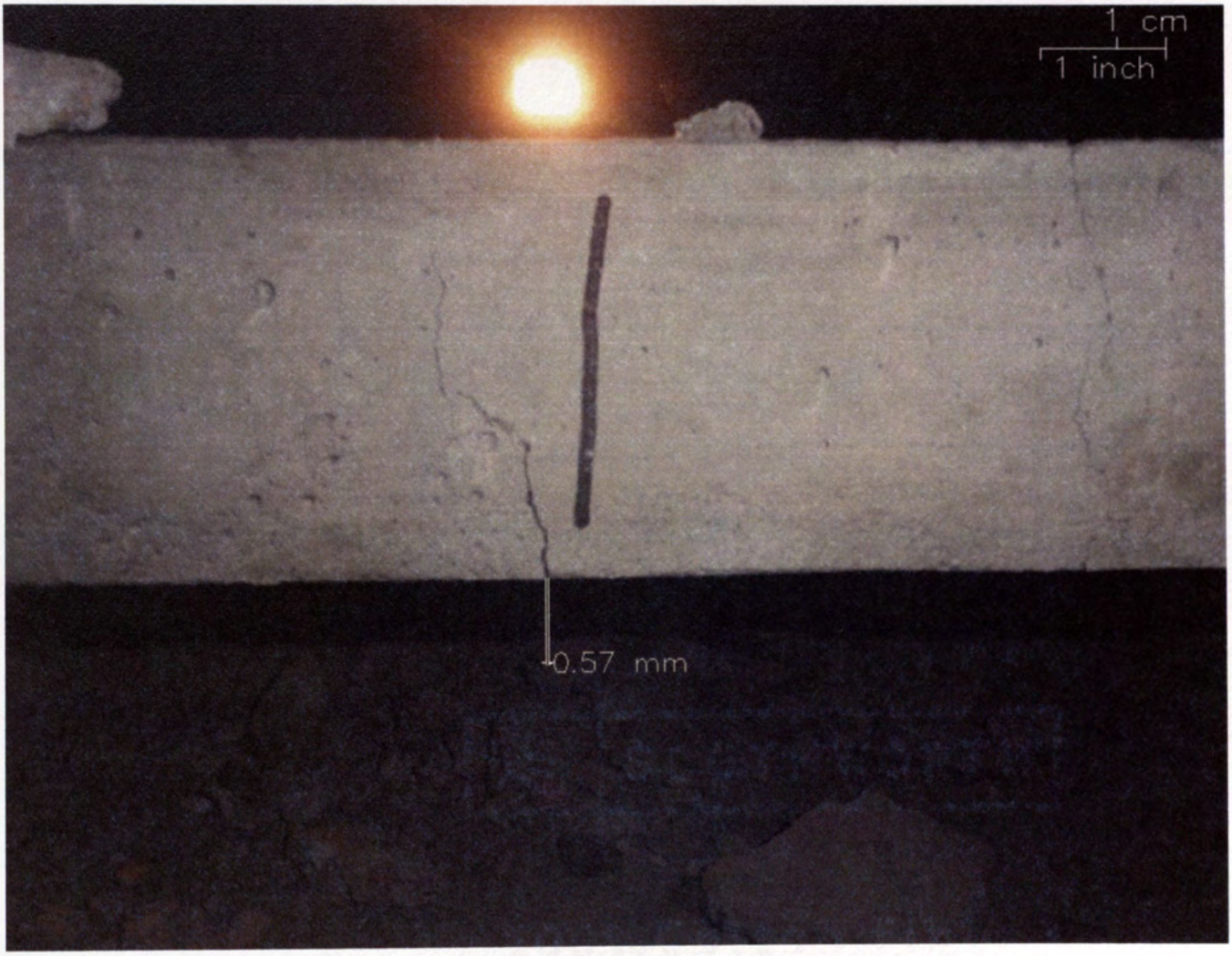

Figure E.3 – Flexural Cracks in the Back Face of 1-RC

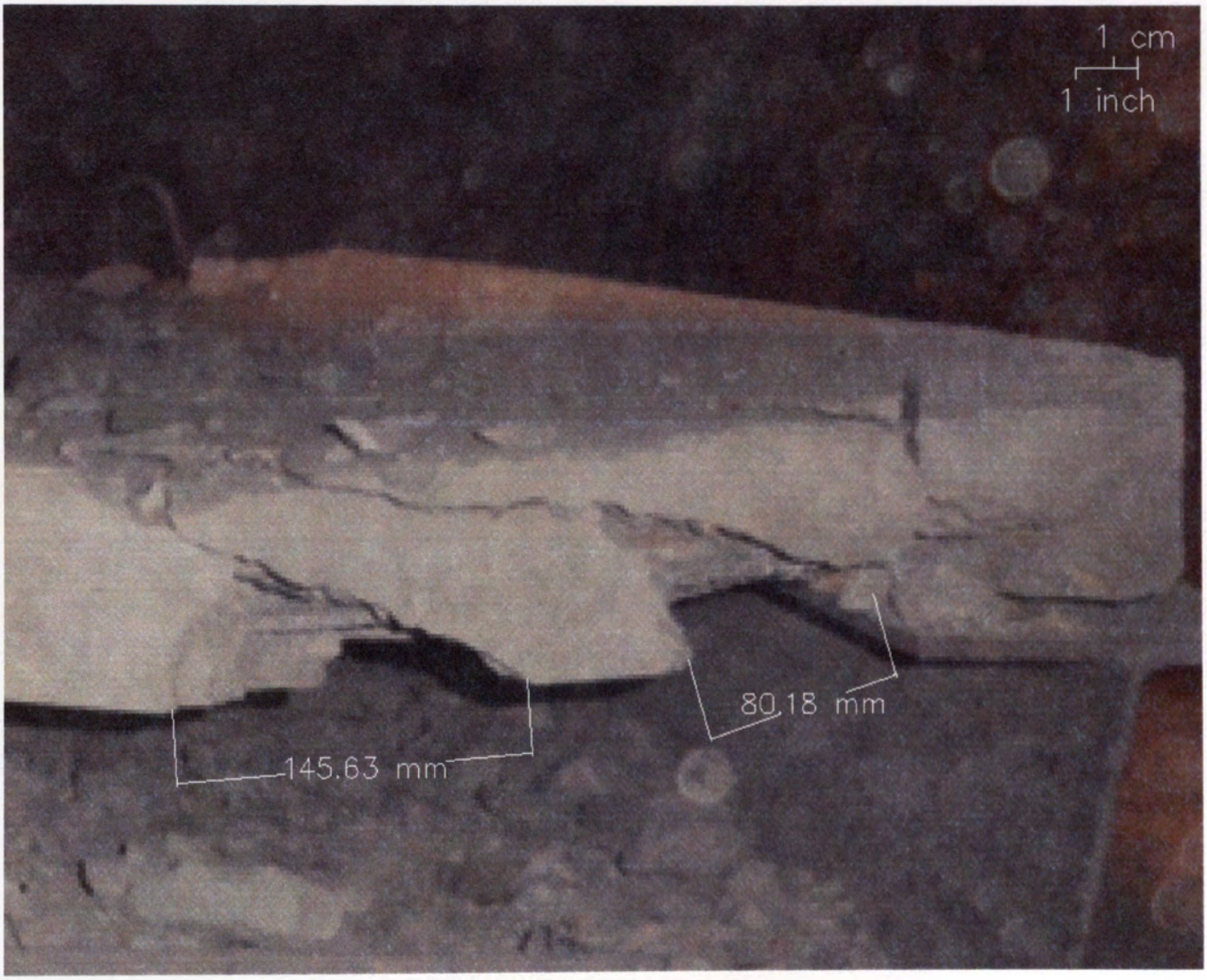

Figure E.4 – Shear Cracks in the Front Face of 1-RC

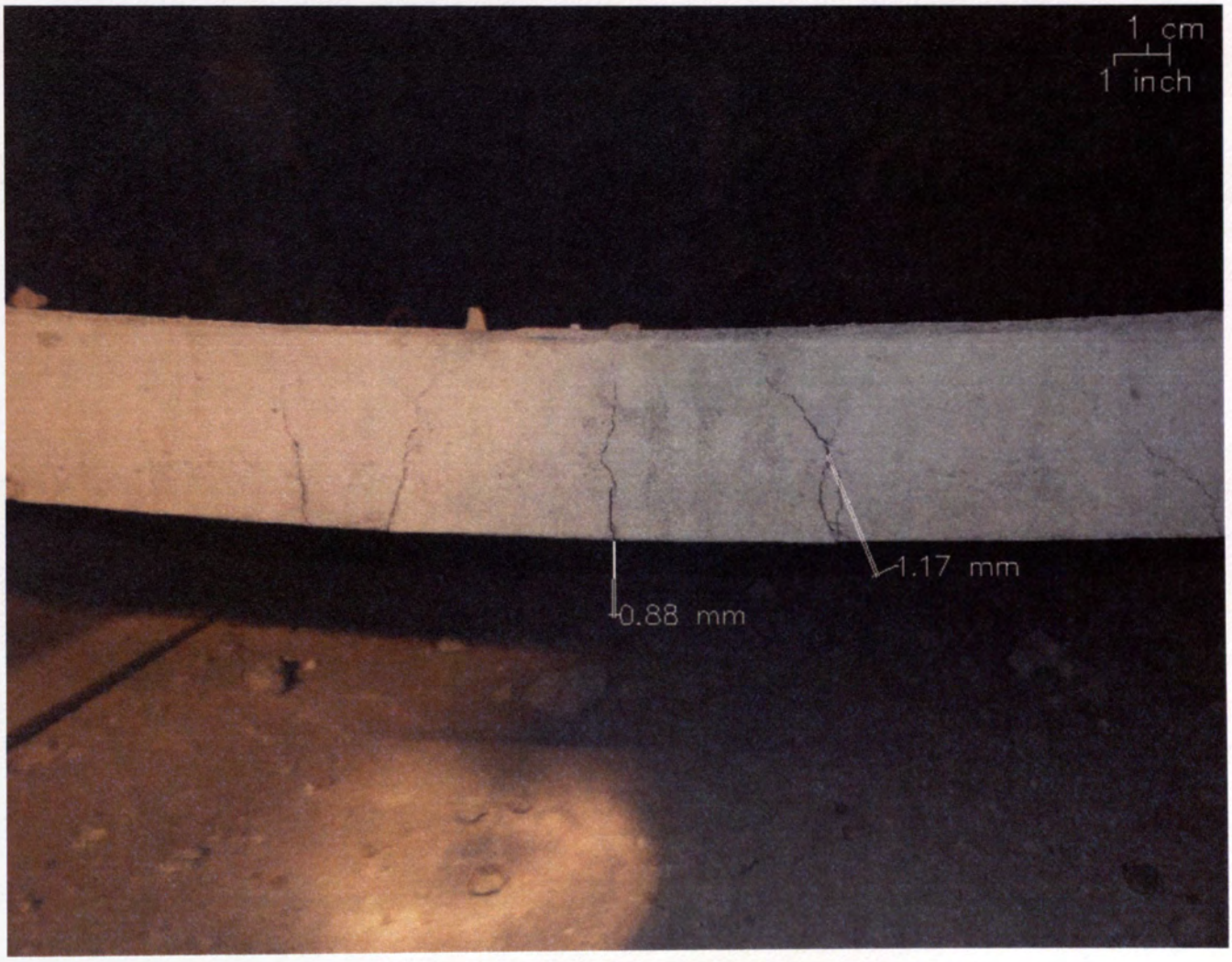

Figure E.5 – Flexural Cracks in the Front Face of 2-RC

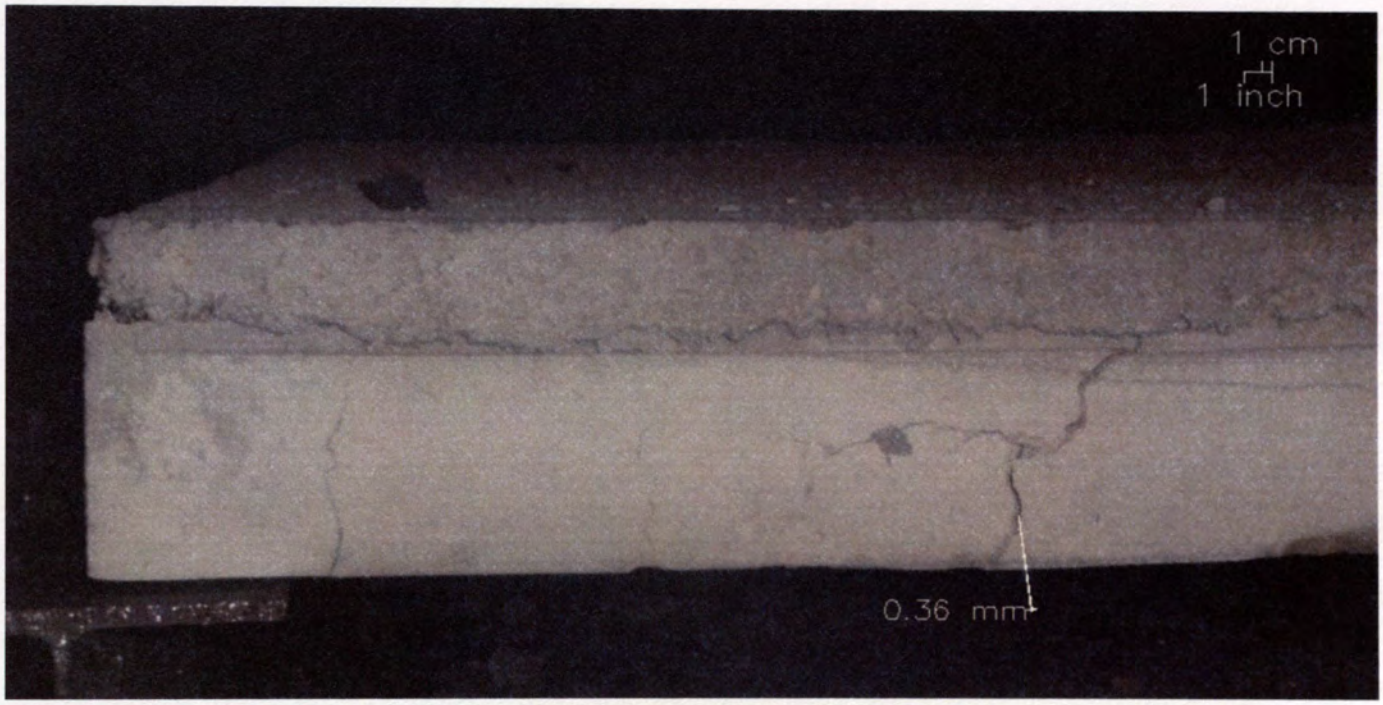

Figure E.6 –Flexural Cracks in the Front Face of 1-H, 1st Event

Figure E.7 – Flexural and Shear Cracks in the Front Face of 1-H, 2nd Event

Figure E.8 – Flexural Cracks in the Back Face of 2-H, 1st Event

Figure E.9 – Flexural Cracks in the Back Face of 2-H, 2nd Event

Figure E.10 – Flexural Cracks in the Front Face of H-FG, 2nd Event

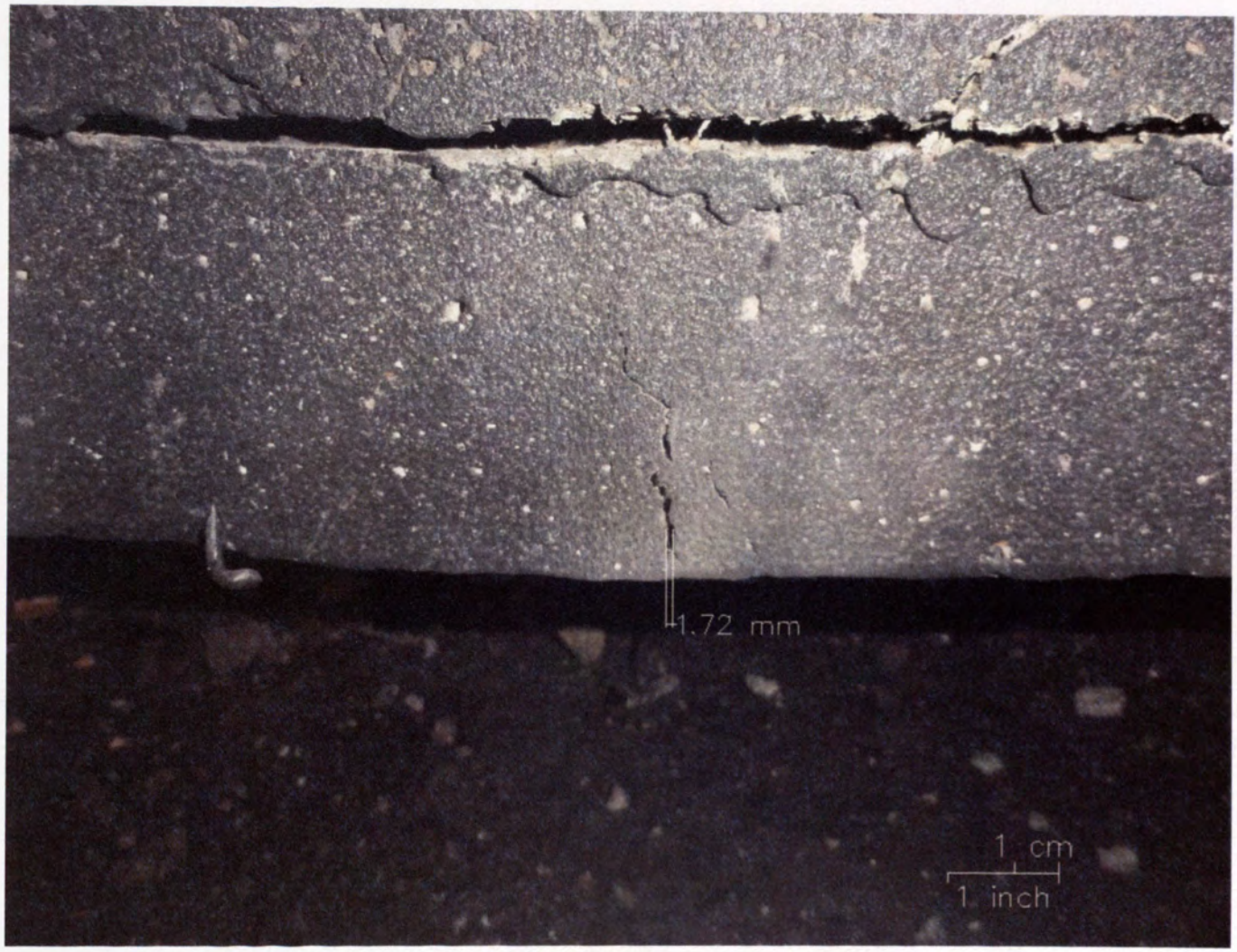

Figure E.11 – Flexural Cracks in the Front Face of H-A, 2nd Event

Figure E.12 – Flexural Cracks in the Back Face of H-A/F, 2nd Event

Figure E.13 – Flexural Cracks in the Back Face of H-FG-A/F, 2nd Event

Figure E.14 – Shear Cracks in the Front Face of H-B, 1st Event

Figure E.15 – Shear Cracks in the Front Face of H-B, 2nd Event

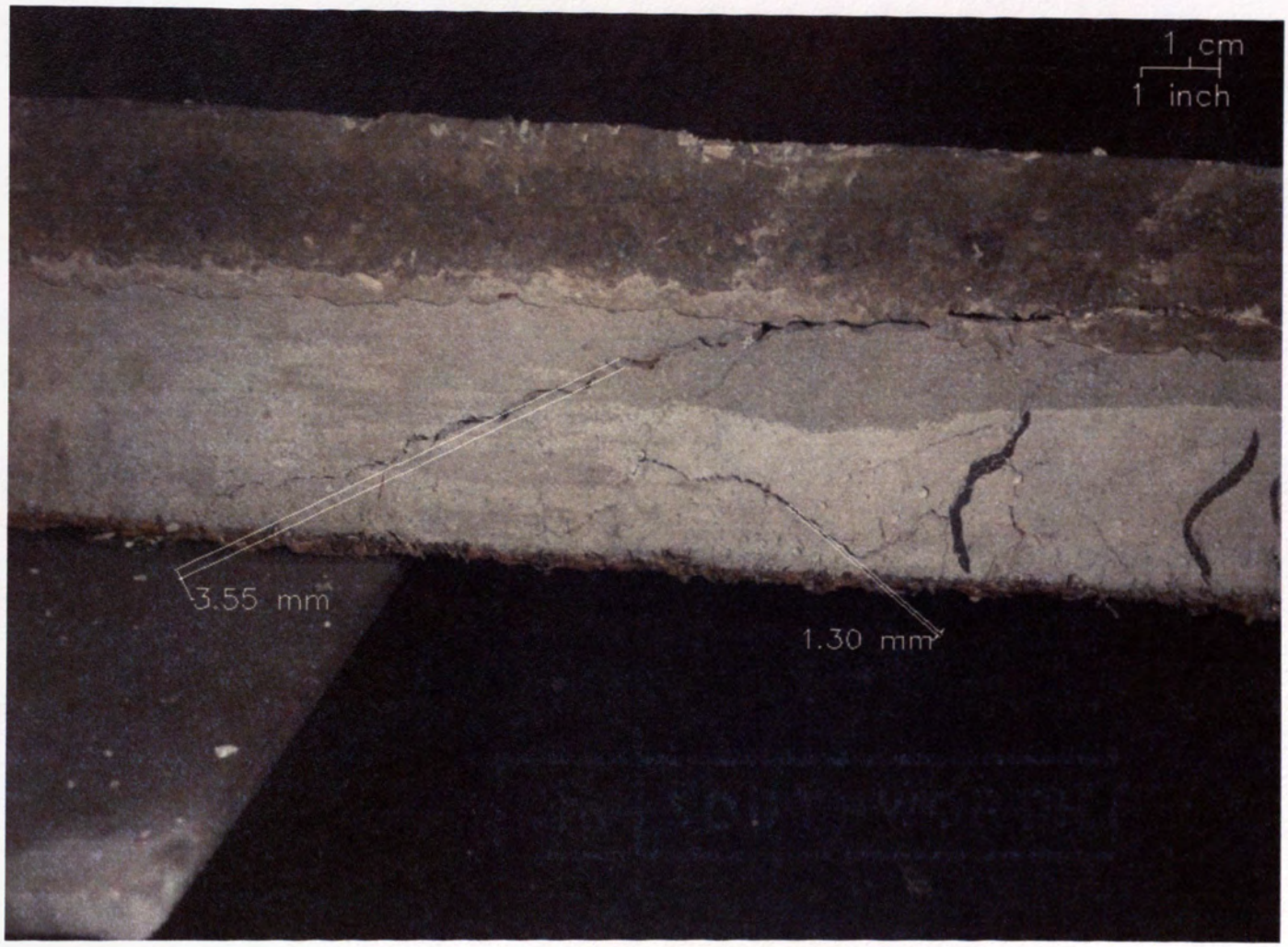

Figure E.16 – Flexural and Shear Cracks in the Front Face of H-B/F, 2nd Event

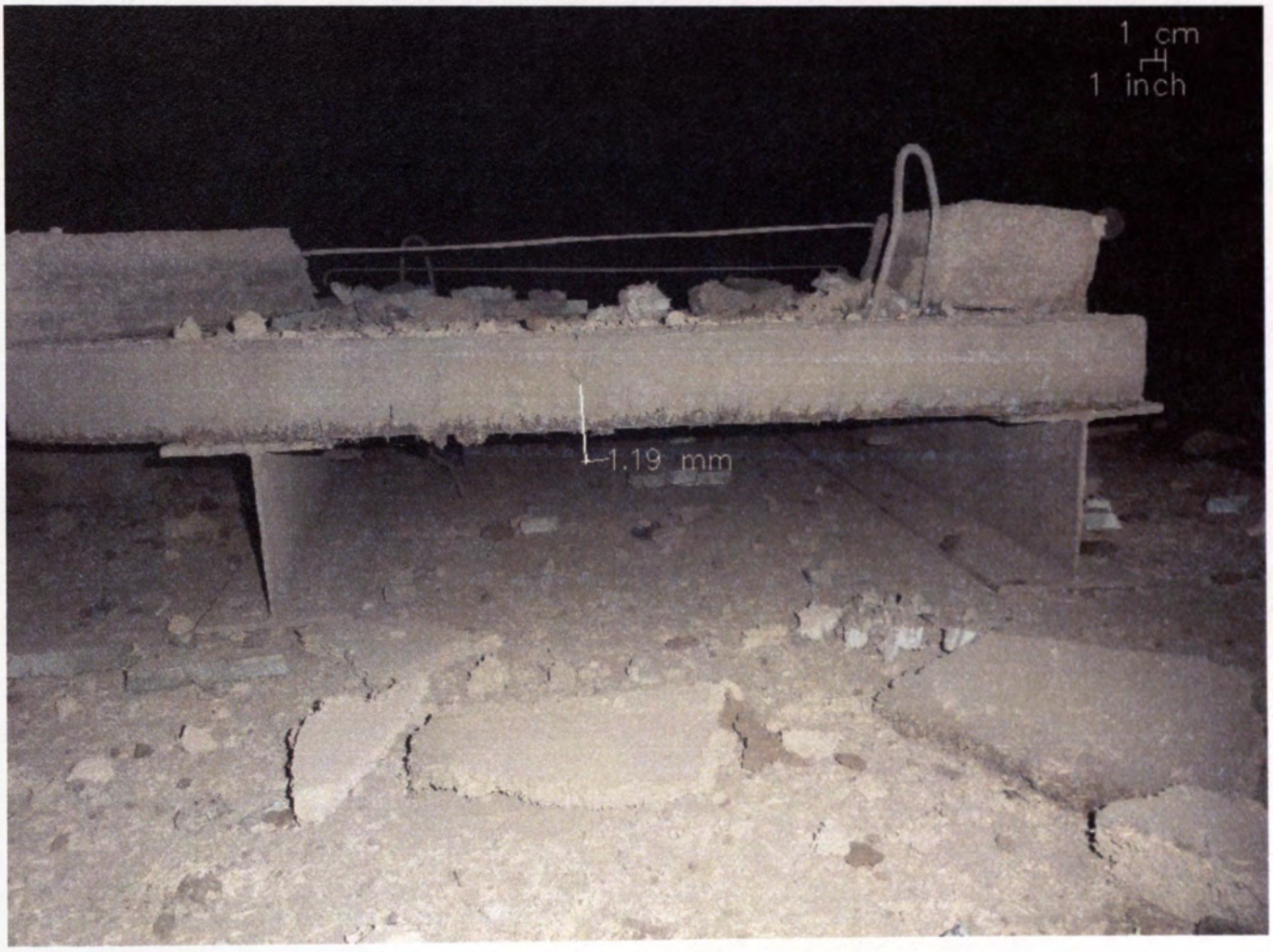

Figure E.17 – Flexural Cracks in the Front Face of H-FG-B/F, 2nd Event

VITA

Anthony Francis Wulfers was born on December 1, 1987 in Fort Collins, CO to Timothy and Rebecca Wulfers. He soon moved to his parents' hometown Cape Girardeau, MO and spent his childhood there. Upon graduating from the local catholic high school he enrolled at University of Missouri-Rolla (now Missouri S&T). As a freshman he joined Phi Kappa Theta fraternity and the university baseball team. He played baseball for 1 ½ years and is now an alumni of Phi Kappa Theta. Anthony graduated from Missouri S&T with a Bachelor's of Science in Civil Engineering in May 2010. He then pursued a Master's of Science in Civil Engineering with an emphasis in Structural Engineering. He is also currently the structural team lead for Missouri S&T Engineers Without Borders Nahualate, Guatemala team.